

SBIR- 09.19-8629

release date 9/18

A HELIUM-3/HELIUM-4 DILUTION CRYOCOOLER FOR OPERATION IN ZERO GRAVITY

Dr. John B. Hendricks, Principal Investigator  
Dr. Michael J. Nilles, Program Manager  
Dr. Michael L. Dingus, Scientist

Alabama Cryogenic Engineering, Inc.  
P.O. Box 2451  
Huntsville, AL 35804

October 17, 1988

April 17, 1986 through October 17, 1988

NOTICE

Rights in Data SBIR Phase II (April 1985)

This SBIR data is furnished with SBIR rights under the NASA Contract No. NAS8-37260. For a period of two years after acceptance of all items to be delivered under this contract the Government agrees to use this data for Government purposes only, and it shall not be disclosed outside the Government (including disclosure for procurement purposes) during such period without permission of the Contractor, except that, subject to the foregoing use and disclosure prohibitions, such data may be disclosed for use by support Contractors. After the aforesaid two year period the Government has a royalty-free license to use, and to authorize others use on its behalf, this data for Government purposes, but is relieved of all disclosure prohibitions and assumes no liability for unauthorized use of this data by third parties. This Notice shall be affixed to any reproductions of this data, in whole or in part.

N93-18397

Unclass

G3/31 0121201

(NASA-CR-183632) A  
HELIUM-3/HELIUM-4 DILUTION  
CRYOCOOLER FOR OPERATION IN ZERO  
GRAVITY Final Report, 17 Apr. 1986  
- 17 Oct. 1988 (Alabama Cryogenic  
Engineering) 148 P

SBIR DATA

Available only on approval of MSFC.

## ABSTRACT

This research effort covered the development of  $^3\text{He}/^4\text{He}$  dilution cryocooler cycles for use in zero gravity. The dilution cryocooler is currently the method of choice for producing temperatures below 0.3 Kelvin in the laboratory. However, the current dilution cryocooler depends on gravity for their operation, so some modification is required for zero gravity operation. In this effort we have demonstrated, by analysis, that the zero gravity dilution cryocooler is feasible. We have developed a cycle that uses  $^3\text{He}$  circulation, and an alternate cycle that uses superfluid  $^4\text{He}$  circulation. The key elements of both cycles were demonstrated experimentally. The development of a true "zero-gravity" dilution cryocooler is now possible, and should be undertaken in a follow-on effort.

## TABLE OF CONTENTS

<u>Section</u>	<u>Page</u>
Abstract.....	i
List of Figures and Tables.....	iii
1.0 INTRODUCTION .....	1
2.0 BASIC PRINCIPLES OF DILUTION CRYOCOOLER OPERATION .....	5
2.1 "Solution" Refrigerator .....	7
2.2 <sup>3</sup> He Circulation Type .....	13
2.3 <sup>4</sup> He Circulation, "Leiden" Type .....	16
2.4 <sup>4</sup> He Circulation, "ACE, Inc." Type .....	19
3.0 ZERO GRAVITY OPERATION OF DILUTION CRYOCOOLERS (THEORY) .....	24
3.1 <sup>3</sup> He Circulation Type .....	25
3.2 <sup>4</sup> He Circulation, "Leiden" Type .....	30
3.3 <sup>4</sup> He Circulation, "ACE, Inc." Type .....	32
4.0 LABORATORY STUDIES OF "ZERO GRAVITY" DILUTION CRYOCOOLER CONCEPTS ..	34
4.1 Solution Refrigerators .....	34
4.2 Phase Separators for <sup>3</sup> He .....	43
4.3 The "ACE, Inc." Cycle .....	64
5.0 CONCLUSIONS .....	72
6.0 RECOMMENDATIONS .....	77
7.0 REFERENCES AND BIBLIOGRAPHY .....	81
8.0 APPENDICES .....	86
APPENDIX A - Theory of Solution Refrigerators .....	A-1
APPENDIX B - Theory of the "Vortex" Cryocooler .....	B-1
APPENDIX C - Test Facility for Cryocooler Development .....	C-1

## LIST OF FIGURES

		<u>Page</u>
Figure 2.1	The $^3\text{He}/^4\text{He}$ Phase Separation Diagram ( $x = n_3/n_3 + n_4$ ).....	6
Figure 2.2	Basic Solution Refrigerator Cycle.....	8
Figure 2.3	Solution Refrigerator Using Superleaks and He II Circulation.....	10
Figure 2.4	Osmotic Pressure as a Function of Temperature and Concentration.....	12
Figure 2.5	The $^3\text{He}$ Circulation Dilution Cryocooler.....	14
Figure 2.6	The "Leiden" Dilution Cryocooler.....	17
Figure 2.7	The "ACE, Inc." Dilution Cryocooler.....	20
Figure 3.1	Schematic Diagram of the Superfluid Phase Separator (SPS).....	28
Figure 3.2	Two Possible Arrangement of Phases in a Zero- Gravity Solution Refrigerator.....	31
Figure 4.1	Schematic Representation of the Solution Refrigerator Test Cell.....	36
Figure 4.2	Temperatures of Solution Refrigerator Stages Versus Power Input to the Fountain Pump.....	38
Figure 4.3	Temperatures of Solution Refrigerator Stages as a Function of Power Input to the Fountain Pump.....	39
Figure 4.4	Temperatures of Solution Refrigerator Stages as a Function of Power Input to the Fountain Pump.....	40
Figure 4.5	Temperatures of Solution Refrigerator Stages as a Function of fountain Pump Power for Another 7% $^3\text{He}$ Test Run.....	41
Figure 4.6	Temperatures of Solution Refrigerator Stages as a Function of Fountain Pump Power for a Test Run with a $^3\text{He}$ Concentration of 14%.....	42
Figure 4.7	Schematic View of Cryostat.....	46
Figure 4.8	$^3\text{He}$ - $^4\text{He}$ Mixture Gas Handling and Pumping System..	49
Figure 4.9	Scale Drawing of $^3\text{He}$ Trapping Sponge Test Cryostat.....	51

	<u>Page</u>
Figure 4.10	Schematic View of Trapping Sponge Holder..... 53
Figure 4.11	Temperature of Sponge and Below the Sponge Versus Time for a 50% <sup>3</sup> He- <sup>4</sup> He Mixture Run..... 56
Figure 4.12	Pressure Above the Sponge as a Function of Time for the 50% <sup>3</sup> He- <sup>4</sup> He Mixture Test Shown in Figure 4.11..... 59
Figure 4.13	Temperature Vs. Time for Another 50% <sup>3</sup> He- <sup>4</sup> He Mixture Test Run..... 60
Figure 4.14	Pressure Above the Sponge Versus Time for the Run Shown in Figure 4.13..... 61
Figure 4.15	Temperature Versus Heat Input to Each Station When the Sponge is Running in Continuous Mode (Mass Flux In = Mass Flux Out)..... 63
Figure 4.16	Test Cell Schematic..... 65
Figure 4.17	Temperature Versus Time Behavior for Ge-3 Thermometer. Fountain Pump Power is 8.6 mV..... 67
Figure 4.18	Dilution Test Cell Schematic for Testing of the ACE, Inc., Cycle..... 69

LIST OF TABLES

	<u>Page</u>
Table 3-1	Baseline Specifications for a Space Based <sup>3</sup> He/ <sup>4</sup> He Dilution Cryocooler..... 24

## 1.0 INTRODUCTION

This report covers experimental and theoretical work on the application of "dilution cryocoolers" in zero gravity. There are basically two ways to reach temperatures below 0.3 K. These are:

- i. The "Adiabatic Demagnetization Refrigerator" (ADR)
- ii. The "Dilution Cryocooler".

The ADR is a magnetic refrigeration system. A magnetic salt is cooled to as low a temperature as possible and at the same time is magnetized with a very strong magnetic field. The salt is thermally disconnected from the precooler, and then the magnetic field is removed. Depending on the salt, temperatures below 0.1 K can be easily reached using this method. For zero gravity operation, the primary advantage of the ADR is that it doesn't depend at all on gravity. The ADR can be tested in one-g and we can be relatively certain of its zero gravity operation. The primary disadvantages of the ADR are:

- i. The high magnetizing field means that large, heavy magnets are required. Permanent magnets are not permitted, as the fields must be turned on and off.
- ii. The refrigeration is cyclic, as the salt must be remagnetized periodically.
- iii. The temperature of the salt is not constant during heat absorption. In order to maintain the temperature, an "isothermal demagnetization" can be used, but this requires a time programmed magnetic field.

The dilution cryocooler does not suffer from these problems. Constant temperatures as low as 3 mK can be reached. The currently available dilution cryocoolers require an external  $^3\text{He}$  vapor circulation pump. A new design for the circulator has recently become available, and this circulator makes long lifetime, zero gravity operation possible. The circulator, called a molecular drag pump, is produced by Alcatel Vacuum. In operation it requires roughly 50 watts of power. Therefore, there is an immediate trade off to consider in the application of the dilution cryocooler. Is the total weight of the ADR system (Magnetic salts, heat switch, magnet, power supplies, magnetic shields, etc.) greater or less than the total weight of the dilution cryocooler (cold head, gas lines, circulator, power supply)? Also, does the average power requirement of the dilution cryocooler (50 watts) create more or less of a system problem than the periodic power requirement of the ADR? These issues must be resolved before a final choice is made for the design of an ultra low temperature spaceborne cryocooler. A zero gravity dilution cryocooler is clearly an attractive option that bears consideration in the selection process.

Both the ADR and the dilution cryocooler require a "heat sink", and a HeII space dewar system operating at 1.5 - 1.8 K can serve for both systems. The heat given off by the cryocooler is absorbed by the evaporation of HeII. Since there is only a finite amount of HeII in the dewar, the lifetime of the mission can be determined by this heat absorption. The heat leaks of the ADR include the heat of magnetization of the magnetic salt, the magnet charging losses, the current lead losses for the magnet, and losses connected with the heat switch. The losses connected with the dilution cryocooler include heat rejected by the refrigeration cycle, losses connected with imperfect heat

exchange between the  $^3\text{He}$  being removed and the  $^3\text{He}$  being introduced, and losses connected with the piping required for the vapor circulation. As far as the cryogenic cycle itself is concerned, we expect the magnetic cycle to have higher intrinsic efficiency than the dilution cycle. However, we expect the losses to be relatively small, and the dominant losses will come from the external "support" systems.

A new dilution cryocooler cycle, that we call the ACE, Inc. cycle, was developed in this research program. It is different from the  $^3\text{He}$  circulation machine in that no external circulator is required. Thus, the drive power for the circulator is also eliminated. The "cost" for this simplification is a higher heat input to the He II dewar system during operation. However, this is balanced by the absence of pumping lines, etc. that are required for the  $^3\text{He}$  circulation machine. Also, a novel design for a spaceborne  $^3\text{He}$  circulation dilution cryocooler has been developed that utilizes surface tension in a porous metallic matrix to achieve phase separation. Experimental data has been obtained that supports the feasibility of both of these newly developed technologies.

In the earth laboratory, the choice between systems is clear. The dilution cryocooler has replaced the ADR except for some very special circumstances. This research program has begun the examination of the situation for space flight. None of the currently available dilution machines can operate in zero gravity.

The object of this research program was to develop dilution machines that could function in zero gravity. This has been successfully accomplished. The

dilution units must now be applied to specific space applications so an overall analysis can be carried out to see if the dilution cryocooler will replace the ADR in space as it has on earth.

## 2.0 BASIC PRINCIPLES OF DILUTION CRYOCOOLER OPERATION

The "dilution" cryocooler is based on three basic principles. The first principle is the heat of mixing of  $^3\text{He}$  in  $^4\text{He}$ . The reversible dilution of  $^3\text{He}$  into  $^4\text{He}$  produces a cooling effect. This cooling is the basis of a "solution" refrigerator using the two liquid helium isotopes. The second basic principle is the phase separation of liquid  $^3\text{He}$  and  $^4\text{He}$  below 0.87 Kelvin. The third basic principle is that the "dilute solution" contains roughly 6.4 % of  $^3\text{He}$ , even at zero temperature. Thus, the heat of mixing is available even at very low temperatures. The phase separation diagram of the two helium isotopes is shown in Figure 2.1.

A fourth principle, that is not used in the conventional  $^3\text{He}$  circulation dilution cryocooler, is useful for alternate cycles. This is the fact that the two isotopes can be easily separated using a "superleak". This is only possible below the superfluid transition temperature of  $^4\text{He}$ . The superleak can serve as a separation membrane in the solution refrigerator.

In this section we will review the basic operation of the solution refrigerator. A more complete theoretical analysis is included as Appendix A to this report. We will then give a brief analysis of the two currently proven dilution cryocooler cycles. The  $^3\text{He}$  circulation machine is the commercially available unit, and is almost universally used for laboratory studies in the 5 mK to 300 mK temperature range. The  $^4\text{He}$  circulation, "Leiden" type dilution cryocooler has been developed in the laboratory. It can operate over the same temperature range as the  $^3\text{He}$  circulation machine, but has not been commercially produced.

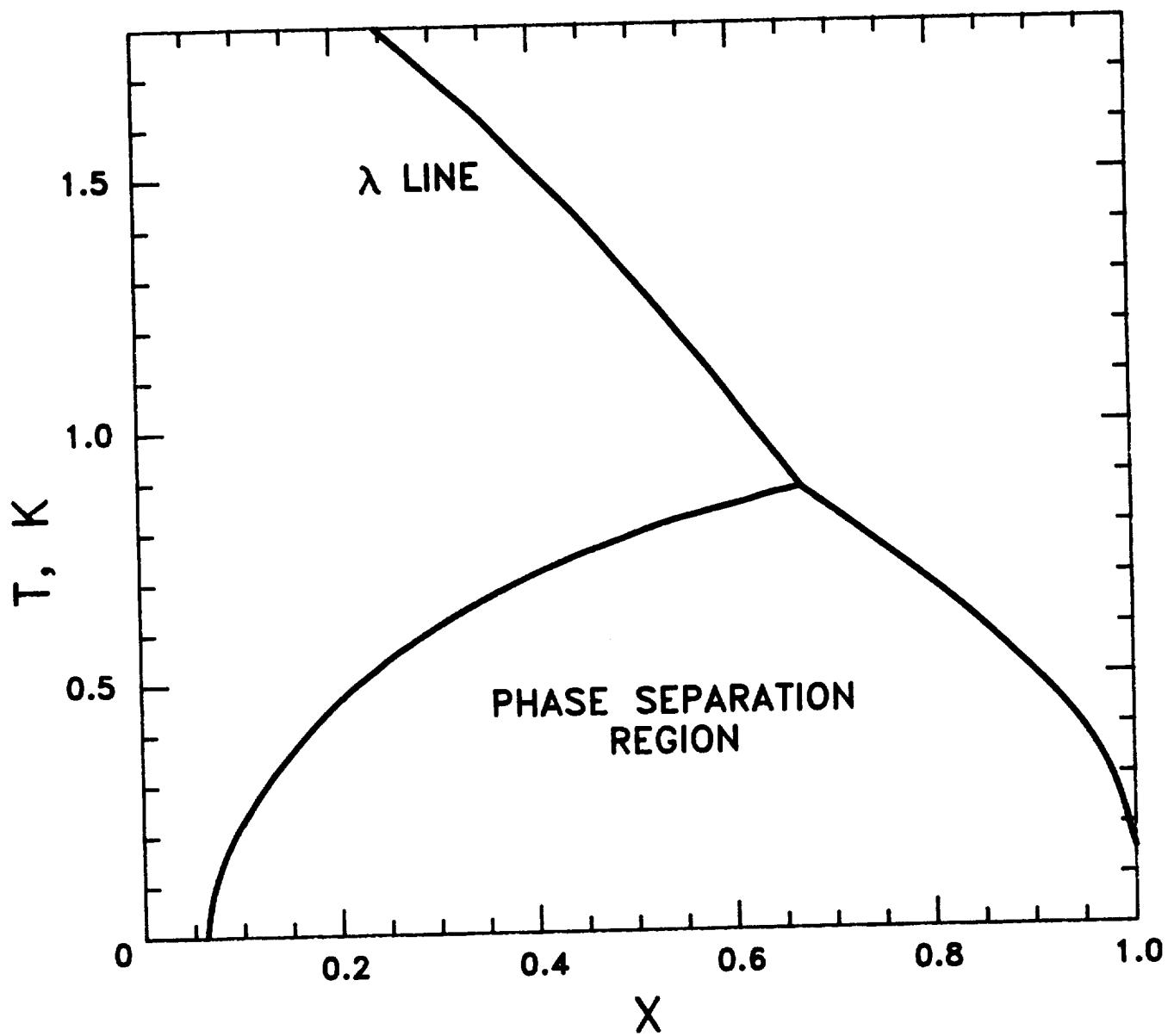


Figure 2.1 The  $^3\text{He}/^4\text{He}$  Phase Separation Diagram  
( $x = n_3/n_3 + n_4$ )

In the final section, a new dilution cryocooler cycle, that was developed in the effort covered by this report, will be described. This machine will be called the "ACE, Inc."  $^4\text{He}$  circulation, dilution cryocooler cycle. Even though it was specifically developed for zero gravity use, it can also operate in gravity, and is a possible replacement for the current commercial models.

In the report we will refer to the three different dilution cryocooler cycles as

- i. The  $^3\text{He}$  circulation cycle
- ii. The Leiden cycle
- iii. The ACE, Inc. cycle.

## 2.1 The Solution Refrigerator

The solution refrigerator is discussed by Radebaugh in Chapter 11 of Walker's (1983) monograph on cryocoolers. The basic cycle is shown in Figure 2.2. The key to the device is availability of a permeable membrane (G) that will allow the free circulation of one component ( $A_1$ ) by restricting the movement of the second component ( $A_2$ ). The heating and cooling effects at the two membranes will be approximately

$$Q = T\Delta S \tag{2.1}$$

A more detailed discussion of the thermodynamics is included in Appendix A. This analysis assumes that the two components are miscible. If there is a

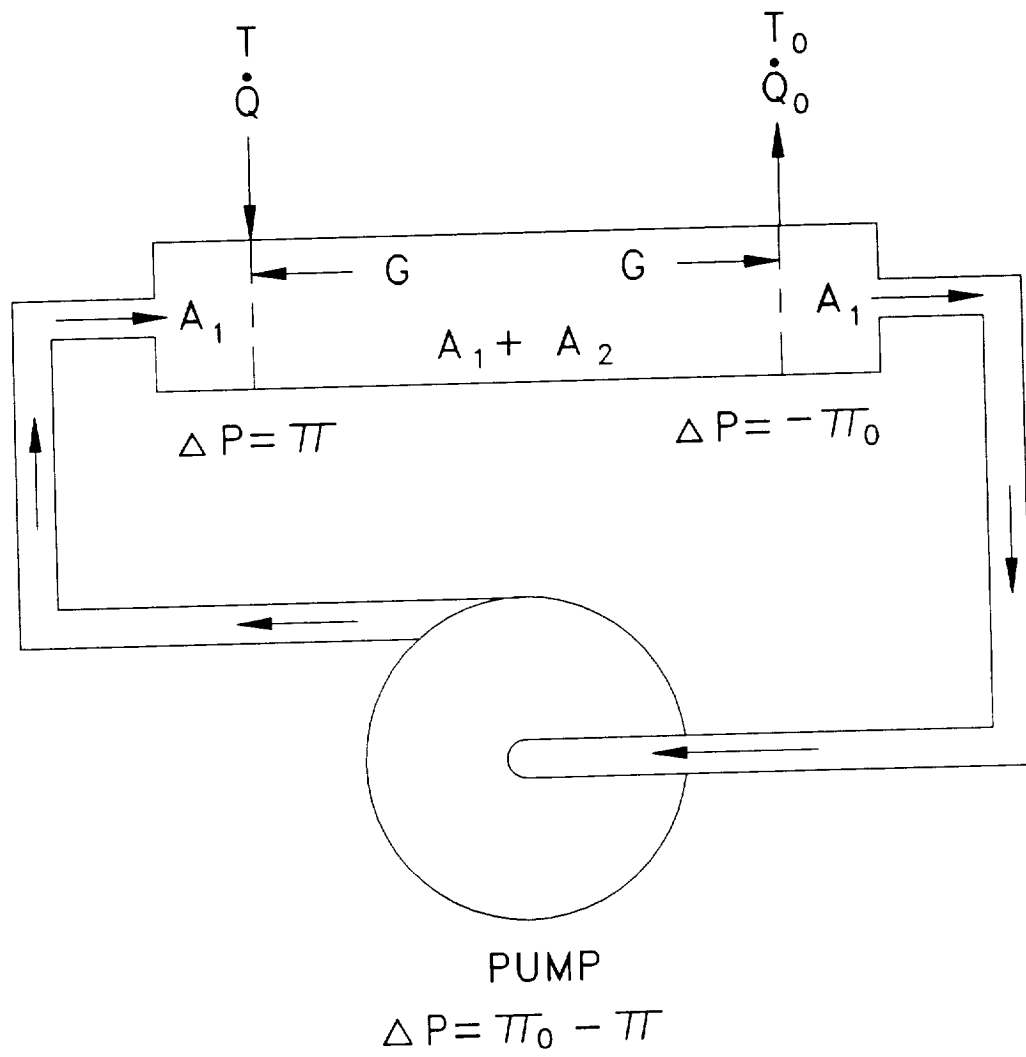


Figure 2.2 Basic Solution Refrigerator Cycle.

phase separation between the membranes, as is the case with the  $^4\text{He}/^3\text{He}$  dilution cryocooler, the analysis can get more complicated.

As the solution refrigerator operates, there is a continuous injection of  $A_1$  at the input and a removal of  $A_1$  at the output. This means that if  $A_1$  and  $A_2$  are miscible,  $A_2$  will take part in the mass transport from the input to output membrane. However, since the net mass flow of  $A_2$  must be zero over time, there must be a countercurrent of  $A_2$ . This countercurrent will be by diffusion, through the moving mixture. The diffusion can be driven by:

- i. concentration gradients,
- ii. temperature gradients,
- iii. osmotic pressure gradients, or
- iv. a combination of the above.

If the circulating fluid is superfluid  $^4\text{He}$ , and the stationary fluid is liquid  $^3\text{He}$ , then the solution refrigerator is closely related to the dilution cryocooler. However, as stated above, the simple analysis is only applicable above the phase separation temperature (0.87 K). Therefore, we will restrict the liquid helium solution refrigerator to temperatures above 0.87 K.

Packed, fine insulating powders can separate the two isotopes easily. These superleaks transmit almost no  $^3\text{He}$ , and can be used to purify  $^4\text{He}$ . The superleaks are connected in series with a drift tube (T) as shown in Figure 2.3. A "fountain pump" or other circulator provides the pressure necessary to drive the superfluid through the device.

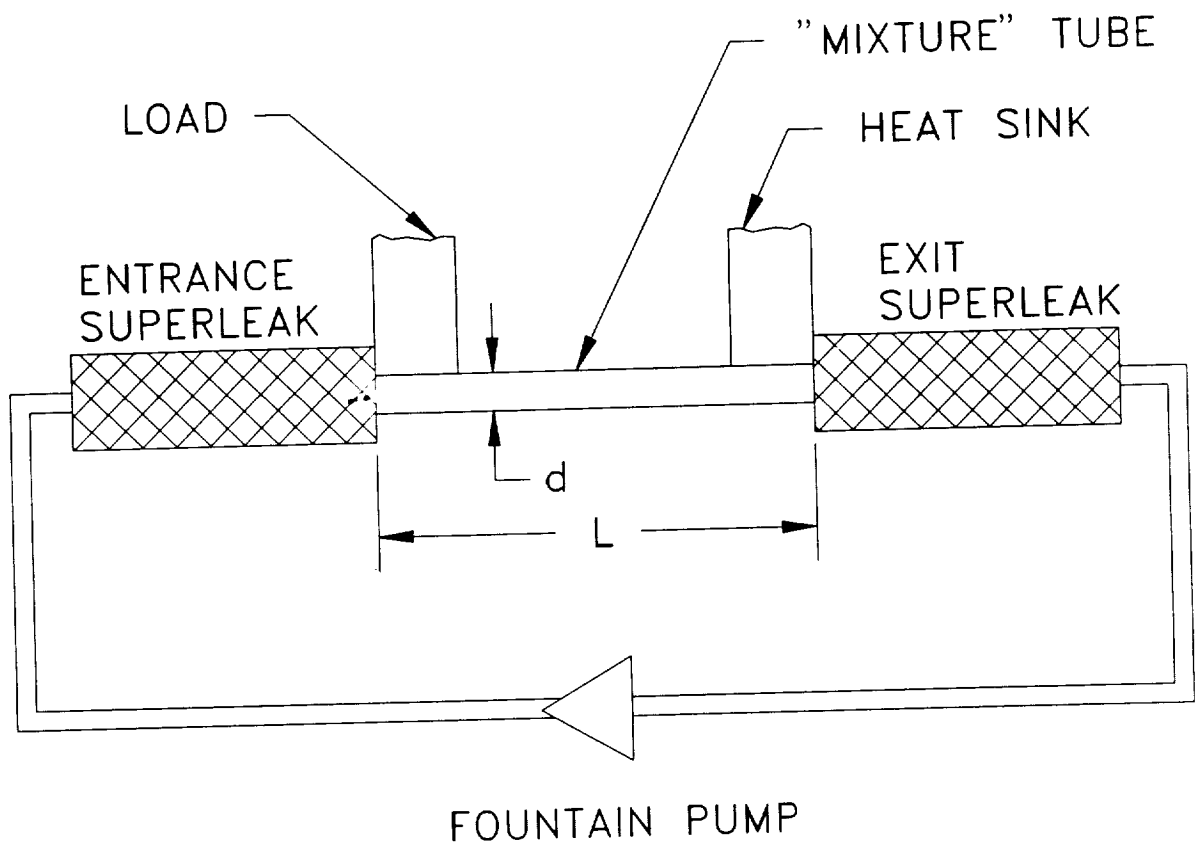


Figure 2.3 Solution Refrigerator Using Superleaks and He II Circulation.

The  $^3\text{He}$  concentration in the drift tube will change with temperature. Radebaugh (1967) has shown that the osmotic pressure in the drift tube will remain constant. This is true only for small relative velocities, however. For a discussion of cases where the mutual friction can become important, see deWaele et al. (1984). A chart of osmotic pressure vs. concentration and temperature is given in Figure 2.4.

A demonstration calculation of a solution refrigerator will be given as an example. Assume end temperatures of 1 K and 1.5 K, and that the  $^3\text{He}$  concentration at the 1 K end is 0.10. The osmotic pressure corresponding to  $T = 1$  K and  $x = 0.1$  is 208.6 Torr. The concentration corresponding to  $\pi = 208.6$  Torr and  $T = 1.5$  K is 0.064. Therefore:

$$Q_1 = T_1 \Delta S_1 = (1) (3.247) \text{ J/mol}$$

$$-Q_2 = T_2 \Delta S_2 = (1.5) (3.315) \text{ J/mol}$$

For a Carnot engine operating between the same two limits, we have

$$Q_2 |_{\text{Carnot}} = (T_2/T_1) Q_1,$$

$$\text{but } (1.5)(3.315) > (1.5/1) (1) (3.247)$$

so the solution refrigerator is less efficient than a Carnot refrigerator, as we would expect. In the above we have used the tables given in Radebaugh (1967).

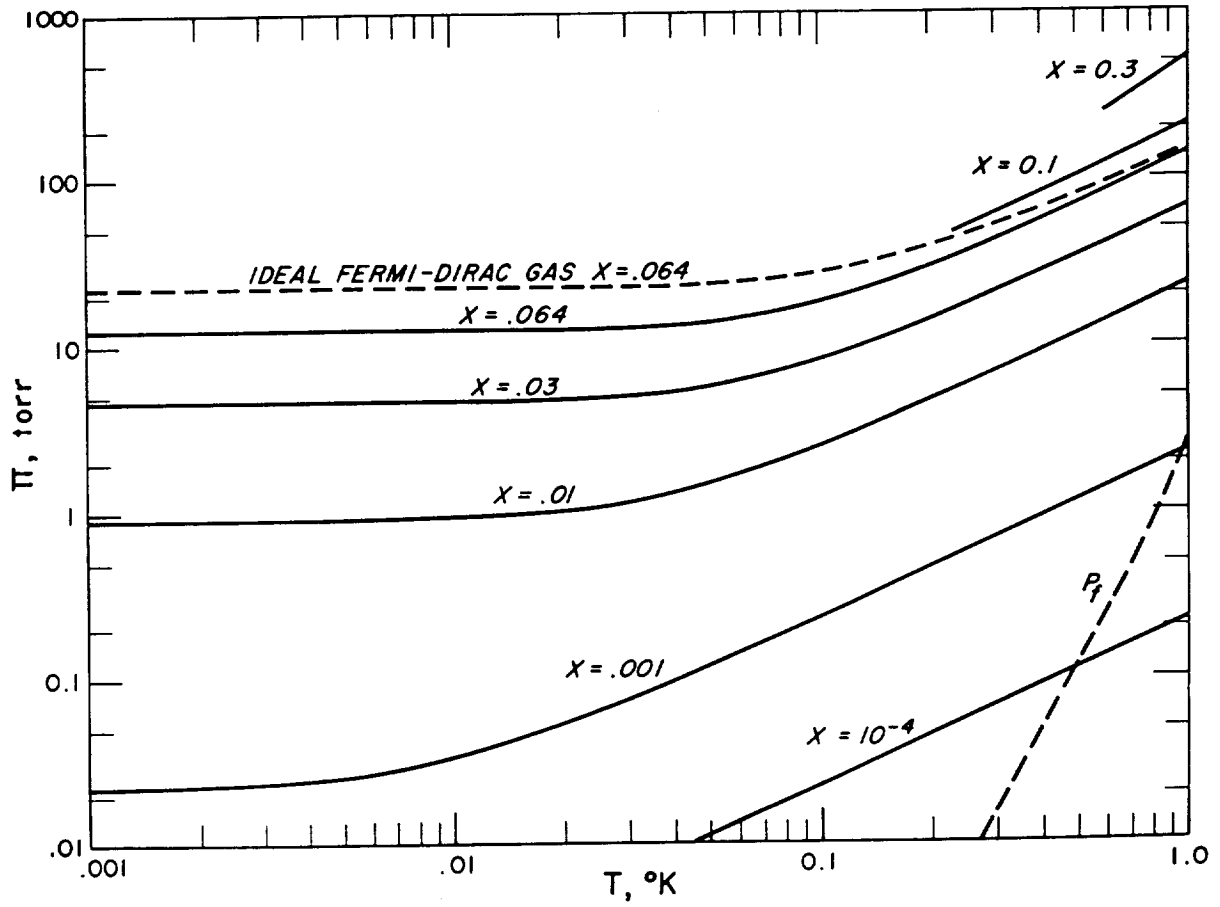


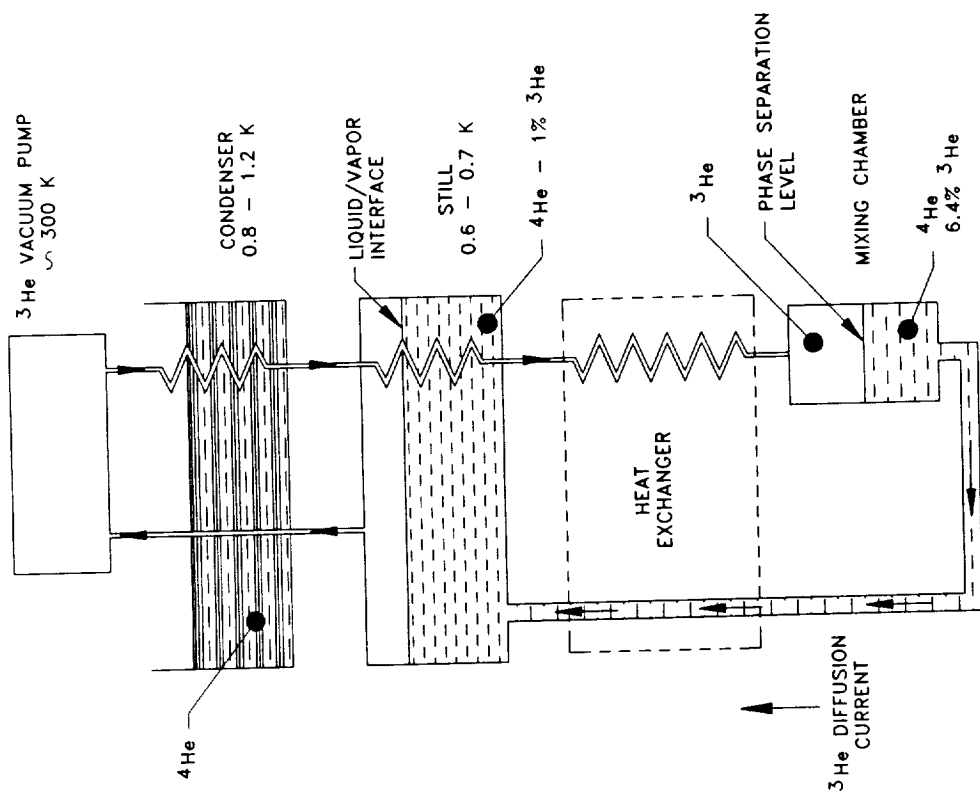
Figure 2.4 Osmotic Pressure as a Function of Temperature and Concentration

## 2.2 The $^3\text{He}$ Circulation Dilution Cryocooler

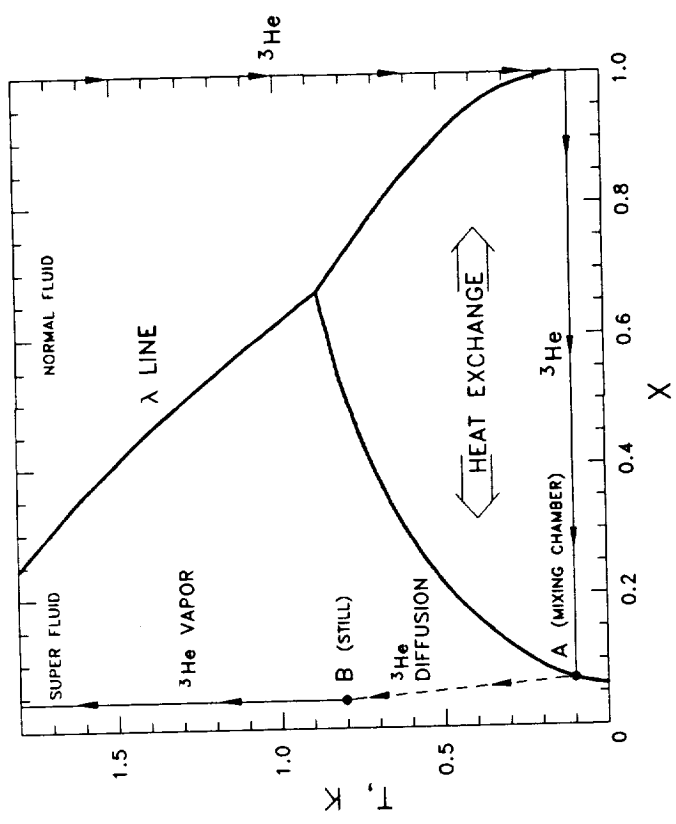
A detailed discussion of the conventional  $^3\text{He}$  circulation dilution cryocooler is not necessary for the purposes of this report. For a complete discussion, the reader is referred to Lounasma (1974), Radebaugh's chapter in Walker (1983), Betts (1976), or Richardson and Smith (1988). All these authors use the same basic techniques and only differ in small details. The theory of the  $^3\text{He}$  dilution cryocooler is well established, and has been supported by over twenty years of laboratory experience.

The basic cycle of the  $^3\text{He}$  circulation machine is illustrated in Figure 2.5(a).  $^3\text{He}$  vapor is brought from room temperature and condensed to liquid in the condenser. The liquid is then cooled, first in the still, and then in the heat exchanger, before it is injected into the mixing chamber. The  $^3\text{He}$  diffuses from the almost pure  $^3\text{He}$  floating on the top of the mixing chamber into the dilute solution in the lower part of the mixing chamber. Below 0.1 K, the concentration of the dilute solution remains almost constant at 6.4%  $^3\text{He}$ , independent of temperature. The "heat of mixing" of the  $^3\text{He}$  into the dilute solution provides the cooling power of the refrigerator.

A continuous column of dilute solution connects the mixing chamber to the still. At the liquid interface, the  $^3\text{He}$  is removed by evaporation. At temperatures below 0.7 K, almost pure  $^3\text{He}$  is evaporated, with no  $^4\text{He}$  removed in the vapor. Thus the  $^4\text{He}$  can be seen as a fixed "mechanical vacuum", with the  $^3\text{He}$  moving through it with no significant interaction. The dilute solution fills the other side of the heat exchanger, and the exchange of heat between the dilute solution and the incoming  $^3\text{He}$  forms one of the most



(a) Cycle Schematic



(b) Cycle Operating Points

Figure 2.5 The  $^3\text{He}$  Circulation Dilution Cryocooler

difficult technical problems in the design of the dilution cryocooler. A discussion of this problem is outside the purpose of this report, but is well covered in the previously cited literature.

The  $^3\text{He}$  concentration in the dilute solution follows the constant osmotic pressure law. This was discussed in the section of the solution refrigerator. For a 6.4%  $^3\text{He}$  concentration in the mixing chamber, we expect a 1%  $^3\text{He}$  concentration in the still, for a still temperature of 0.7 K. Since there will be a deficit of  $^3\text{He}$  in the still, due to evaporation, and an excess of  $^3\text{He}$  in the mixing chamber due to inward diffusion; the  $^3\text{He}$  will flow from the mixing chamber to the still. This is a diffusion current, driven by the constant osmotic pressure requirement. The cycle is shown in Figure 2.5(b).

The cooling power of a  $^3\text{He}$  circulation machine, with the flow of  $^3\text{He}$  returning to the cryocooler shut off (non-continuous operation) is

$$Q_m = 84 n_3 T_m^2 \quad \text{J/sec} \quad (2.2)$$

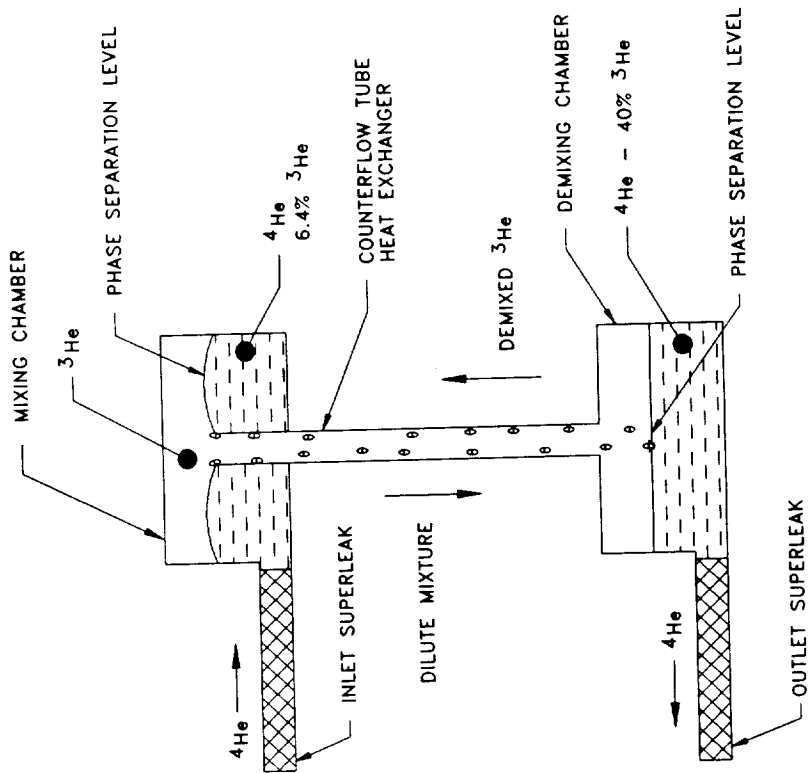
Circulation of  $^3\text{He}$  will reduce this cooling power, depending on the effectiveness of the heat exchanger. This can be used as a limiting value for comparison to other dilution cycles. Since the cooling power is directly proportional to the  $^3\text{He}$  circulation rate,  $n_3$ , it is important to make this as large as possible. However, this is set by the capacity of the room temperature pump. Modest vacuum pumps will have a speed of 5 liter/sec., correspond to  $n_3 = 30 \times 10^{-6}$  mole/sec. In order to get large flow rates, Roots blowers and other high capacity vacuum pumps are employed. Circulation

rates of  $2 \times 10^{-3}$  mole/sec have been used, but these are extreme values due to the pumping problems.

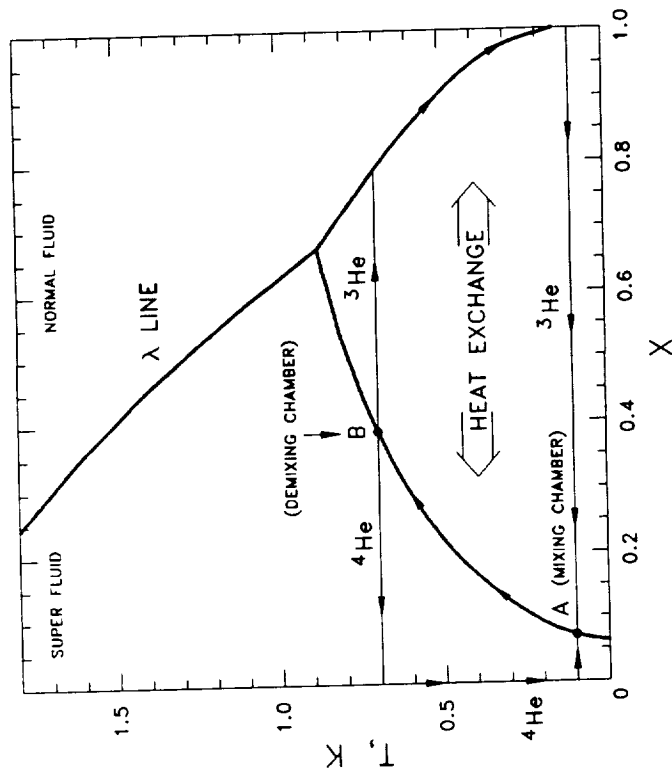
### 2.3 The $^4\text{He}$ Circulation, "Leiden" Dilution Cryocooler

In the "Leiden" type dilution cryocoolers, liquid  $^4\text{He}$  is circulated, rather than  $^3\text{He}$ . The Leiden machine uses superleaks for injecting and withdrawing superfluid  $^4\text{He}$  from the unit. A schematic of the cycle is shown in Figure 2.6(a). The system is arranged so that phase boundaries exist in both the mixing and the demixing chambers. The dilute solution in the mixing chamber is trapped below the "lip" of the counterflow tube. The  $^3\text{He}$  floats on top of the dilute solution, and fills the counterflow tube down to the demixing chamber. In the demixing chamber, the  $^3\text{He}$  floats on top of the dilute mixture in the lower chamber. Pure  $^4\text{He}$  is injected through the inlet superleak, and forms more dilute solution in the mixing chamber. This process is accompanied by cooling. As excess dilute solution is formed in the mixing chamber, it "pours" over the lip and falls through the counterflow tube as drops of dilute solution or as a sheet of dilute solution covering the walls of the tube. The cold dilute solution exchanges heat with the  $^3\text{He}$  as the drops fall. The  $^4\text{He}$  is removed from the tube by an exit superleak that is placed in the dilute solution in the demixing chamber. Heat is given off as the demixing takes place. This heat must be removed by an external cooler at a temperature below the phase separation point. This is typically done with a  $^3\text{He}$  vapor cycle refrigerator.

The cycle is indicated on a phase diagram in Figure 2.6(b). The entire process in the counterflow tube is in phase equilibrium, so the state path is



(a) Cycle Schematic



(b) Cycle Operating Points

Figure 2.6 The "Leiden" Dilution Cryocooler

along the phase separation line. As the temperature changes,  $^3\text{He}$  must diffuse into the falling drops to increase the concentration. As the  $^3\text{He}$  rich solution increases in temperature, the  $^4\text{He}$  fraction increases also. This means that the  $^3\text{He}$  rich phase has an increasing density as we move down the tube. Therefore, there is no gravitational instability in this cycle.

One of the basic problems with the Leiden cycle machine is the outlet superleak. The superfluid  $^4\text{He}$  is removed from a solution containing roughly 40%  $^3\text{He}$ . Therefore, as the  $^4\text{He}$  is removed, a relatively large amount of  $^3\text{He}$  must be removed, and must "diffuse" away from the superleak. If  $^3\text{He}$  builds up, it can form a blockage, and stop the superfluid  $^4\text{He}$  removal. This is a limiting factor on the circulation rate of the machine.

The Leiden machine cooling power can be calculated from the  $^3\text{He}$  circulation machine equation. For temperatures below 0.1 K, the  $^4\text{He}$  rate can be written as:

$$n_4 = [(1.0 - 0.064)/0.064]n_3 = 14.6 n_3 \quad (2.3)$$

Therefore, the maximum refrigeration rate according to Eqn. 2.2 will be:

$$Q_m = 5.7 n_4 T_m^2 \quad \text{J/sec} \quad (2.4)$$

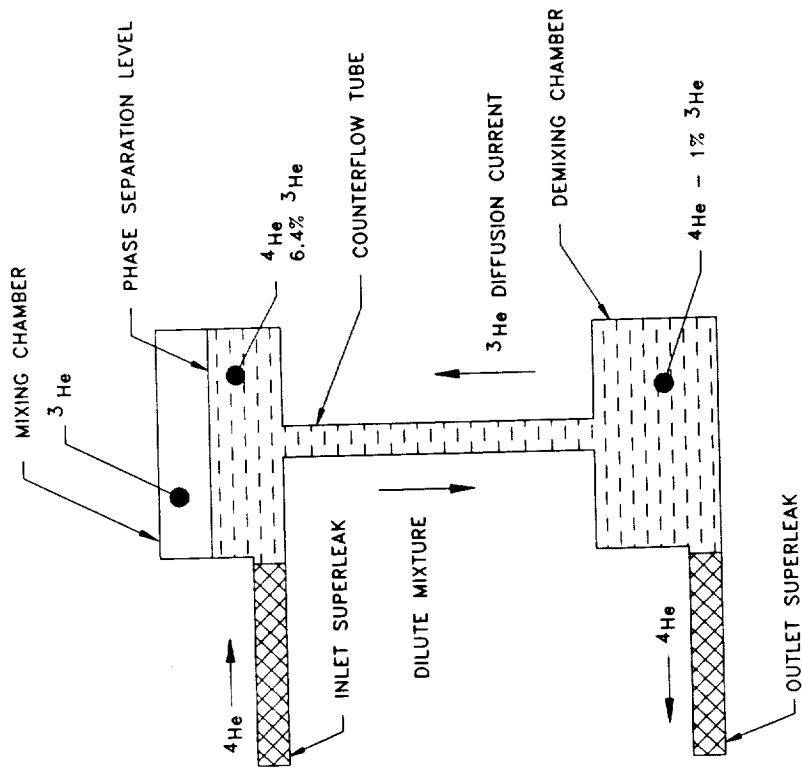
It is much easier to get large  $^4\text{He}$  circulation rates, as the entire circulation circuit can be maintained at superfluid temperatures, and the flow can be driven by a "fountain pump". Rates as high as  $2 \times 10^{-3}$  mole/sec are easily obtained using this method.

The main drawback to the Leiden machine is the precooler requirement. Since a  $^3\text{He}$  vapor cycle is required, we have gained no real advantage over the  $^3\text{He}$  circulation machine. All the external vacuum pumps are still required. The primary advantage in the Leiden cycle is the elimination of the recuperative heat exchangers in the low temperature section. This can lead to a considerable simplification in the design of the cryogenic section.

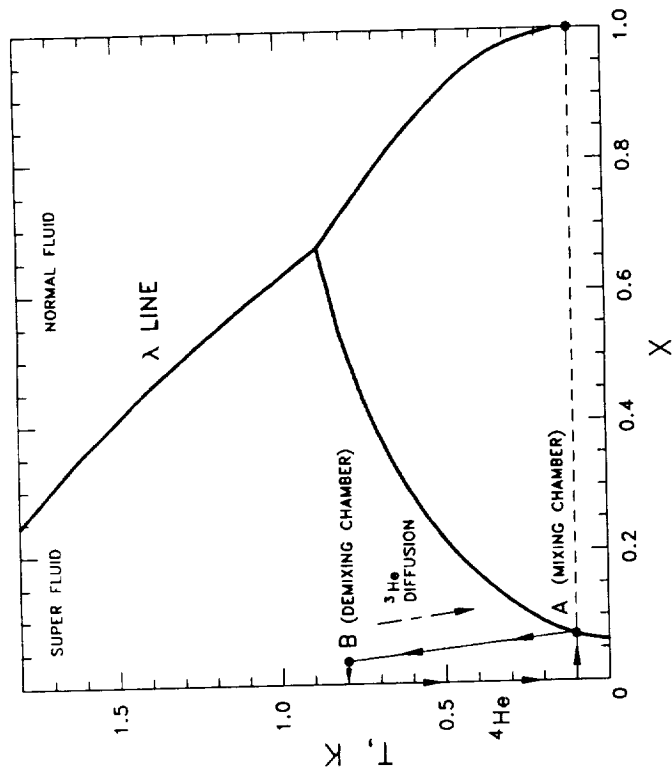
The Leiden dilution cryocooler is described in detail in the same references that were given for the  $^3\text{He}$  circulation machine. A recent paper by Satoh, et al. (1987) contains a description of the best machine built to date. A base temperature of 3.4 mK was reached at a circulation rate of  $3.5 \times 10^{-3}$  mole/sec. This base temperature compares well with typical  $^3\text{He}$  machines.

#### 2.4 The $^4\text{He}$ Circulation, "ACE, Inc. Dilution Cryocooler"

The schematic of the "ACE, Inc." cycle is shown in Figure 2.7(a). The cycle is similar to the Leiden cycle, as  $^4\text{He}$  is circulated through superleaks. However, it is different because there is only one phase boundary, and that is in the mixing chamber. The principal differences between the Leiden and ACE, Inc. cycles can be seen on the phase diagram, Figure 2.7(b). Only the mixing chamber operating point is on the phase separation line. The rest of the dilute solution in the counterflow tube and the demixing chamber has sub-critical  $^3\text{He}$  concentration. The relative concentrations of  $^3\text{He}$  in the mixing and demixing chambers are set by the "constant osmotic pressure" requirement, as in the  $^3\text{He}$  circulation cycle.



(a) Cycle Schematic



(b) Cycle Operating Points

Figure 2.7 The "ACE, Inc." Dilution Cryocooler

A substantial advantage of the ACE, Inc. cycle over the Leiden cycle is that the demixing chamber can operate at temperatures above the phase separation point. A higher demixing temperature will lower the overall cycle efficiency. However, if the requirement of a  $^3\text{He}$  vapor cycle precooler can be eliminated, it can result in a much simpler machine.

The  $^3\text{He}$  will be removed from the dilute solution in the demixing chamber. Therefore, an excess concentration of  $^3\text{He}$  will exist there. This excess will diffuse up the counterflow tube, then replenish the  $^3\text{He}$  being absorbed in the mixing chamber. This diffusion is similar to the diffusion that takes place between the mixing chamber and still of the  $^3\text{He}$  circulation machine. It is in the opposite direction, however; and it moves against the mass transport velocity,  $v$ , of the dilute mixture. From the experiments of Satoh, et al. (1982) on vortex cryocoolers, we know that the  $^3\text{He}$  will be swept out of the counterflow tube if the velocity exceeds the critical value. If we take the critical velocity to follow:

$$v_c = 10^{-6}/d \text{ m/sec.}$$

$$\text{then: } n_4 \leq 2.8 \times 10^{-2} d \tag{2.5}$$

where  $d$  is in meters and  $n_4$  is in mole/sec. Therefore,

$$Q_m \leq 0.16 d T_m^2 \tag{2.6}$$

However, the counterflow tube also conducts heat. This is calculated from

$$Q_c = k (A/L) \Delta T \quad (2.7)$$

Experimentally, the thermal conductivity values for solutions from 1.3% to 6.4%, lie in the  $k = 0.1$  W/mK range. Also,  $\Delta T = T_D - T_m \approx T_D$ , so we can write the available cooling power as:

$$Q_a = Q_m - Q_c = 0.16 d [T_m^2 - .49(d/L) T_D] \quad (2.8)$$

we can define a critical value when  $Q_a = 0$ . The value of  $(d/L)$  corresponding to the critical value is:

$$\begin{aligned} (d/L)_c &= T_m^2 / .49 T_D \\ &= 2.04 \times 10^{-2} \text{ for } T_m = 0.1 \text{ K and } T_D = 1 \text{ K} \end{aligned} \quad (2.9)$$

To insure that the conduction term is negligible,  $d/L$  should be less than one tenth  $(d/L)_c$ . Given this requirement, then the maximum cooling power is

$$Q_a|_{\max} = 0.16 d T_m^2$$

With a 4 mm tube, and  $T_m = 0.1$  K, the maximum cooling power is 6.4 micro-watt. The drift tube length,  $L$ , is 2 meters.

The above analysis depends critically on the critical velocity equation. There is almost no data available on superflow at temperatures below 1 Kelvin. The temperature dependence is also unknown, except that theory indicates a constant value with temperature. Finally, the mutual friction between the superfluid and the  $^3\text{He}$  is not well known. Castelijn, et al. (1984) has

considered the effect of the  $^3\text{He}$  velocity on the performance of the  $^3\text{He}$  circulation dilution cryocooler. The velocity of  $^3\text{He}$  in the ACE, Inc. cryocooler is not much larger than in the  $^3\text{He}$  circulation cycle, so we suspect this effect is not important. If the critical velocity becomes the limiting element, the drift tube can be split into a number of parallel tubes having small diameters. This increases  $v_c$  for a given cross-sectional area.

### 3.0 OPERATION OF DILUTION CRYOCOOLERS IN ZERO GRAVITY

In Section 2.0 the basic principles of dilution cryocooler operation were presented. These principles apply to earth based machines, that use gravity to provide physical separation of the phases present in the cryocooler. In this section we will develop the theory of machines that will operate in zero gravity. One approach to the problem is to provide an artificial gravity. This could be done by rotation of the device (centrifugal forces) or by use of electric fields. The latter method has been demonstrated in models by the group at the Jet Propulsion Laboratory, Israelsson (1988). We have rejected this approach in this effort. We intend to design a machine for zero gravity operation without artificial gravity.

For the design studies we have selected the baselined specifications given in Table 3-1. The specifications are based on the Adiabatic Demagnetization Refrigerator (ADR) systems that have been developed for space based sensor systems and represent the current state of the art in detector technology. The three dilution cryocooler types that were presented in Section 2.0 will be discussed in turn. The solution refrigerator does not depend on gravity in any way, so it will not be covered further.

TABLE 3-1

Baseline Specifications for a Space Based  $^3\text{He}/^4\text{He}$  Dilution Cryocooler

Operating Temperature	0.1 K
Operating Heat Load	10 $\mu\text{W}$
Heat Sink Temperature (Superfluid Helium Dewar)	1.5 K to 1.8 K

### 3.1 Operation of a $^3\text{He}$ Circulation Dilution Cryocooler in Zero Gravity

The  $^3\text{He}$  circulation dilution cryocooler, Figure 2.5(a), has three phase boundaries. These include:

- i. The vapor/liquid interface in the  $^3\text{He}$  condenser.
- ii. The "dilute solution"/"concentrated solution" interface in the mixing chamber.
- iii. The vapor/liquid interface in the still.

Each interface will be discussed in turn.

The vapor/liquid interface in the condenser is set by the thermal gradient in the condenser. Above the cold condenser section, the pressure is below that saturation pressure at the wall temperature. The tube is thus acting as a heat exchanger to cool the vapor. When the vapor reaches the condenser, the wall temperature falls rapidly, over a short section, to a value that is below the saturation temperature corresponding to the line pressure. Thus the fluid goes from single phase vapor to single phase, over pressurized liquid over a short distance. In addition, the tube has a small diameter so the fluid in the tube is roughly isothermal. Under these conditions gravity is not an important factor. The zero gravity heat transfer coefficients are probably different from the one g values, but not drastically so. We don't expect any free convective effects in such a confined space, so this indicates no important gravity effects. In conclusion, we do not expect the condenser to be a problem in a zero gravity  $^3\text{He}$  circulation dilution cryocooler.

The next interface that we reach in the circuit around the refrigerator is the phase boundary in the mixing chamber. This boundary is where the actual cooling effect is produced, so in order to make use of the cooling power, we must make thermal contact to the phase boundary. The usual schematic of the  $^3\text{He}$  circulation unit shows the  $^3\text{He}$  being introduced into the concentrated phase, and indicates "diffusion" across the phase boundary. As a matter of fact, the  $^3\text{He}$  is usually introduced into the dilute solution directly. This encourages stirring, and maintains concentration equilibrium in the mixing chamber. This experimental evidence supports the conclusion that a clear, defined phase interface is not a requirement for dilution cryocooler operation. The thermal contact requirement is the vital one.

The position of the phase boundary in the mixing chamber is set by the amount of  $^4\text{He}$  in the system. To first order, the  $^4\text{He}$  serves as a "mechanical vacuum". If the  $^4\text{He}$  phase boundary in the "still" is fixed, then the position of the phase interface will be fixed, depending on the volumes of the parts. In this way we can insure that the still and connecting lines are full of dilute solution, and that the phase boundary is somewhere in the mixing chamber.

The phase arrangement in the dilute solution channel will be self correcting. The  $^3\text{He}$  is being injected in the mixing chamber and removed in the still. Therefore, we expect the mixing chamber to be colder than the still with circulation on. Assuming such stable operation, now place a "blob" of pure  $^3\text{He}$  in the dilute solution channel. The temperature in the channel will be somewhere between the still temperature,  $T_s$ , and the mixing chamber temperature,  $T_m$ . Therefore, the particular point should be somewhere between

points A and B on the phase diagram, Figure 2.5(b). Now all these points are in the dilute phase, and are not in equilibrium with the concentrated phase. Therefore, we expect the "blob" to slowly "evaporate" into the dilute mixture and cease to exist. The only place where concentrated solution can exist is in the coldest part of the cryocooler; that is, in the mixing chamber.

The final phase boundary is in the still. Here, the problem is much more complex. In the still the dilute solution is a superfluid. This means that the walls of the still are coated with a superfluid film (Rollin film). This film can creep into the pumping lines and can contribute a substantial  $^4\text{He}$  circulation to the cryocooler. This  $^4\text{He}$  will reduce the cooling power of the machine, so some method of controlling the film is usually included in the still. In zero gravity the situation is much worse. The creeping  $^4\text{He}$  film could reach throughout the cold section of the pumping lines and the  $^4\text{He}$  level would be much higher than in one g operation. Therefore, the phase boundary in the still must be controlled for successful zero gravity operation.

A similar control problem with superfluid helium exists for dewars filled with He-II and operated in space. A device, called the superfluid porous plug has been developed that controls the superfluid. A device, based on similar principles can operate as a still phase separator (SPS). The SPS will be formed of a relatively high thermal conductivity material. This could take, the form of a plate perforated by small holes, or a pressed, sintered, porous metal disk. A schematic is shown in Figure 3.1. The passages in the SPS are represented by a uniform circular tube with diameter  $d$ . The matrix is represented by the disk, having an effective thermal conductivity,  $k$ . The

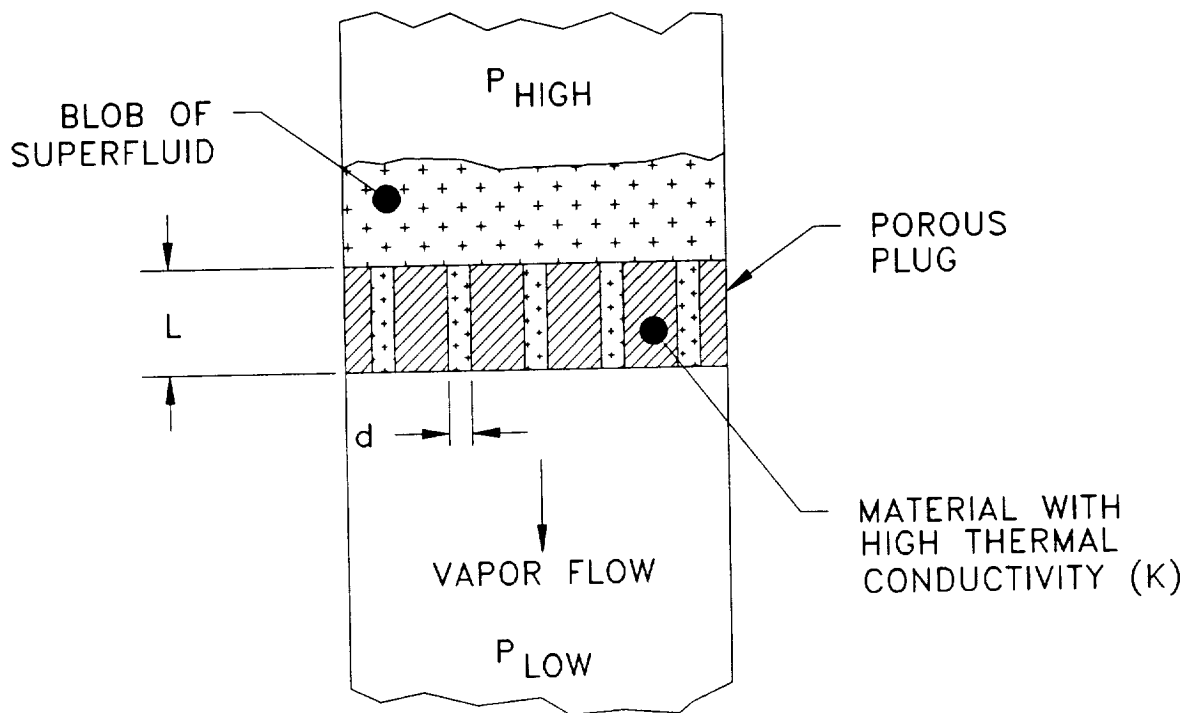


Figure 3.1 Schematic Diagram of the Superfluid Phase Separator (SPS). Surface tension in the pores prevents the liquid from escaping from the high pressure area  $P_{HIGH}$  to the downstream low pressure  $P_{LOW}$ .

disk will have  $n$  passages per unit area, and the effective length of the passages is  $L$ .

A qualitative description of the device follows. The dilute solution, at a temperature of 0.6 K to 0.8 K is on the upstream side to the plug. The downstream side is connected to a pumping line, and the pressure on the downstream side is reduced. Since it is a superfluid, a certain portion of the dilute solution will leak through the plug. The  $^3\text{He}$  in the dilute solution will evaporate and the liquid will cool. A fountain pressure,

$$P_f = \rho S \Delta T \tag{3.1}$$

will be generated that tends to drive the superfluid towards the hotter end of the plug; that is, back into the SPS. In steady state, the downstream end of the plug will be slightly colder, due to the  $^3\text{He}$  evaporation. Heat will be removed from the dilute solution on the upstream end, and transmitted through the SPS to the evaporating interface.

The holes in the SPS should have a small diameter, so that the surface tension force

$$P_{st} = \frac{2\sigma}{d} \tag{3.2}$$

is relatively large. This will assist in the definition of the evaporation interface. However, the holes should be large enough to allow the  $^3\text{He}$  to pass through with a relatively small pressure drop. According to the mechanical vacuum model, we can treat the  $^3\text{He}$  as a vapor, except that we replace the free

mass,  $m_3$ , by an effective mass  $m_3^*$ . For stable operation, the sum of the surface tension pressure and the fountain pressure should be much greater than the pressure drop of the  $^3\text{He}$  passing through the SPS.

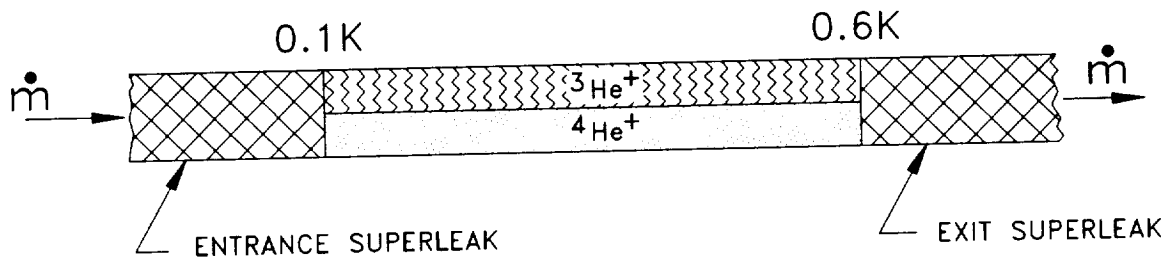
This device is related to the normal fluid phase separator that was developed by Alabama Cryogenic Engineering, Inc. in an earlier research effort.

### 3.2 Zero-Gravity Operation of the "Leiden" Dilution Cryocooler

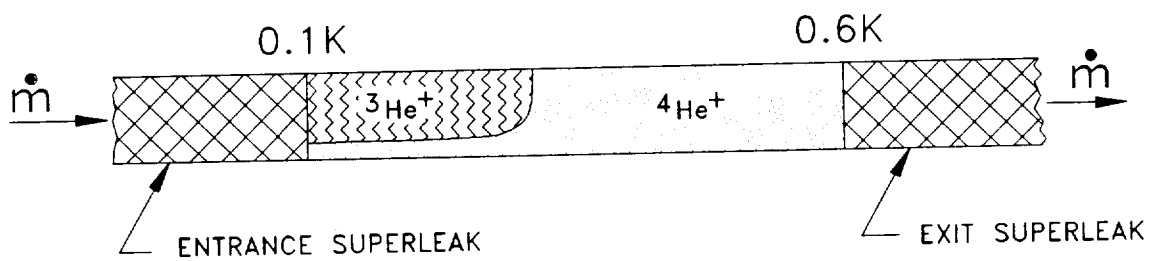
According to our analysis performed during this research program, the "Leiden" cycle is not applicable in zero gravity. This is contrary to the conclusions that were drawn in the Phase I effort, and this caused a substantial adjustment in the Phase II program. To illustrate, consider the situation shown in Figure 3.2(a). We assume that a solution type refrigerator device is filled with  $^3\text{He}/^4\text{He}$  mixture, and the end temperatures are set to the values shown. Is the indicated phase arrangement stable? There are two separate requirements:

- i. The concentrations along the phase boundary must follow the phase separation line.
- ii. The osmotic pressure in the dilute solution must be constant.

Reference to the property tables indicates that these two conditions cannot be met at the same time. An additional indication that this is not an equilibrium state is a calculation of the cooling power with circulation of



a) "Unstable" Phase Arrangement



b) "Stable" Phase Arrangement

Figure 3.2 Two Possible Arrangement of Phases in a Zero-Gravity Solution Refrigerator.

$^3\text{He}$  through the superleaks. We find that  $Q_{\text{out}}$  at 0.6 K is less than  $Q_{\text{in}}$  at 0.1 K. Thus, the second law is violated.

The solution to the problem is shown in Figure 3.2(b). An internal "convection" will take place, driven by the osmotic pressure. The  $^3\text{He}$  will thus collect at the cold end of the tube, and the dilute solution will fill the remaining space. Therefore, the "Leiden" machine becomes the ACE, Inc. cycle. We conclude that the "Leiden" cycle is only possible in gravity, and is not a candidate for zero gravity operation.

### 3.3 Zero-Gravity Operation of the ACE, Inc. Dilution Cryocooler

The ACE, Inc. cycle avoids the problems of the Leiden cycle by having a phase boundary only in the mixing chamber. Since this is the coldest region in the unit, the  $^3\text{He}$  phase can exist there stably at all temperatures. The arrangement of the phases is similar to the  $^3\text{He}$  circulation dilution cryocooler. To simplify things, the amount of  $^3\text{He}$  in the active region could be reduced, so that at the lowest temperatures there would be not concentrated  $^3\text{He}$  phase. This is possible, but it will reduce the cooling power at temperature higher than 0.1 K. For maximum refrigeration power there should be enough  $^3\text{He}$  to provide a phase separation at a relatively high temperature. This will speed up the cooldown process, and insure that the full cooling power is available at the lowest temperatures.

Since the ACE, Inc. cycle is new, the question of testing for zero gravity arises. As with all the dilution cycles there is a strong effect of gravity. The pure  $^3\text{He}$  is much lighter than the dilute solution, so it tends

to raise to the highest point in the machine. In addition, if the  $^3\text{He}$  concentration changes along the counterflow tube, then the density also will change. A "gravitational instability" of this type must be suppressed in the  $^3\text{He}$  circulation cycle. This is usually done by adding a "U-Tube" trap at the exit of the still.

For testing in gravity, the ACE, Inc. unit must be in one of two positions. Either the mixing chamber must be higher than the demixing chamber or they must be at the same height (horizontal operation). If the demixing chamber is above, a gravitational instability will occur, and the unit cannot operate stably.

#### 4.0 LABORATORY STUDIES OF "ZERO GRAVITY" DILUTION CRYOCOOLER CONCEPTS

In this section, test results will be presented for a solution refrigerator using  $^3\text{He}$ - $^4\text{He}$  liquids as working fluids. This type of refrigerator was introduced in Section 2. A description of the experimental apparatus will be given, and the test results for pure  $^4\text{He}$  and for two different  $^3\text{He}$ - $^4\text{He}$  mixtures will be presented. It will be shown that these results indicate that the principle of the  $^3\text{He}$ - $^4\text{He}$  solution refrigerator is valid and that functioning of the solution refrigerator was observed as expected.

##### 4.1 Solution Refrigerator Test Results

In this section, test results will be presented for a solution refrigerator using  $^3\text{He}$  -  $^4\text{He}$  liquids as working fluids. This type of refrigerator was introduced in Section 2. The solution refrigerator differs from the dilution refrigerator in that the latter works at temperatures below the 0.86 K threshold for the  $^3\text{He}$  rich -  $^4\text{He}$  rich phase transition. Solution refrigerators could in principal be tested for any two weakly interacting species if a membrane can be constructed that is permeable to one species but impermeable to the other. One component is trapped between two membranes, which it cannot penetrate. The second component is circulated in through one membrane, and out the other. An entropy increase occurs on the downstream side of the first membrane as the two components mix together, while an entropy decrease occurs at the second membrane where the two components are separated. These changes are due to the entropy of mixing of the two distinguishable, non-interacting components. At this point in the description

of the solution refrigerator, the argument is usually given that these entropy changes result in cooling at the first membrane and heating at the second one since

$$Q = T\Delta S \tag{4.1}$$

where  $Q$  is the heat flow,  $T$  is the temperature, and  $\Delta S$  is the change in entropy of the system due to mixing. However, equation 4.1 may not always be justified (see Appendix A).

Solution refrigerator tests were conducted on an auxiliary cryostat, which will be described in detail in Section 4.2. This cryostat provides a 1.4 K superfluid helium supply and heat sink for test use. Figure 4.1 shows a schematic representation of the test cell used for the  $^3\text{He} - ^4\text{He}$  solution refrigerator.  $^3\text{He}$  is trapped between two superleaks, which consist of stainless steel tubes tightly packed with jeweler's rouge.  $^3\text{He}$  is admitted to the chamber between the superleaks by means of a stainless steel capillary that runs to room temperature.  $^3\text{He}$  cannot pass through the superleaks, so it is trapped between them. Superfluid  $^4\text{He}$  ( $T < 2.17$  K) can go through the superleaks, and is circulated through the refrigerator by a fountain pump. The fountain pump makes use of the thermomechanical effects (see Guenin and Hess, 1980) to drive fluid from the pot through the device and back into the pot. An intermediate heat exchanger is required between the fountain pump and the solution refrigerator to ensure that the liquid entering the refrigerator is at the base temperature of approximately 1.4 K.

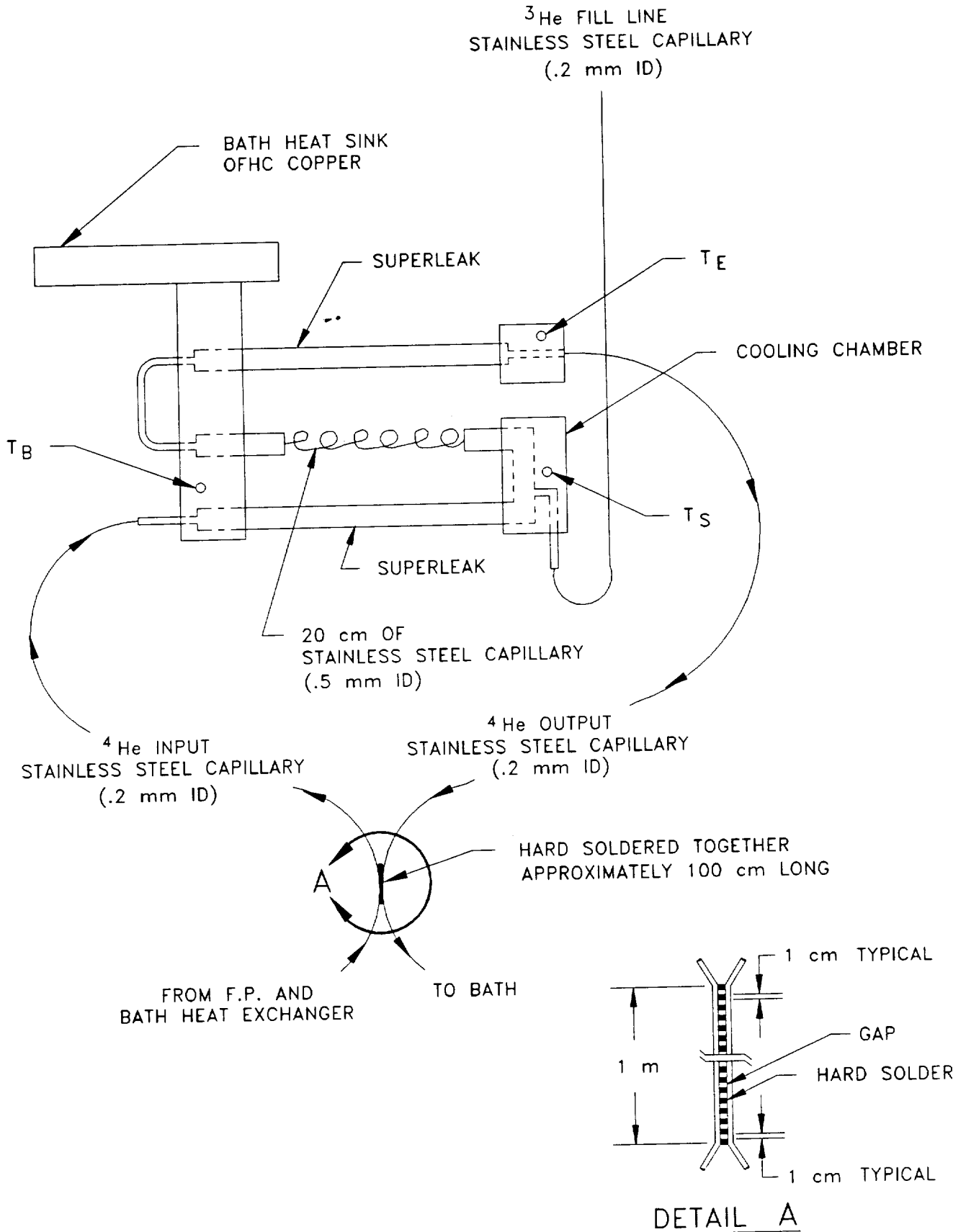


Figure 4.1 Schematic representation of the solution refrigerator test cell.

In Figures 4.2 and 4.3, the temperatures of three stations of the refrigerator are shown plotted against fountain pump power. The data shown in these figures are for pure  $^4\text{He}$  ( $X=0$ ) in the chamber. The temperature at the end of the exit superleak  $T_e$  can be seen to decrease dramatically as the fountain pump power is increased; the exit superleak and capillary is effectively acting like a vortex cooler, and sharp cooling is observed. The temperature of the bath heat sink  $T_B$  rises slowly as the fountain pump power is increased. This is to be expected because the heat input to the fountain pump must be dissipated into the bath. The solution refrigerator's cooling chamber temperature  $T_C$  shows no appreciable cooling for the pure  $^4\text{He}$  ( $X=0$ ) cases shown.

After completing these runs, pressurized  $^3\text{He}$  was forced into the test cell, pushing out some of the  $^4\text{He}$  superfluid in there. Metering of the amount of gas input gave estimates of the concentration. Figures 4.4 and 4.5 show the same parameters plotted for the case when the cell was filled with approximately 7%  $^3\text{He}$  ( $X=0.07$ ); Figure 4.6 shows the same parameters for 14%  $^3\text{He}$  ( $x=0.14$ ). In all three of these figures, a noticeable cooling was observed in the cooling chamber as the fountain pump power was increased. Thus, the cooling seems to be related to the presence of  $^3\text{He}$  in the cell.

#### 4.1.1 Conclusions of the Solution Refrigerator Tests:

1. That the solution refrigeration principle was demonstrated for the  $^3\text{He}$ - $^4\text{He}$  system.

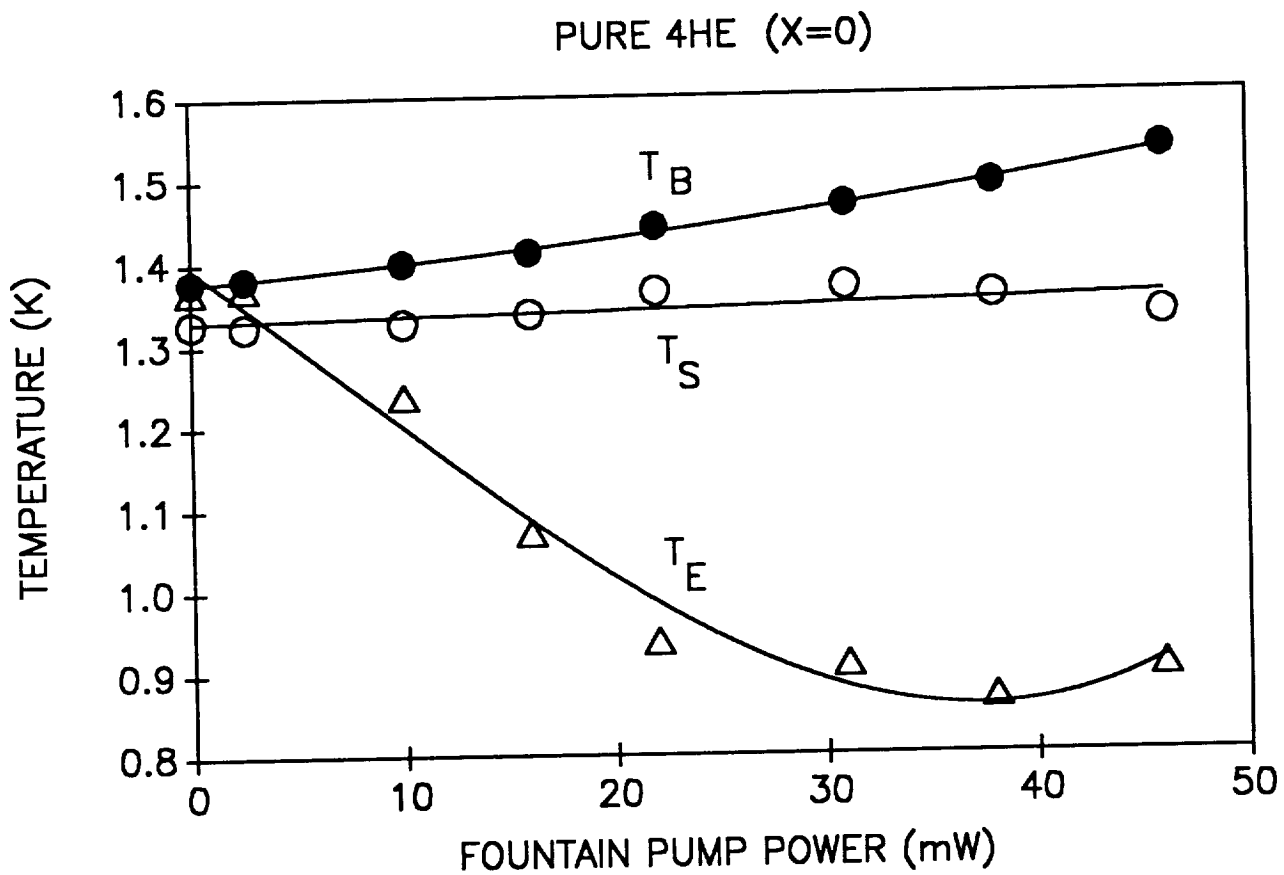


Figure 4.2 Temperatures of solution refrigerator stages versus power input to the fountain pump.  $T_S$  is the temperature of the cooling chamber. These results are for pure  $^4\text{He}$ , so no refrigeration effect is expected.

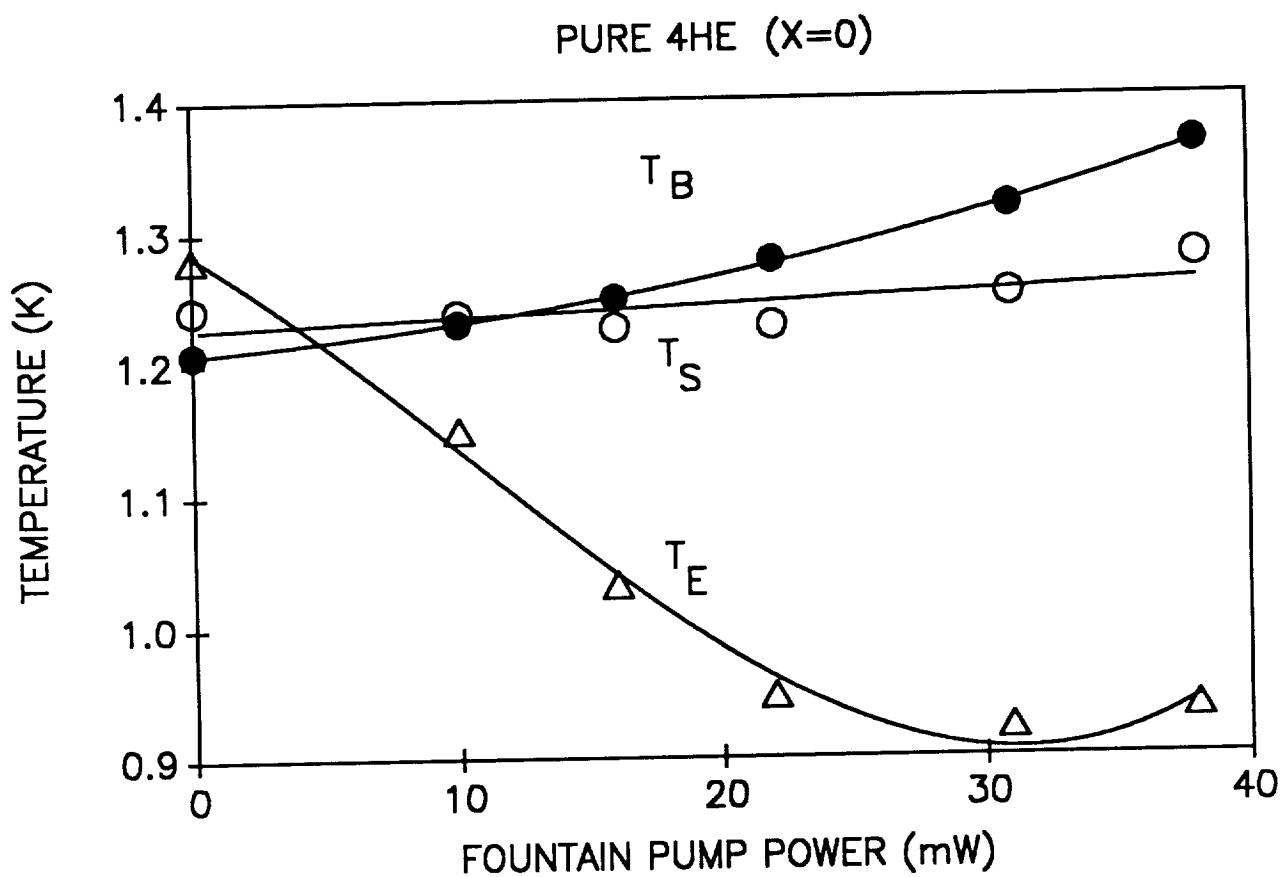


Figure 4.3 Temperatures of solution refrigerator stages as a function of power input to the fountain pump. This graph shows results for another run with pure  $^4\text{He}$  as the working fluid.

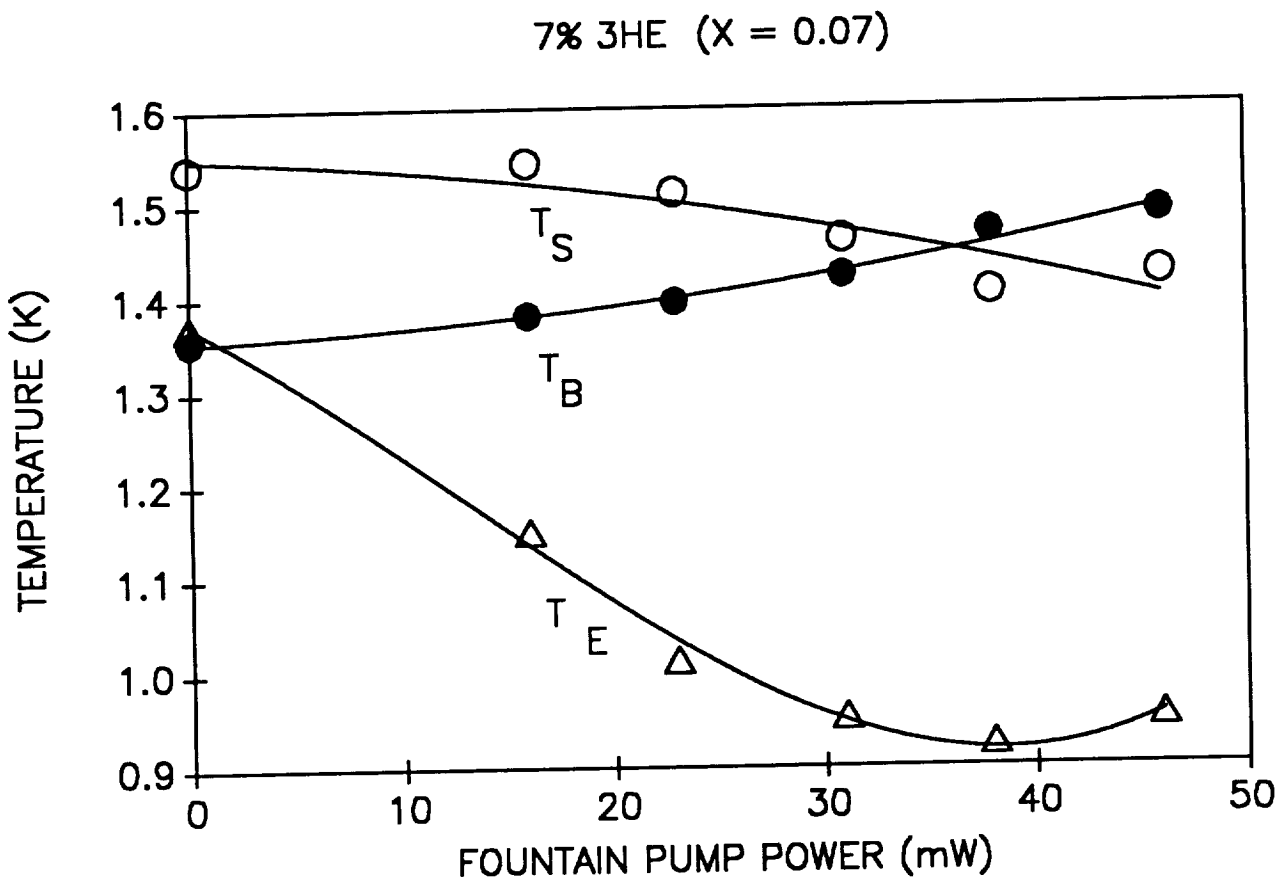


Figure 4.4 Temperatures of solution refrigerator stages as a function of power input to the fountain pump. This data is for a 7%  $^3\text{He}$  mixture test, and cooling of the cooling chamber is evident.

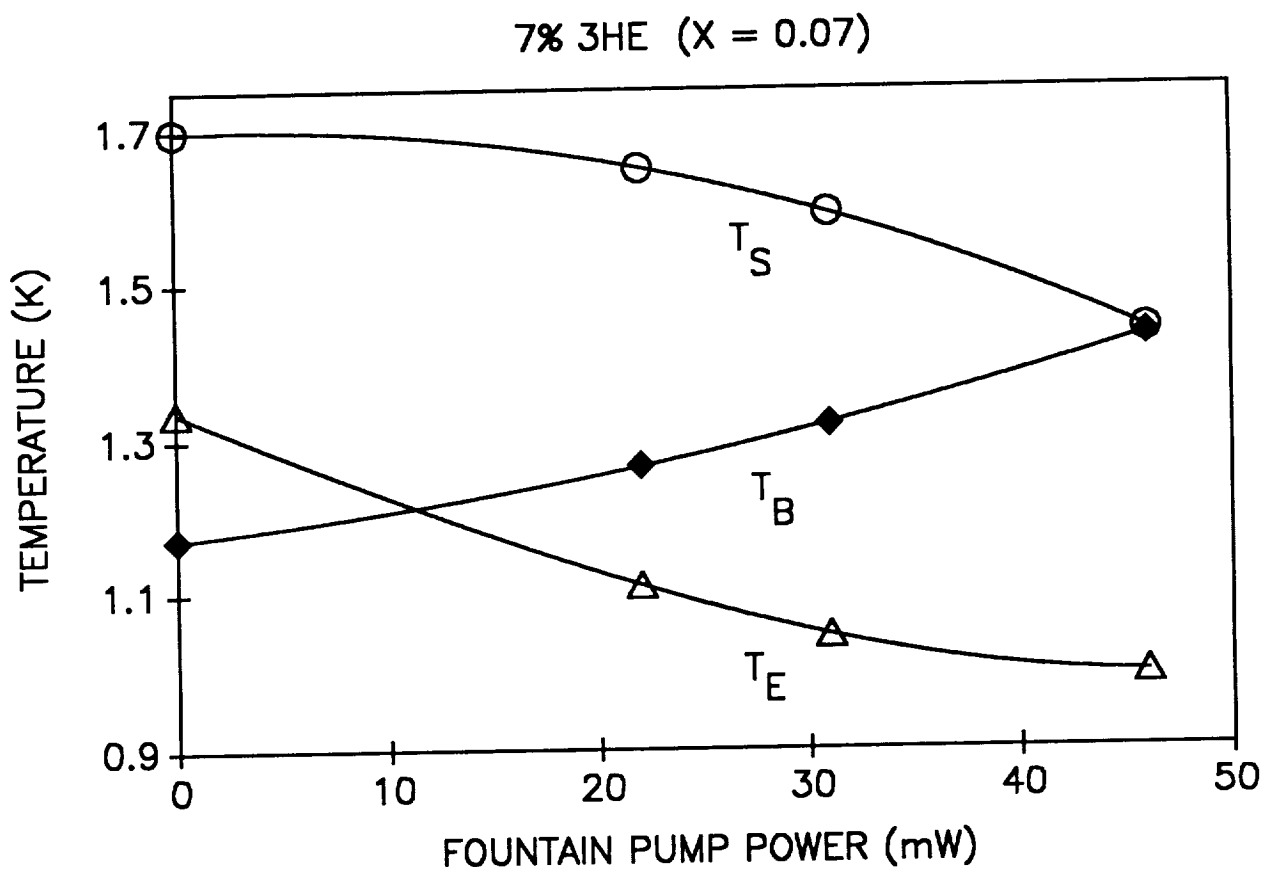


Figure 4.5 Temperatures of solution refrigerator stages as a function of fountain pump power for another 7%  $^3\text{He}$  test run.

14%  $^3\text{He}$  ( $X=0.14$ )

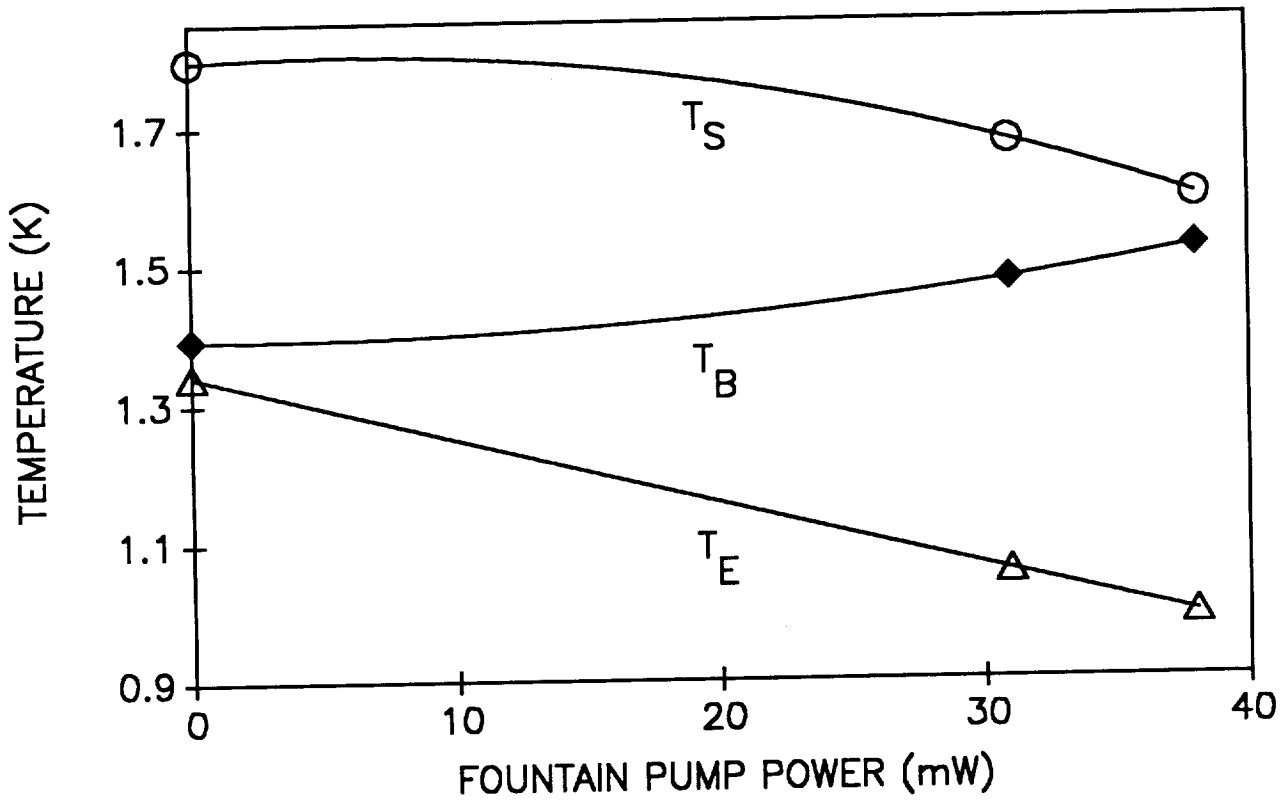


Figure 4.6 Temperatures of solution refrigeration stages as a function of fountain pump power for a test run with a  $^3\text{He}$  concentration of 14%.

2. That further study is needed to optimize the performance of the refrigeration effect and to discover the limits of attainable minimum temperatures.

#### 4.2 Dilution Cryocooler Phase Separators for $^3\text{He}$

Below 0.86 K,  $^3\text{He}$  -  $^4\text{He}$  mixtures undergo a phase transition that results in the creation of a  $^3\text{He}$  rich and a  $^4\text{He}$  rich phase. This transition is illustrated in the phase diagram presented in Figure 2.1. For the traditional earth-based dilution refrigerator to operate gravity is used to separate these two phases. The  $^3\text{He}$  rich phase floats on top of the  $^4\text{He}$  rich phase due to the mass density difference between the two isotopes. In space based applications, gravity will not be available to provide this needed phase separation.

A possible alternative method would be to utilize surface tension to separate the two phases. The surface tension of  $^4\text{He}$  is approximately 2.3 times as large as that of  $^3\text{He}$  at 0.5 K (Wilks, 1967, pg. 422). As the temperature goes toward absolute zero, the  $^3\text{He}$  rich phase approaches pure  $^3\text{He}$ , and the  $^4\text{He}$  rich phase decreases the concentration of  $^3\text{He}$  asymptotically to 6.4%  $^3\text{He}$ . Thus, separation of these two phases via their differences in surface tension should be achievable.

A promising method for achieving phase separation for both binary liquid and liquid-vapor systems involves using a porous metallic matrix to retain liquid in zero gravity. Such a trapping method has been successfully demonstrated by ACE, Inc., for pure  $^3\text{He}$  for the -1-g "inverted" configuration

(see NASA contract # NAS8-35254 Final Report, Long Lifetime, Spaceborne, Closed Cycle Cryocooler). In this application, the porous matrix or "sponge" was used to trap liquid in a liquid-vapor phase separator. This sponge corresponds to the still phase separator (SPS) discussed in Section 3.1.

Since  $^3\text{He}$  has the lowest surface tension of the two isotopes, successful trapping of  $^3\text{He}$  indicates that trapping should be achievable for either the  $^3\text{He}$  rich phase or the  $^4\text{He}$  rich phase. Since the  $^4\text{He}$  rich phase has the higher surface tension, it should cling more strongly to the porous material. The exact distribution between the  $^3\text{He}$  rich and  $^4\text{He}$  rich components within the pores is difficult to predict beyond the expected preferential attraction of  $^4\text{He}$  to the pore walls.

Phase separation between liquid and vapor must occur in the still of the dilution refrigerator. In the still, pumping is applied to the liquid mixture of  $^3\text{He}$ - $^4\text{He}$  to remove the  $^3\text{He}$  from the still for recirculation. Because of the high partial pressure of  $^3\text{He}$  at this temperature, nearly pure  $^3\text{He}$  is removed from the still. This  $^3\text{He}$  is circulated and introduced to the mixing chamber to provide the cooling action of the refrigerator. In zero gravity, the liquid must be prevented from escaping the system through the pumping lines. Furthermore, the method used to achieve liquid-vapor phase separation in the still must not interfere with the evaporation of the  $^3\text{He}$ . To explore the idea of using the porous matrix to trap the mixture in the still, experiments with  $^3\text{He}$ - $^4\text{He}$  mixtures as the working fluid were conducted using the -1-g test apparatus that was designed for the pure  $^3\text{He}$  experiment. What follows now is a description of this test apparatus, followed by a presentation of the mixture test data.

#### 4.2.1 Test Facility and Instrumentation

This section will describe the test facility that was used for the surface tension phase separation tests for both pure  $^3\text{He}$  and  $^3\text{He}$ - $^4\text{He}$  mixtures and for the solution refrigerator tests described in Section 4.1. A description will be given of the basic cryostat and dewar configuration, as well as the electronic instrumentation.

##### 4.2.1.1 Basic Cryostat

Figure 4.7 shows a schematic diagram of the basic cryostat configuration. The cryostat consisted of a 6 liter liquid helium pot which was suspended in a liquid nitrogen cooled Cryofab, Inc., model CSM-85 dewar. The space around the  $^4\text{He}$  pot was supported from the dewar top flange. A thin walled stainless steel pumping line served as a helium vapor exhaust port. A large capacity mechanical pumping system was used to pump the  $^4\text{He}$  pot down below the lambda transition to a minimum temperature of 1.4 K. At the bottom of the superfluid pot 4 mini-conflat connectors made access to the liquid helium in the pot possible. These connectors were welded to the pot and provide access to the liquid. The  $^4\text{He}$  pot had a removable copper radiation shield attached to it to protect the experimental space from radiation leaks due to the dewar's 77 K walls. Copper radiation baffle plates attached to the pumping line reduced radiation leaks to the pot from the room temperature dewar top flange.

All electrical leads were of 0.005" manganin wire, and were passed through the dewar top flange via room temperature ceramic feed-throughs.

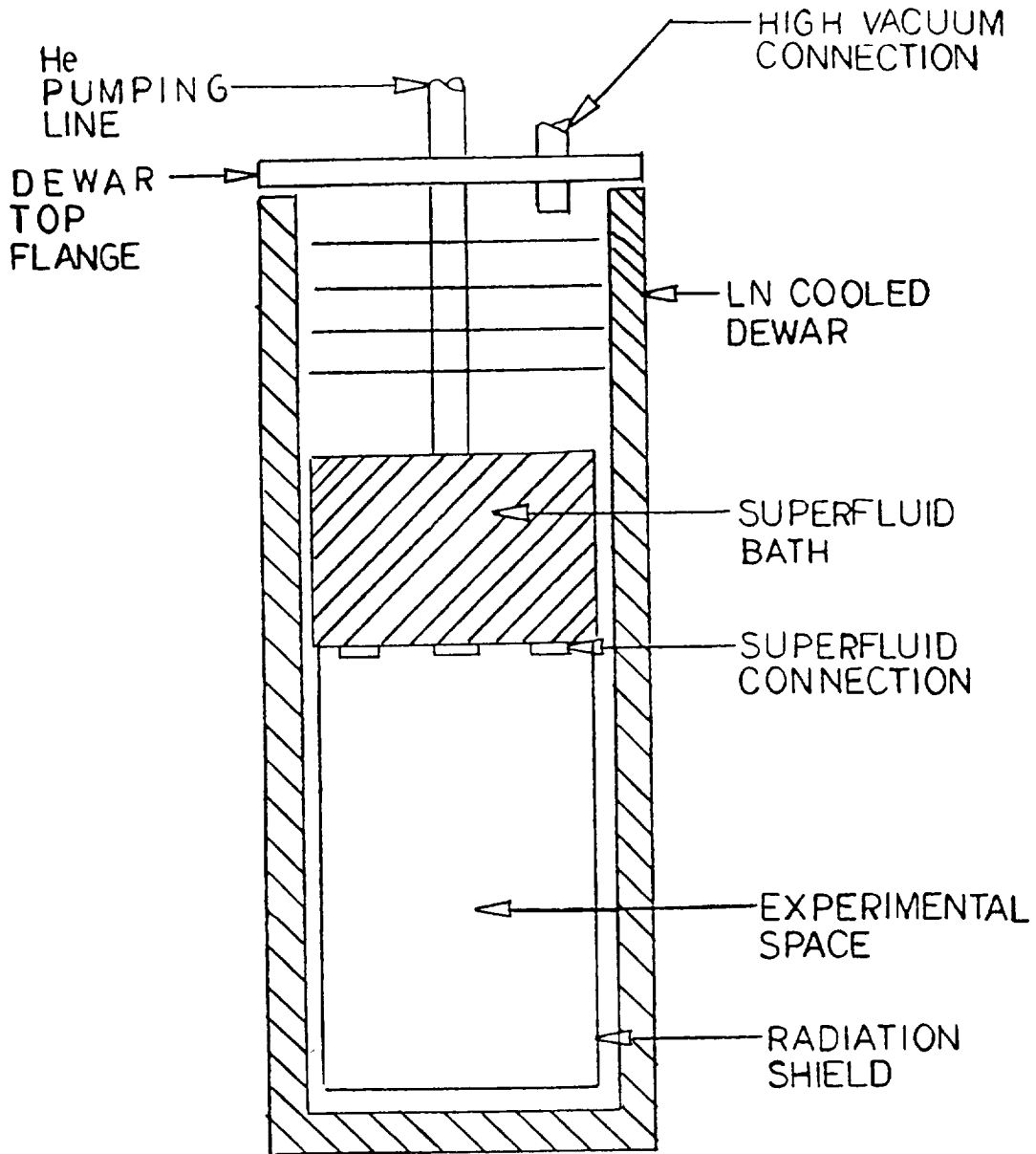


Figure 4.7 Schematic view of cryostat.

These leads were well heat sunk on the pumping line. This made use of the cold helium gas being removed from the system to minimize the heat leak to the pot via the leads. All capillaries and electrical leads were also well heat sunk to the superfluid pot itself.

When the cryostat radiation shield was in place, a thermal blanket consisting of 20 layers of NRC-2 superinsulation was wrapped around the pot and radiation shield to reduce the radiation leak to the pot from the 77 K dewar walls. The pot walls and radiation shield were also covered with a single layer of 3M No. 425 aluminum tape. Shu, Fast and Hart (1986) have shown that this combination of superinsulation and aluminum tape can significantly decrease heat leaks in cryogenic environments. With these precautions taken, the 6 liter helium pot could hold liquid for up to 24 hours.

The experimental space inside the copper radiation shield was a cylindrical chamber 7" in diameter and 11" in length. This space provided adequate room mounting the cryocooler and associated hardware.

One final feature of the cryostat design that facilitated modification of the apparatus was that the entire cryostat could be decoupled from support vacuum lines and electrical leads and be lifted from the dewar. Also, the dewar could be lowered as an optional method of obtaining access to the experimental space.

#### 4.2.1.2 Electronic Instrumentation

The heart of the electronic instrumentation system is a Biomagnetic Technologies Potentiometric Conductance Bridge (PCB). This bridge was used to measure the resistance of Cryocal Model CR100 and Lake Shore Cryotronics Model GR-200A-100 Germanium Thermometers. The PCB applies very small load currents (picowatts) to the resistors, and thus avoids self-heating in the thermometer elements.

Hastings ST Series mass flowmeters were used to measure the helium gas flow rates. These gauges give a 0-5 volt D.C. output that is linear with mass flow over their calibration range; also, these devices are pressure independent. Setra Pressure gauges were used to monitor pressures to the system. These gauges give out a 0-5 volt D.C. voltage that is linear with pressure.

#### 4.2.1.3 Pumping and Gas Handling System

In Figure 4.8 a schematic representation of the pumping system is given. In normal operation, the nearly pure  $^3\text{He}$  vapor was removed by the pump via the "out" port of the sponge chamber. The vapor then passed through a low impedance cold trap designed to prevent back streaming of pump oil into the chamber. The pumping speed is then regulated by the block and metering valves shown at the pump inlet. After passing through the Alcatel Model 2012H hermetically sealed pump, the  $^3\text{He}$  vapor passes through an oil mist eliminator, and into a charcoal cold trap. The output of the pump is then measured with a Hastings ST-10 mass flowmeter. The gas then enters the main body of the gas

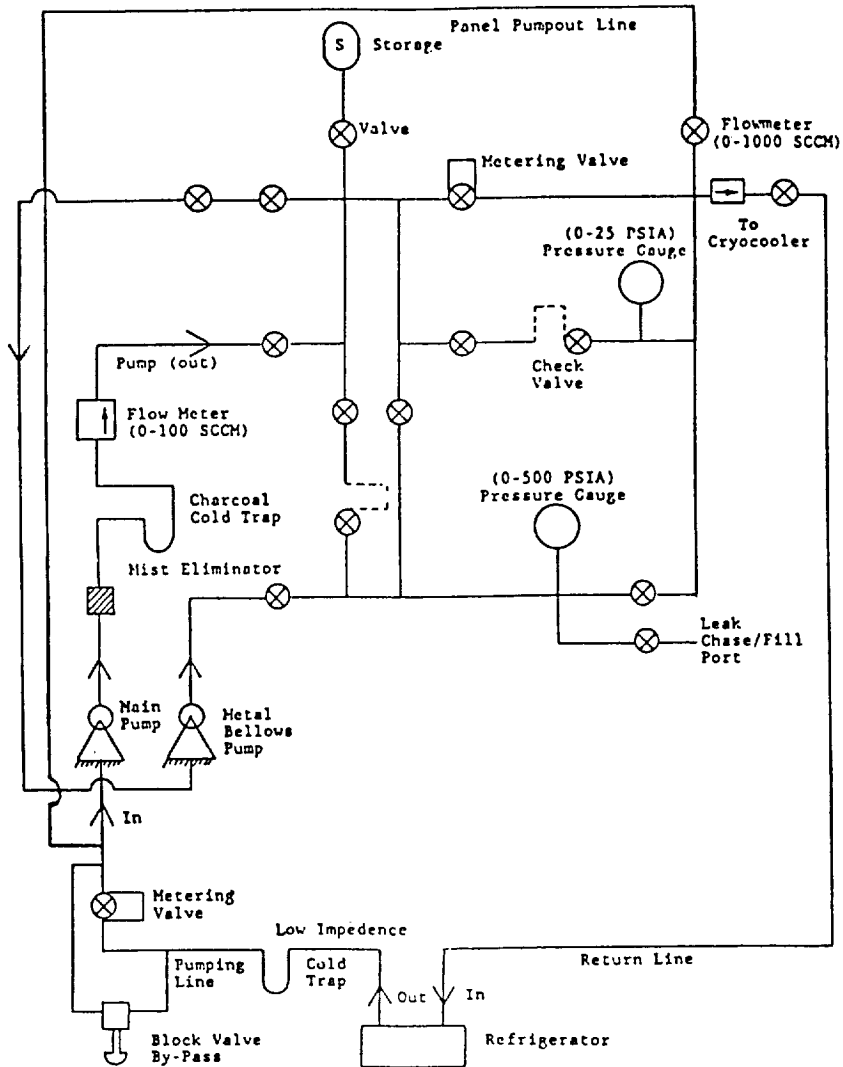


Figure 4.8  $^3\text{He}$ - $^4\text{He}$  mixture gas handling and pumping system.

panel, where pressure monitoring is done with Setra pressure gauges. After passing through a needle metering valve, the  $^3\text{He}$  enters a Hastings ST-10 mass flowmeter, and then back into the cryocooler via a return line. This is the typical configuration used during a continuous cycle run.

Other important features of the system are a 37.4 liter storage volume, where the  $^3\text{He}$ - $^4\text{He}$  sample is stored. A Metal Bellows hermetically sealed pump is also attached to the gas handling panel to facilitate removal of the gas from the storage can during its condensation into the trapping sponge. This gas handling and pumping system offered great flexibility in controlling the refrigeration cycle and in monitoring system parameters.

#### 4.2.2 Porous Metallic Sponge Assembly

Figure 4.9 shows a scale drawing of the trapping sponge, pumping line, and return capillary.  $^3\text{He}$ - $^4\text{He}$  mixtures entered the system via a 10 feet length of coiled stainless steel capillary that passed through one of the superfluid pot pumping lines. This scheme is designed to make use of the cold  $^4\text{He}$  vapor coming out of the superfluid pot to precool the incoming gas in the capillary. The capillary is coiled to increase its total surface area, thus improving heat transfer.

After it passed through the pumping line, the capillary entered the  $^4\text{He}$  bath, where it was well heat sunk to the bath temperature by contact with the high conductivity superfluid. In this region of the capillary, the incoming gas condensed to form liquid, which trickled down below the bath.



After passing through the bath, the liquid then dripped into the upper chamber, where it was trapped by the porous sponge. A 1/2" diameter thin walled stainless steel pumping line was used to remove the vapor from the cryocooler. This line was firmly heat sunk to the 1.5 K bath at  $^4\text{He}$  pot level, and had bends to eliminate radiation leaks from room temperature. Finally, the 1.5 K radiation shield described in the cryostat section surrounded the entire sponge assembly to block radiation leaks from the 77 K walls of the nitrogen dewar after moving through the bath. Then the fluid collected in the chamber above the sponge. This fluid was drawn into the porous silver trapping sponge by capillary action. Evaporation then occurred at the lower face of the sponge.

If a loss of trapping occurred, some or all of the fluid above the sponge would fall into the lower chamber. This chamber was thermally isolated from the liquid reservoir held above the sponge by the low thermal conductivity of its stainless steel walls. The lower chamber and U-shaped tube below the chamber were all made of copper and were isothermal. Thus, the device is schematically represented as previously shown in Figure 4.10. Presence of liquid in either the upper or lower chamber is determined by applying heat loads to heaters shown and measuring the temperatures of the chambers with resistive thermometers.

#### 4.2.3 Porous Trapping Plug

The porous sponge used in the device was prepared in the following fashion. First, 400 A silver powder was compressed to 3000 psi with a hydraulic press. The powder was contained in a stainless steel jig and

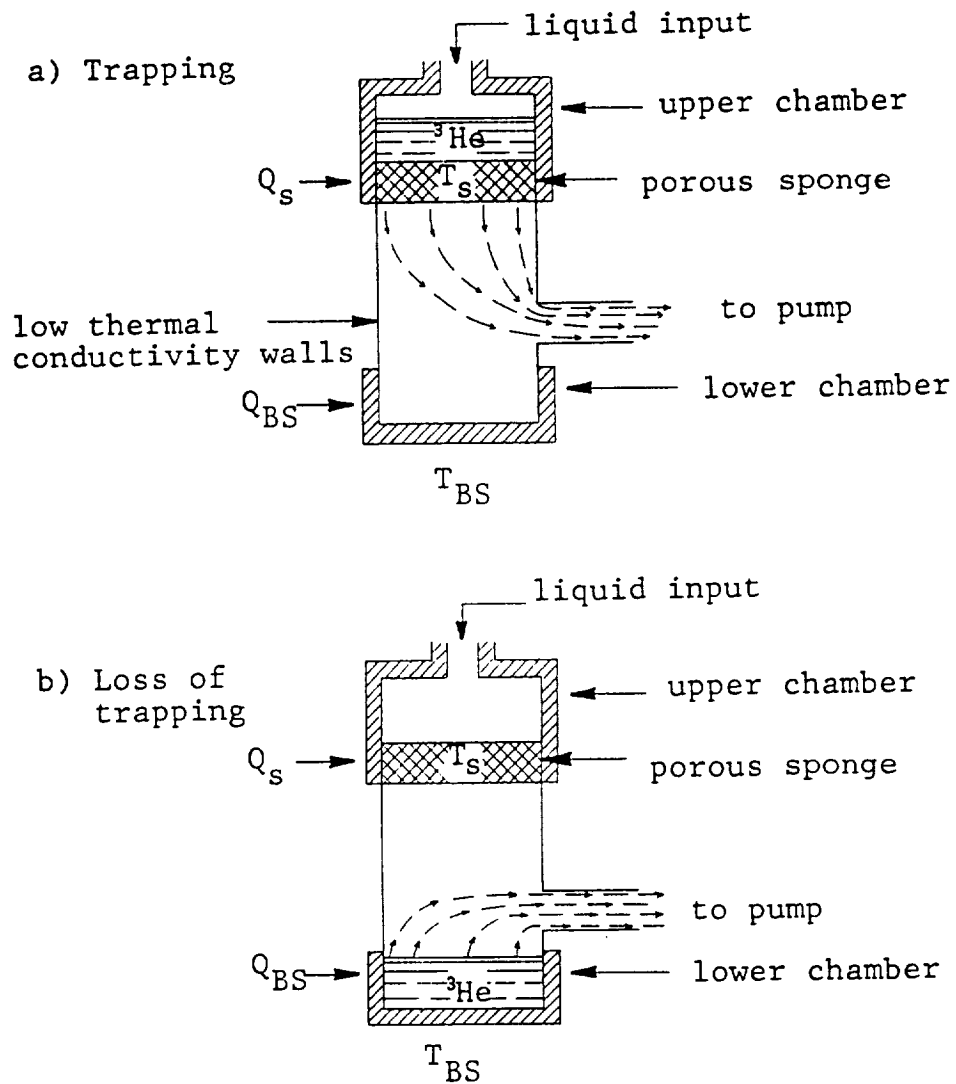


Figure 4.10 Schematic view of trapping sponge holder  
 (a) retention of liquid against gravity (-1-g) is shown.  
 (b) depicts the situation occurring with a loss of liquid trapping.

compressed with a stainless steel piston. This jig produced compressed cylindrical silver plugs approximately 1/4" in thickness and 3/4" in diameter. These plugs were then placed in a vacuum oven, which was evacuated and then backfilled with helium gas. The plug was then heated to 200 C in forty minutes and kept at 200 C for 1-1/2 hours. At this time, the oven was turned off and allowed to cool slowly to room temperature. This method was similar to that used by Franco (1984), and resulted in plugs with a packing fraction of approximately 50%. The resulting plug was then epoxyed into an OFHC copper plug holder with Stycast 2850GT epoxy.

#### 4.2.4 Results and Discussion

In this section, the results of the -1-g trapping tests of  $^3\text{He}$ - $^4\text{He}$  mixtures in the porous silver sponge will be discussed. After the data is presented, conclusions drawn from the tests will be given.

##### 4.2.4.1 Preliminary Test: Pure $^3\text{He}$

To verify that the trapping plug apparatus was working properly, tests were conducted with pure  $^3\text{He}$ . These results agreed well with previous tests that demonstrated the sponge's ability to trap  $^3\text{He}$  against gravity (See NASA Contract No. NAS8-35254). After condensing liquid  $^3\text{He}$  above the trapping sponge, pumping from below the sponge was applied, and cooling occurred until a steady equilibrium was reached at  $T \approx 0.6$  K. This temperature was maintained until the  $^3\text{He}$  was completely exhausted from the sponge. The mass flow into and out of the sponge assembly was measured, along with the pressure above the sponge and the temperature of both the sponge ( $T_S$ ) and the chamber

below the sponge ( $T_{BS}$ ). Loss of trapping could be detected by observing the drop of  $T_{BS}$  below  $T_S$  and by applying heat to each station. If liquid was present in either station, the mass flow was seen to follow the latent heat relation

$$Q = mL \tag{4.2}$$

where  $Q$  is the heat input,  $m$  is the mass flow out, and  $L$  is the latent heat of vaporization. Using this technique, loss of liquid trapping or film flow through the plug could be easily detected.

#### 4.2.4.2 Trapping Plug Results for $^3\text{He}$ - $^4\text{He}$ Mixtures

In Figure 4.11, the temperature of the sponge station and the temperature of the station below the sponge are shown as a function of time for a test run with molar concentration  $X=0.5$ . Here we define the molar concentration  $x$  as

$$x = N_3 / (N_3 + N_4)$$

where  $N_3$  is the number of moles of  $^3\text{He}$  in the sample and  $N_4$  is the number of moles of  $^4\text{He}$ . First, the sample was admitted above the sponge. Care was taken to avoid fractionation of the mixture so that the concentration of the sample would be well defined. After pumping was applied below the sponge the system rapidly cooled to  $T \approx 0.6$  K and stayed constant in temperature for approximately one hour. During this time, nearly pure  $^3\text{He}$  was being pumped from the system due to the high partial pressure of the  $^3\text{He}$  in the mixture.

X=0.5  
NO HEATING TO EITHER STATION

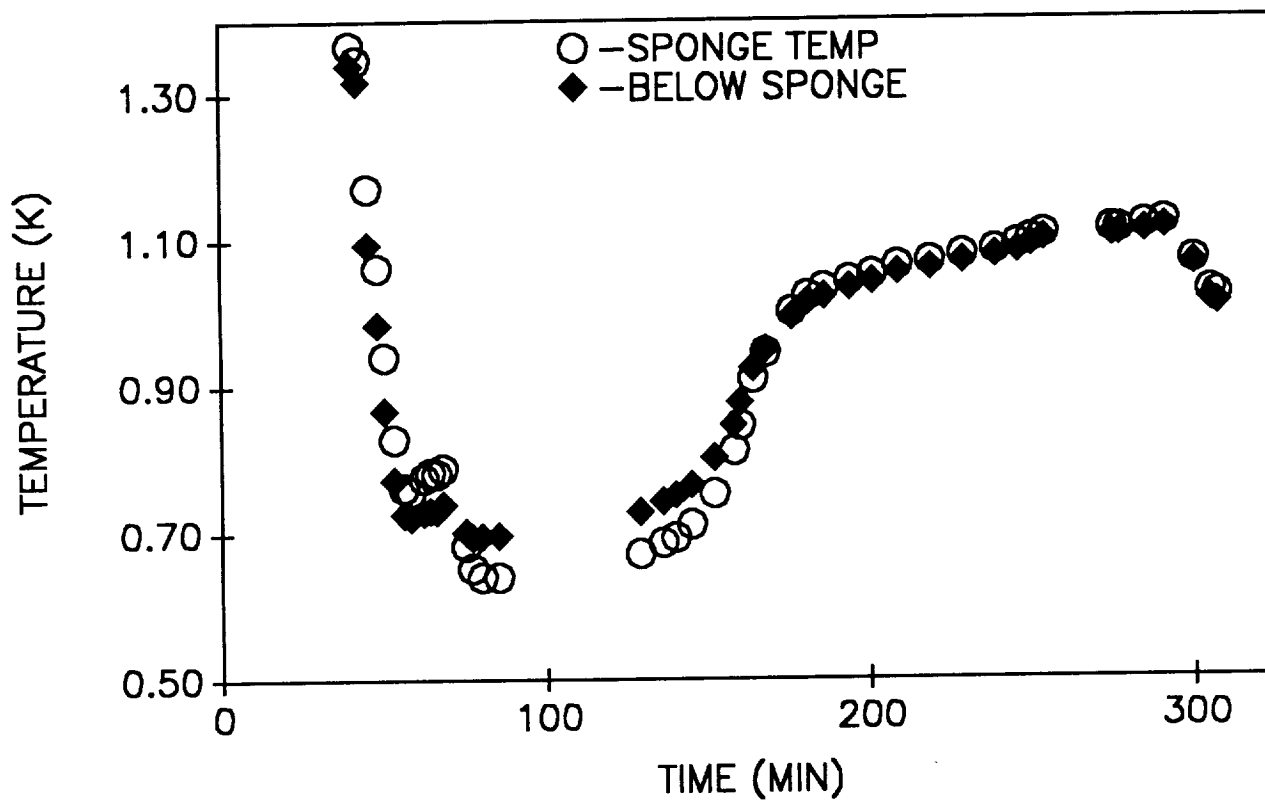


Figure 4.11 Temperature of sponge and below the sponge versus time for a 50%  $^3\text{He}$ - $^4\text{He}$  mixture run.

It should be noted that the same minimum temperature was reached during this part of the run as was achieved using pure  $^3\text{He}$  as the working fluid. This is because the  $^4\text{He}$  acts like a mechanical vacuum due to its low partial pressure, and does not appear to interact with the mechanism of transport of  $^3\text{He}$  through the sponge. During this phase, the sponge temperature is somewhat lower than the temperature below the sponge, indicating that liquid had not broken through. Liquid trapping was confirmed using the mass flow test described previously.

At  $T \approx 160$  minutes, a sharp rise begins in the temperature of both the sponge and below the sponge. This temperature rise is due to the exhaustion of the  $^3\text{He}$  from the liquid mixture, leaving only  $^4\text{He}$  trapped by the sponge. Since the vapor pressure of  $^4\text{He}$  is much less than that of  $^3\text{He}$  at 0.6 K, the system temperature rises due to the insufficient cooling power of the  $^4\text{He}$ . Temperature equilibrium is again reached at  $T \approx 1.0$  K, which is the often observed practical minimum cooling temperature of  $^4\text{He}$  evaporative coolers. The slight drop in temperature at the end of the run is not well understood, but is thought to be due to a thin layer of  $^3\text{He}$  which phase separated when the mixture was colder, and was excluded from the plug due to the surface tension of the  $^4\text{He}$  rich phase. It should be noted that after the  $^3\text{He}$  is exhausted from the system, the temperature of the station below the sponge decreases to a lower value than the sponge. Also, heat tests then reveal the presence of liquid in the station below the sponge. We believe that superfluid film flow accounts for these effects. When  $^3\text{He}$  is present, the thermal conductivity of the liquid mixture is greatly reduced, and the temperature gradient across the sponge is relatively large. Thus, the sponge acts like a porous plug phase separator (See Hendricks and Karr, 1986) when  $^3\text{He}$  is present, and all liquid

is retained by the sponge. It is important that no film flow is seen when  $^3\text{He}$  is present because downstream film flow in the still of dilution refrigerator serves to introduce heat leaks into the system and decreases the rate of  $^3\text{He}$  being pumped from the still.

In Figure 4.12, the pressure above the sponge is shown as a function of time for the same run illustrated in Figure 4.11. After initially pumping down the system, the pressure reaches a minimum value and stays at that minimum throughout the duration of the run. This minimum pressure is somewhat higher than the vapor pressure at  $T_S$  due to the pressure drop across the sponge. The fact that the equilibrium temperature rises when the pressure remains constant is another direct indication that  $^3\text{He}$  is pumped away from the mixture first.

Figure 4.13 shows the results from another test of the  $X=0.5$  mixture. Here, the general performance is the same as in Figure 4.11, but a lower minimum temperature is reached. This graph is on a shorter time scale than Figure 4.11; equilibrium at a higher temperature is not shown. Figure 4.14 shows the pressure above the sponge as a function of time for this test run.

Additional tests were conducted with a mixture concentration of 75%  $^3\text{He}$  ( $X=0.75$ ). Very similar results were obtained with this concentration to the data from the  $X=0.5$  test runs. The only difference in the results was that the portion of the run with  $T \approx 0.6$  K lasted much longer, since more  $^3\text{He}$  was available. These results substantiate the observation that all the  $^3\text{He}$  is preferentially removed from the sponge before the  $^4\text{He}$  in the mixture is expelled.

X=0.5  
NO HEATING TO EITHER STATION

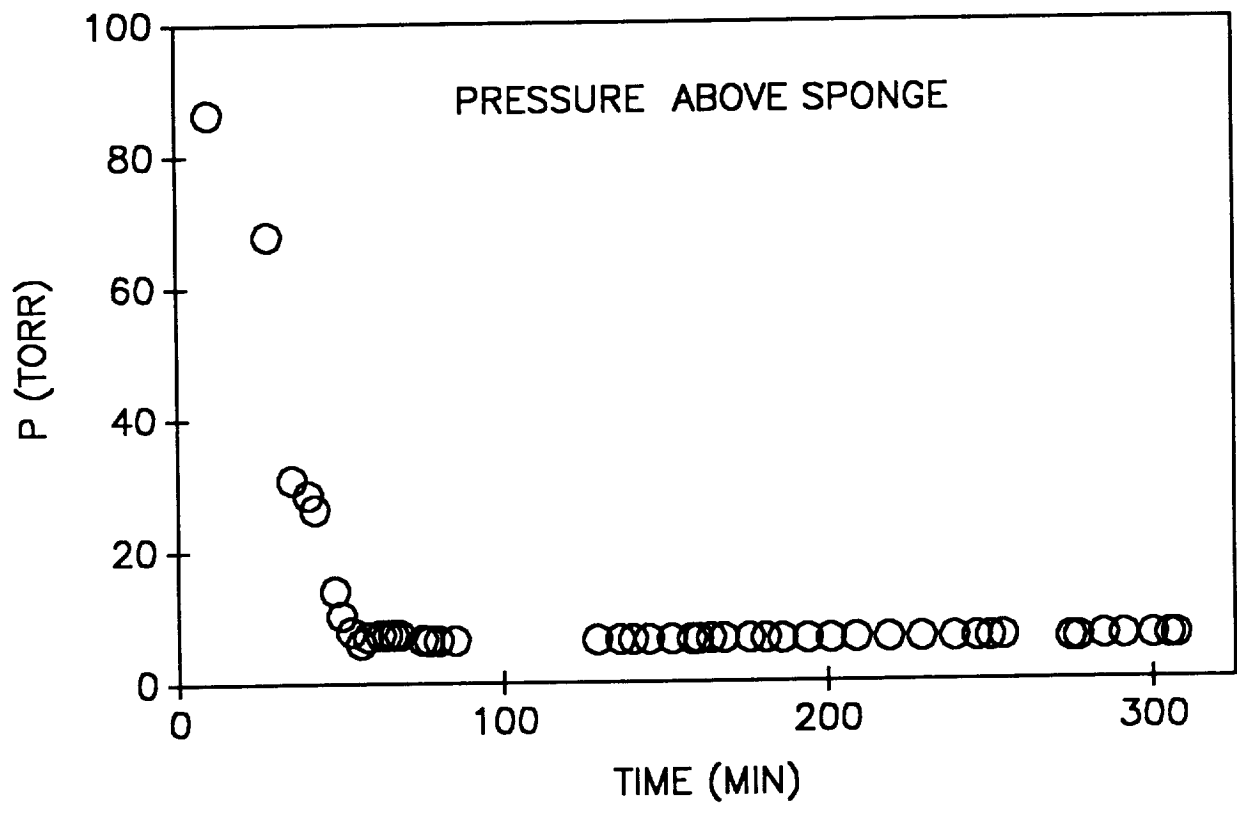


Figure 4.12 Pressure above the sponge as a function of time for the 50% <sup>3</sup>He-<sup>4</sup>He mixture test shown in Figure 4.11.

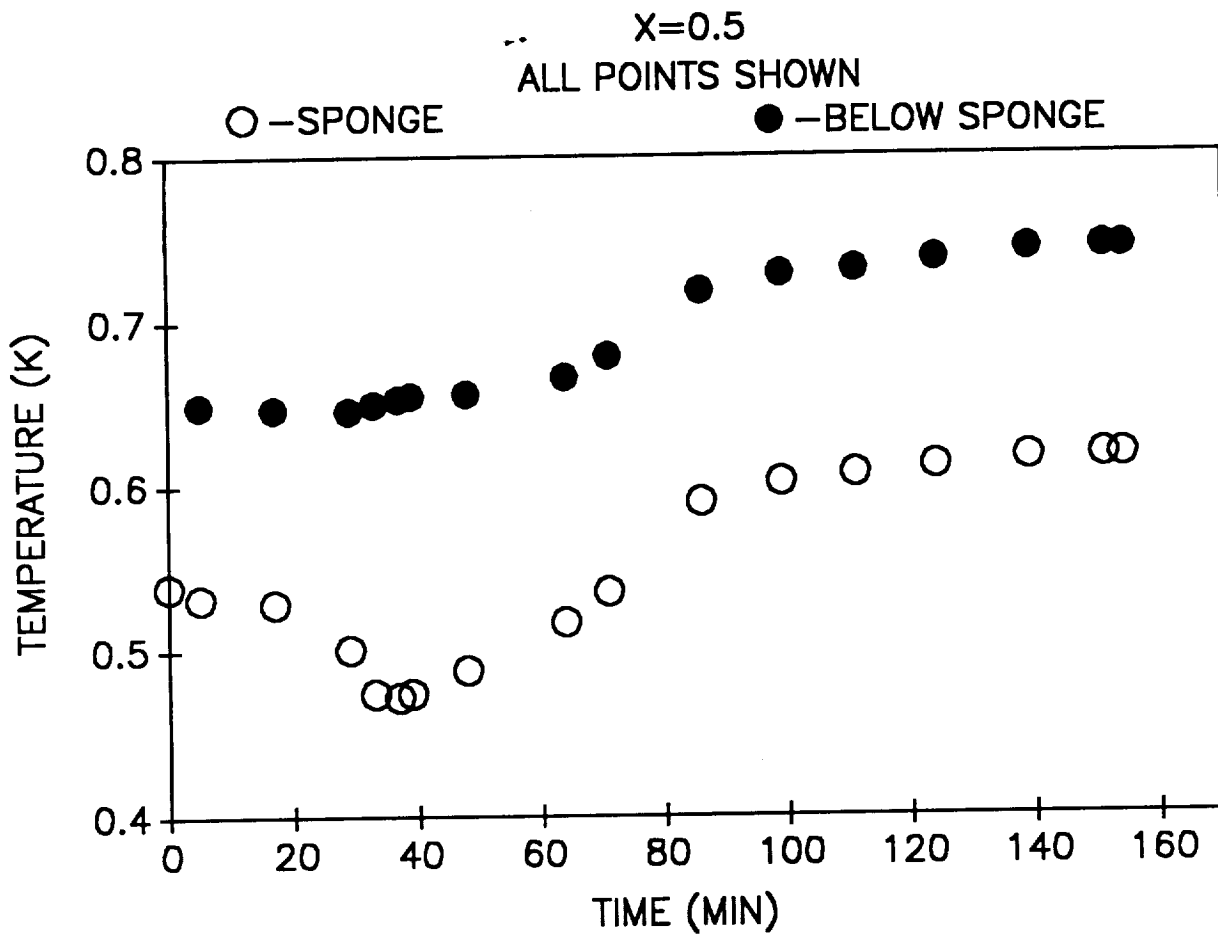


Figure 4.13 Temperature vs. time for another 50%  $^3\text{He}$ - $^4\text{He}$  mixture test run.

X=0.5  
NO HEATING

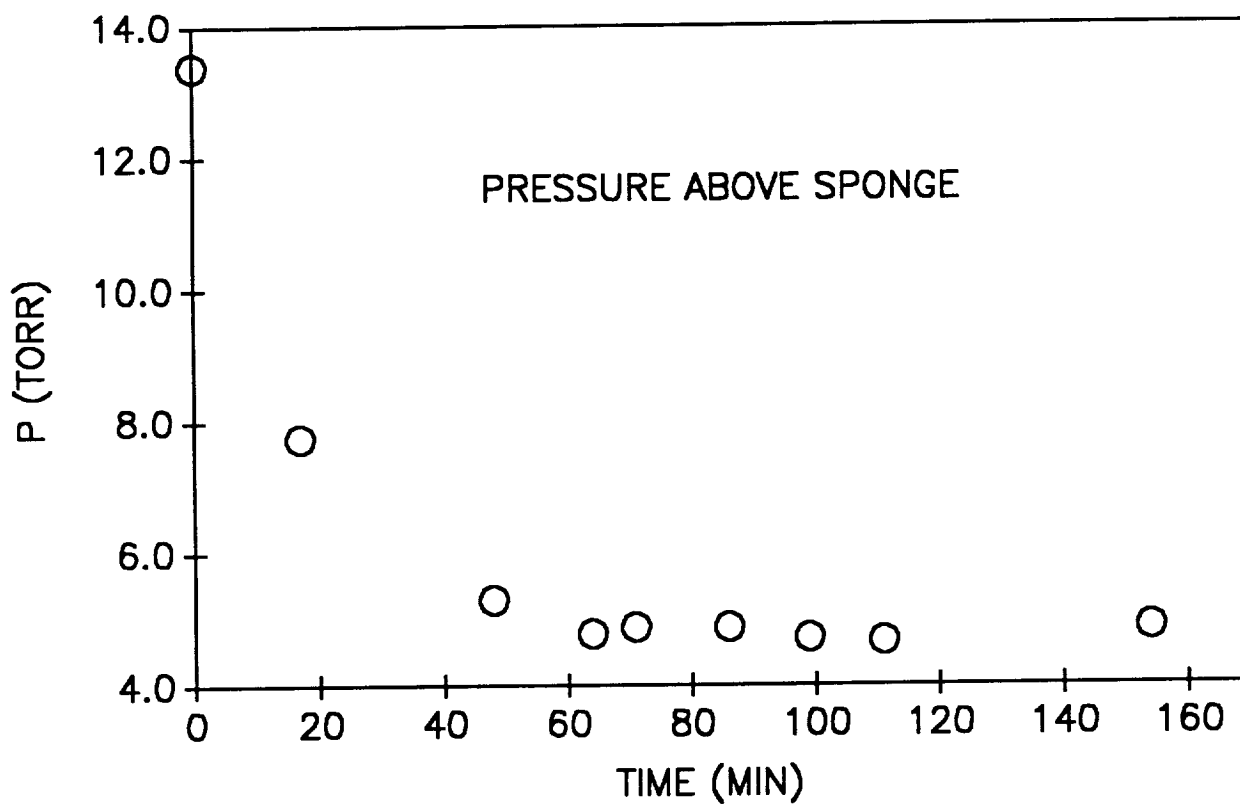


Figure 4.14 Pressure above the sponge versus time for the run shown in Figure 4.13.

The previous results were obtained by filling the chamber above the sponge, shutting off the input mass flow, and then pumping on the sponge from below. In an actual dilution cryocooler application, continuous circulation of  $^3\text{He}$  through the system is required to provide constant operation. To test the feasibility of continuous operation, the trapping sponge was filled with mixture, and pumping started from below while the output flow from the pump was brought to room temperature, sent back into the cryostat to recondense, and fed back into the chamber on top of the sponge. This arrangement led to a steady minimum temperature of the sponge that could be maintained indefinitely, since the  $^3\text{He}$  was not depleted. In Figure 4.15, typical results for such a continuous cycle run are shown. Equilibrium temperatures for each station are plotted as a function of heater power applied to that station for both the sponge and below the sponge. The rapid increase in the temperature of the station below the sponge for a given input heat flux is proof that loss of liquid trapping has not occurred, and that the liquid mixture is being held above the sponge against gravity.

#### 4.2.5 Conclusions

The following conclusions have been reached based on the results of the surface tension phase control test program for  $^3\text{He}$ - $^4\text{He}$  mixtures:

1. That a highly conductive, porous metallic matrix can be used to retain liquid mixtures of  $^3\text{He}$ - $^4\text{He}$  against the pull of gravity (-1-g) provided that the  $^3\text{He}$  concentration of the mixture is not severely depressed.
2. The above result implies that the porous metallic matrix method can be used to achieve liquid-vapor phase separation in zero gravity, since

X=0.5  
EACH STATION HEATED SEPARATELY  
CONTINUOUS MODE

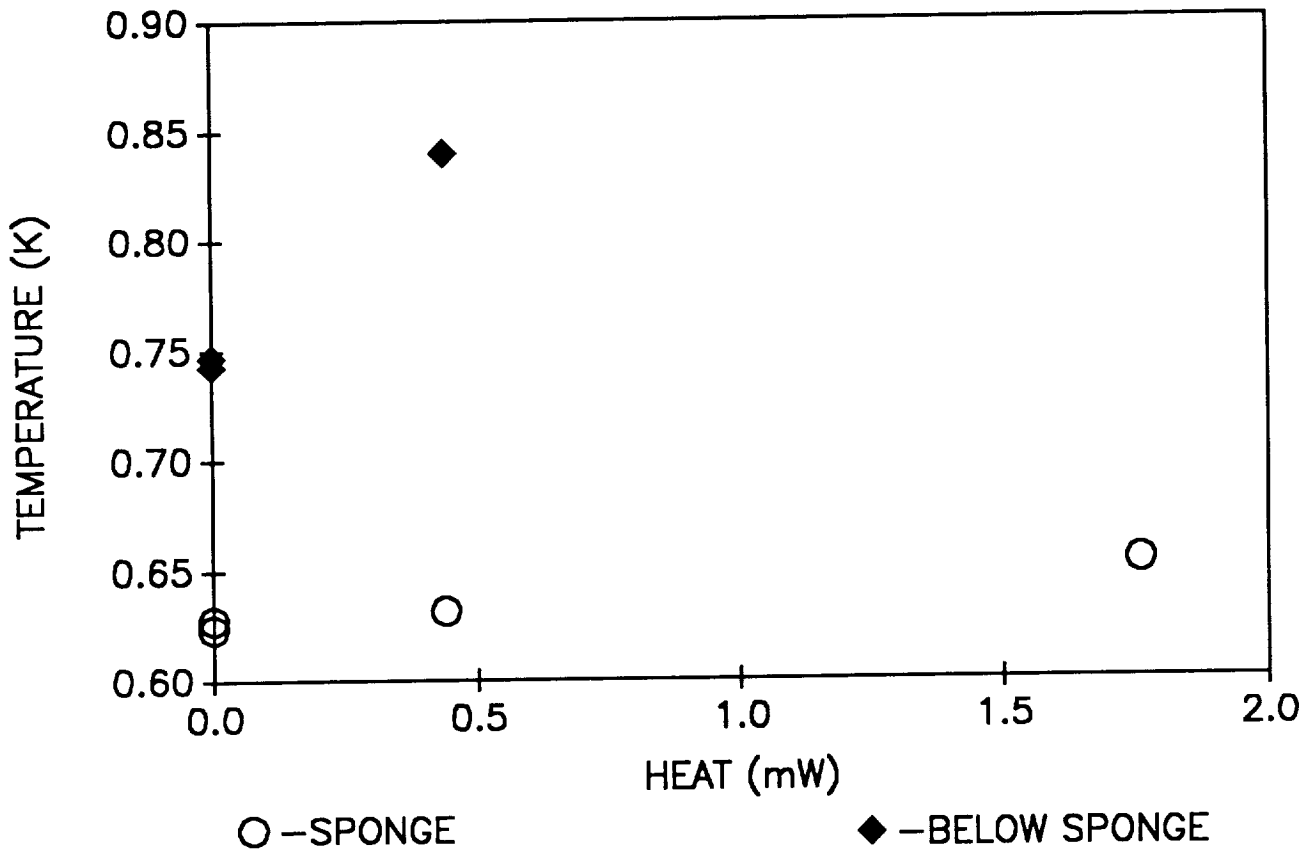


Figure 4.15 Temperature versus heat input to each station when the sponge is running in continuous mode (mass flux in = mass flux out).

zero-g operation is a less strenuous requirement than the inverted (-1-g) configuration.

3. That the above mentioned phase separation technique was successfully tested in a continuous operation mode, where  $^3\text{He}$  was reintroduced as liquid above the porous sponge at the same rate  $^3\text{He}$  vapor was drawn from the sponge by pumping from below.
4. The results listed above demonstrate the feasibility of operating the "still" portion of a  $^3\text{He}$  circulation dilution cryocooler in zero gravity.
5. That the  $^3\text{He}$  rich -  $^4\text{He}$  rich phase separation that must occur in the mixing chamber of the dilution cryocooler can be accomplished using porous matrix phase separation techniques. It should be noted that direct testing of this concept was not carried out, but the differences in the surface tension of the two phases indicates that it should be possible.
6. That a  $^3\text{He}$  circulation dilution refrigerator that operates in zero gravity is a viable technology that can be successfully achieved.

#### 4.3 The ACE, Inc. Cycle

Testing of this cycle was done using the rig illustrated in Figure 4-16. In this configuration, the cycle is run in a minus one-g situation. He II flows through superleak 1 to dilution chamber 1, up the counterflow tube to dilution chamber 2, and then returns to the  $^4\text{He}$  pot through superleak 2. The superleaks are 12" long by .092" O.D. and are packed with jewelers rouge powder. The counterflow tube is .125" O.D. and is 10" long. It is spiraled three times around a 2" rod to minimize the vertical separation between the

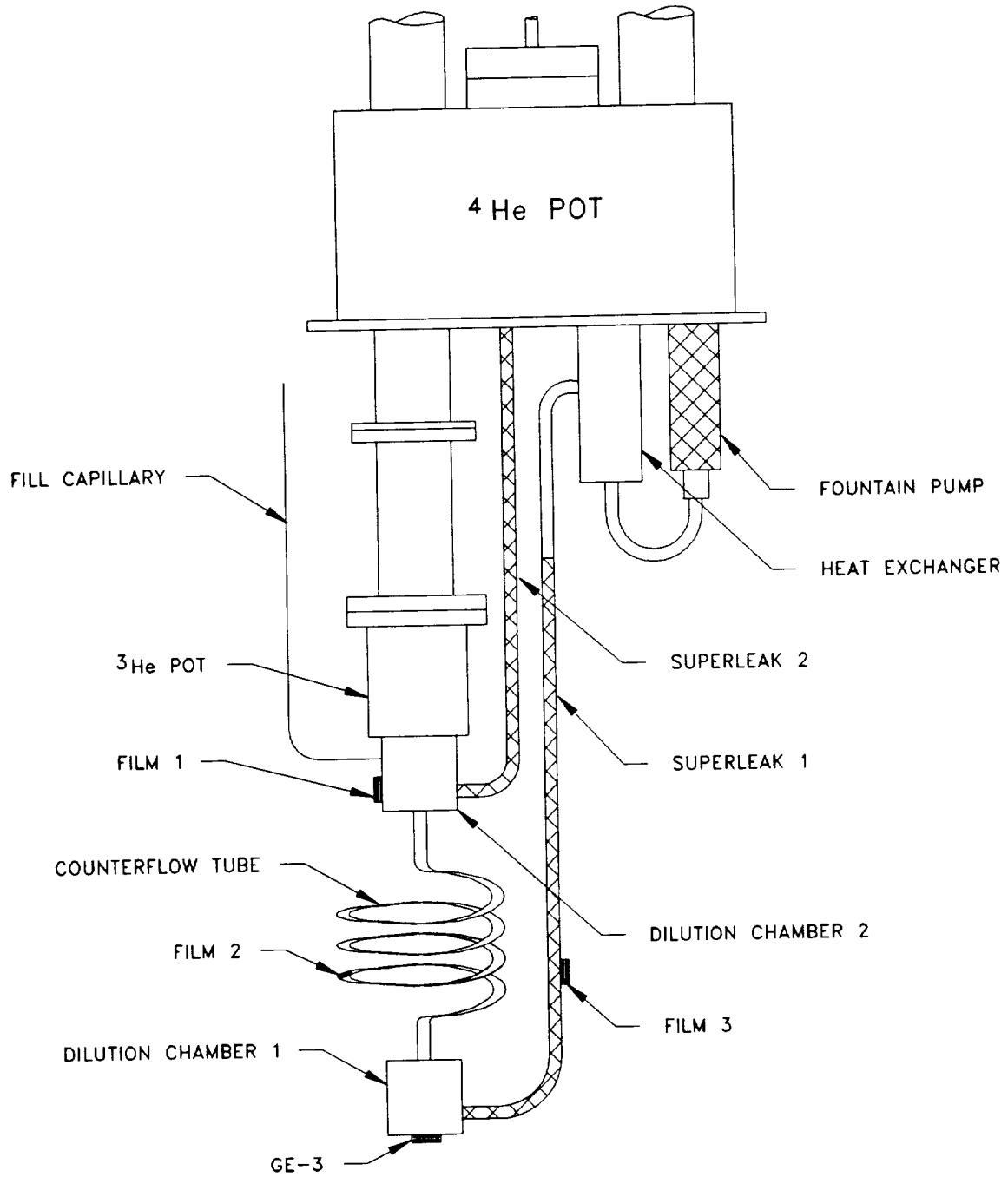


Figure 4.16 Test Cell Schematic

two dilution chambers, which is about 4". The  $^3\text{He}$  fill capillary is .020" I.D. with a .018" O.D. wire inside, to minimize fluid thermal conduction from the  $^4\text{He}$  pot to the test cell. All electrical leads to the thermometers are anchored to the  $^4\text{He}$  pot and the  $^3\text{He}$  pot. A heat exchanger, between the fountain pump and superleak 1, dumps the heat load from the fountain pump back to the  $^4\text{He}$  pot. The overall bath temperature does increase as a result of the heat load from the fountain pump.

#### 4.3.1 1 K Testing

The rig was tested at 1 K and at 0.5 K. At 1 K, this system is just the solution refrigerator, discussed in section 4.1. With the configuration shown in Figure 4.16, a thermal oscillation in dilution chamber 1 was observed that had not been seen with the previously described rig. These oscillations are shown in Figure 4.17 which displays the response of thermometer Ge-3 on chamber 1. They are characterized by a rapid cooling followed by a relatively slow heating. The frequency and amplitude of these oscillations varied. This effect was only seen when  $^3\text{He}$  was present in the test cell. During this run, the fountain pump power was steadily increased. Only when the power level reached 8.6 mW did the oscillations occur. After 20 minutes of observation the fountain pump was turned off and the oscillations disappeared.

The oscillations indicate there is some hydrodynamic instability associated with flowing He II through a tube containing a solution of  $^3\text{He}$ . Since there is no phase separation at this temperature and  $^3\text{He}$  concentration, a convective instability due to density differences is unlikely. It appears that  $^3\text{He}$  is being flushed to the opposite end of the counterflow tube where it

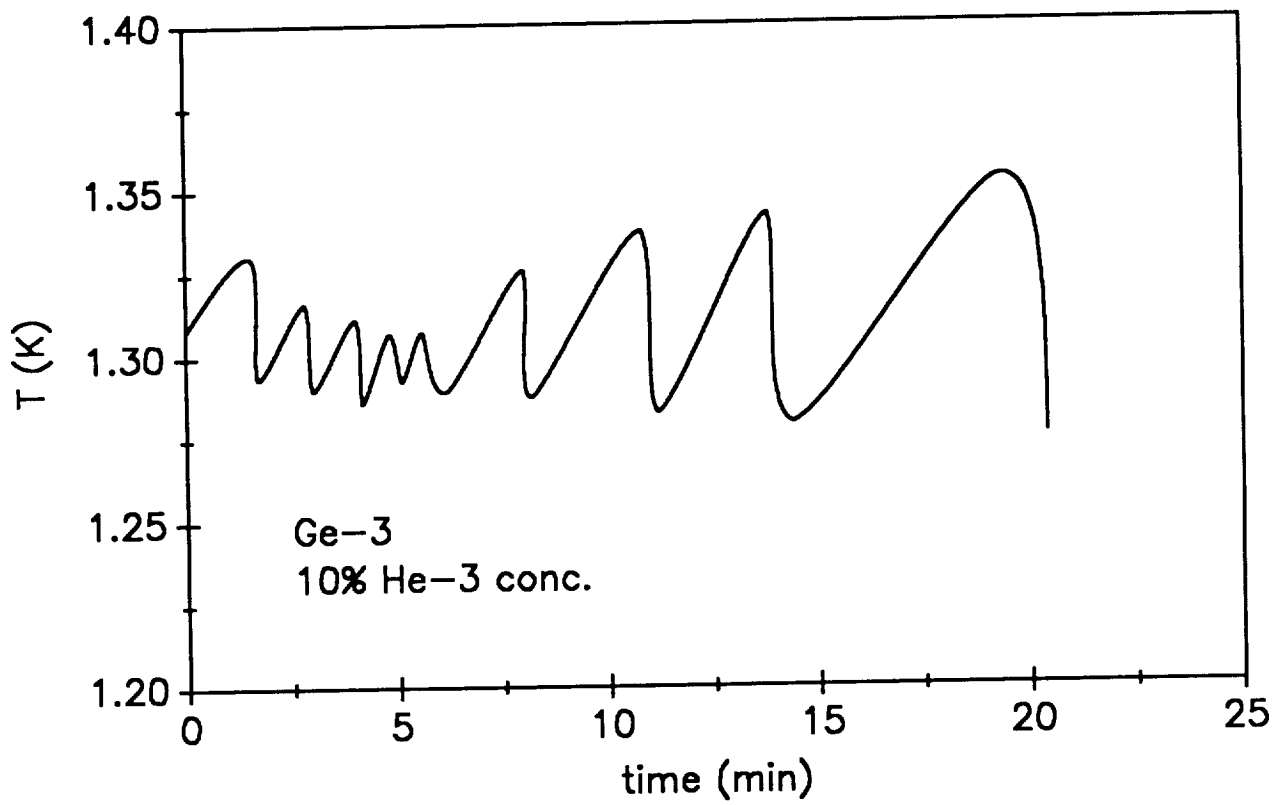


Figure 4.17 Temperature versus Time Behavior for Ge-3 thermometer. Fountain pump power is 8.6 mW.

collects. Periodically, the  $^3\text{He}$  is then redistributed through the counterflow tube, resulting in a cooling effect as for the solution refrigerator.

The principle difference between the two testing configurations lies in the counterflow tube. The first test setup uses a 0.5 mm I.D. tube and the second test setup uses a 3.5 mm I.D. tube. The surface area to volume ratios of the two tubes are  $8 \text{ mm}^{-1}$  and  $1.1 \text{ mm}^{-1}$ , respectively. Any significant fluid wall interaction could result in different flow characteristics between the two testing arrangements. At this point, the reason for the different thermal behavior is unknown.

#### 4.3.2 0.5 K Testing

The previous test cell arrangement is not suitable for testing the ACE, Inc. cycle. A second test cell, shown schematically in Figure 4.18, was constructed. Dilution chamber 1, the entrance side, is now above the exit side, dilution chamber 2. The  $^3\text{He}$  rich solution would float at the top of the test cell.  $^3\text{He}$  would dissolve into the flowing  $^4\text{He}$  by diffusing across the phase boundary. A cooling effect would then occur in chamber 1.

A number of important experimental aspects have affected the low temperature (below 1 K) testing of the ACE, Inc. cycle. Early testing at a temperature of 0.4 K with no  $^3\text{He}$  present in the test cell showed that a temperature difference of 0.1 K existed between the two dilution chambers, with dilution chamber 1 being warmer. In order to improve the thermal isolation of the test cell, capillaries of 0.1 mm I.D. and 300 mm length were inserted on the superleaks and fill capillary between the  $^4\text{He}$  pot and the test

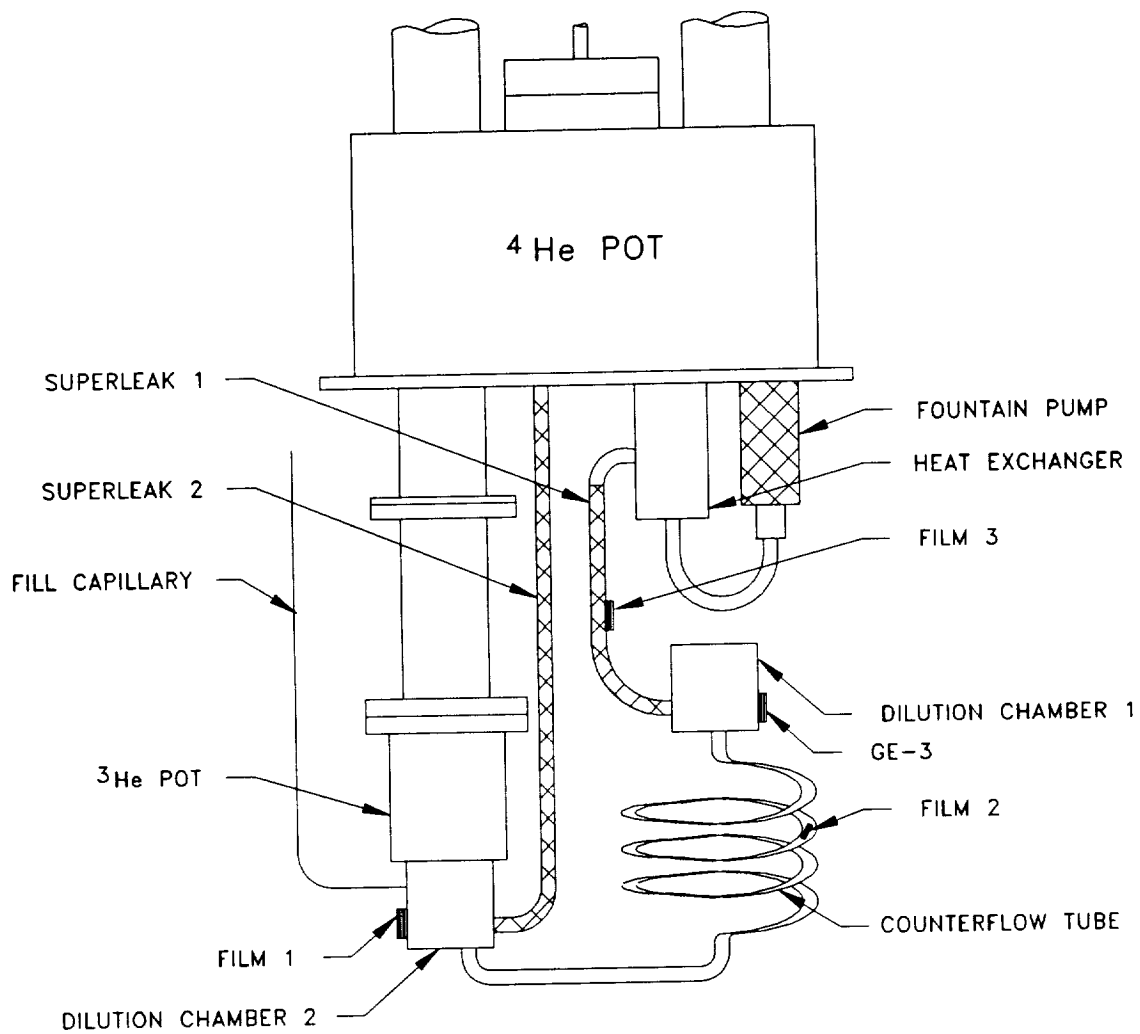


Figure 4.18 Dilution Test Cell Schematic for testing of the ACE, Inc. cycle.

cell. As a result, the ends of the superleaks are no longer thermally anchored to the  $^4\text{He}$  pot.

When  $^3\text{He}$  is loaded into the test cell, its temperature increases. Generally, the test cell temperature, measured by thermometer Ge-3, rises about 0.3 K. The test cell is then cooled off by pumping on the  $^3\text{He}$  pot.  $^3\text{He}$ - $^4\text{He}$  mixtures have higher specific heats and lower thermal conductivities than pure  $^4\text{He}$ . The cooldown rate of the first dilution chamber is about 60 mK/hr. Thus, to cool the test cell to 0.5 K from 1.3 K would take over 13 hours. We attempted to increase the cooldown rate by turning on the fountain pump at a very low power level, .01 mW, in order to flow He II through the test cell. Instead, the cooling rate decreased. An increase in the fountain pump power to .034 mW resulted in dilution chamber 1 warming up. Thermometers film 2 and film 3 also showed warming trends, at a slower rate than Ge-3. Higher fountain pump powers resulted in still further heating.

The theory of the ACE, Inc. cycle was developed during the time the experimental testing was taking place. This theory has illuminated aspects of the hardware design that affect the performance of the ACE, Inc. cycle. As the overall cooling power is only a few microwatts, minute sources of heat inputs can significantly degrade the operation of the cycle.

As discussed previously, the current test cell arrangement has the superleaks connected to the  $^4\text{He}$  pot through 0.1 mm I.D. capillaries. Since the superleaks act as entropy filters, the specific entropy at the superleak entrance increases while He II is flowing. This effect results in a heat load on the test cell.

Additionally, dilution chamber 1 is cooled by conduction through the counterflow tube. It may be necessary to have the  $^3\text{He}$  rich phase in this chamber before  $^4\text{He}$  is circulated in order to have a cooling effect. The mass flow of  $^4\text{He}$  may be carrying the  $^3\text{He}$  downstream to the exit chamber, dilution chamber 2. If this is the case, then the entrance chamber could then be considered to be acting as a vortex cooler, which does not cool below 0.7 K. Instead a heating effect could be expected to be seen.

#### 4.3.3 Conclusions

To summarize, the solution refrigerator has been shown to operate at 1 K. The situation for the ACE, Inc. cycle has not been fully determined experimentally. The theory of this cycle does point to crucial hardware designs that can have significant affects on the operation of this cycle. These designs can be readily modified so as to reduce the extraneous heat loads on the test cell and allow validation of the ACE, Inc. cycle.

## 5.0 CONCLUSIONS

The primary conclusion of the research program is that a zero gravity cryocooler using the principle of the  $^3\text{He}/^4\text{He}$  dilution refrigerator is feasible. The zero gravity dilution refrigerator can take two forms:

- a) A cycle in which the  $^3\text{He}$  is circulated as a vapor, and
- b) A cycle in which the  $^4\text{He}$  is circulated as a liquid through "superleaks".

Each of these methods have been demonstrated in the earth laboratory, but each requires an innovation in order to successfully operate in a zero gravity environment. The two cycles will be considered separately.

### 5.1. $^3\text{He}$ Circulation Dilution Cryocooler

The  $^3\text{He}$  circulation dilution cryocooler has three phase boundaries. These include:

- a) The  $^3\text{He}$  vapor/liquid interface in the condenser at the input of the cycle.
- b) The  $^3\text{He}/^4\text{He}$  phase separation interfaces in the "mixing chamber".
- c) The dilute mixture/vapor interface in the "still".

In this effort, we have demonstrated by analysis that the only interface that must be controlled is the interface in the still. The other interfaces do not

create a fundamental difficulty, and we do not have to provide a substitute for gravity in order to preserve cycle operation.

The vapor/liquid interface in the still must be controlled for successful zero gravity operation. In this research effort, we have demonstrated that a sintered silver "porous plug" can serve as a "still" phase separator. This was demonstrated with  $^3\text{He}/^4\text{He}$  mixtures in a "minus one g" arrangement. That is, gravity is assisting the liquid breakout, and the interface is maintained against the gravity force via surface tension. This is more demanding than zero gravity conditions, and has been used for earlier superfluid porous plug work to demonstrate zero gravity operation.

Measurements have shown, that as long as  $^3\text{He}$  is present in the liquid above the plug, there is no "superfluid film" downstream of the phase separator. This means that the phase separator is serving as a "superfluid film" stopper. Thus, the phase separator provide the two necessary functions of a "still" control device:

- a) The liquid/vapor interface position is defined.
- b) There is no superfluid film downstream of the still.

The  $^3\text{He}$  circulation dilution cryocooler requires a "circulator" for operation. In the typical laboratory operation, this is provided by a "diffusion" pump or a mechanical "Roots Blower". In both cases, a mechanical pump is required as a high pressure "backing pump". These vacuum pumps are not adaptable to zero gravity operation. In this effort, we have identified two pumping systems that can be operated in zero gravity. These include:

- a) The "Molecular Drag" vacuum pump,
- b) A charcoal "absorption pump".

In our original proposal, we excluded the use of an absorption pump as it is not continuous. Therefore, our analysis focused on the "Molecular Drag" pump. This pump is commercially available from Alcatel Vacuum Products. The key characteristics include:

- a) Full pumping speed at pressures as high as 0.1 Torr
- b) High fore-pressure tolerance (< 50 Torr) so the dilution cycle condenser can be used as a forepump
- c) Constant pumping speed at pressures down to  $10^{-6}$  Torr
- d) Low vibration
- e) Long bearing life
- f) No oils or other contaminants that can limit the operating time of the cryocooler.

We conclude that the Molecular Drag pump is an excellent candidate for zero gravity, continuous operation.

## 5.2. $^4\text{He}$ Circulation Cycle

The previously demonstrated  $^4\text{He}$  circulation cycle, called the "Leiden" cycle, has been shown to be unsuitable for zero gravity operation. This was demonstrated by analysis, and was based on two principles. These are:

- a) The phase separation condition
- b) The requirement that the osmotic pressure is constant in the dilute solution.

Using the analysis developed in this effort, we have developed a new  $^4\text{He}$  circulation cycle that can operate in zero gravity. The new cycle is called the ACE, Inc., cycle.

The ACE, Inc., cycle has been demonstrated at relatively high temperatures, and was shown to produce some cooling. However, due to experimental limits, we were not able to find the actual cooling power nor could we measure the low temperature limits of operation. However, we can draw some conclusions, based on the analysis and the experiments. These include:

- a) The ACE, Inc., cycle is closely related to the  $^3\text{He}$  circulation and the solution refrigerator cycle, so it should be feasible.
- b) The ACE, Inc., cycle will be limited by the thermal conductivity of the dilute solution.
- c) The flow velocities in the refrigerator must be below the "critical" value. If the velocity is greater, then the  $^3\text{He}$  will be swept out of the active volume, and it no longer operates as a dilution refrigerator.
- d) Our analysis, based on extrapolations of higher temperature critical velocity values, indicate that a temperature of 0.1 K is possible with a reasonable geometry.

- e) The ACE, Inc., cycle is not "gravity independent". Therefore, testing must be done in a portion that compensates for gravity effects. However, the cycle does not depend on gravity for successful operation.

We conclude that the ACE, Inc., cycle is feasible. However, its limits have not been defined, and therefore it now has a higher degree of "technical risk" than the  $^3\text{He}$  cycle with a still phase separator.

### 5.3. "Vortex" Cryocooler

The "vortex" cryocooler is a "solution" type refrigeration that uses only the two phases (normal fluid and superfluid) of He II. Since this device is analogous to the dilution refrigerator, it became vital to understand the fundamental limits of its operation. We were successful in the task of developing a theory of operation that can account for the observed operation of the vortex cryocooler. The principal limit to low temperature operation is the Joule-Thomson coefficient of the He II. This limits the minimum temperature to the 0.6 K - 0.7 K range.

The Joule-Thomson coefficient of  $^3\text{He}/^4\text{He}$  mixtures is orders of magnitude less than the value for pure He II, so the limiting effect in the "vortex" cryocooler should be negligible in the dilution cryocooler. However, if the  $^3\text{He}$  concentration of the mixture becomes very small, due to velocity effects or other non equilibrium processes, then the Joule-Thomson effect can become large and can prevent low temperature ( $T < 0.6$  K) operation.

## 6.0 RECOMMENDATIONS

The feasibility of two different  $^3\text{He}/^4\text{He}$  dilution cryocooler cycles has been proven in this research effort. The cycles could provide substantially improved performance over the currently available adiabatic demagnetization refrigerator (ADR). However, additional development work is necessary in order to define the precise operational characteristics of the dilution cycles. Since this development could have a substantial impact on the design of current and future astrophysics observatories that use sensor temperatures of approximately 0.1 Kelvin, we recommend that the additional development work be started immediately. This recommended effort should cover two parallel concepts. These are:

- i. The "phase separator" for a  $^3\text{He}$  circulation dilution cryocooler, and
- ii. The effect of "critical velocity" on the operation of the ACE, Inc.,  $^4\text{He}$  circulation dilution cryocooler.

A statement of work for each of the efforts will be given to illustrate the scope of the recommendations.

### 6.1. Phase Separator for a $^3\text{He}$ Circulation Dilution Cryocooler

The object of this effort is to use the previously demonstrated phase separator concept in an actual, operating, dilution cryocooler. Zero-g operation will be simulated by a "minus one-g" setup. This is more demanding than zero-g operation, and can serve as a "proof" of zero-g operation. The effort will consist of the following tasks:

1. Set Baseline Requirements
  - a) Dilution cryocooler cooling power
  - b) Heat rejected at 1K station
  - c) Heat rejected at 1.5 to 1.8 K helium pot.
2. Design high powered vortex cryocooler to serve as 1 K station.
3. Design the dilution cryocooler with phase separator included. This design will be based on the existing SHE "Mini-Fridge", except for the different "still" concept.
4. Construct the high power vortex cryocooler of task 2.
5. Test the vortex cryocooler of task 4, to verify operation. This task will use the test facility constructed in an earlier development effort (NAS8-35254).
6. Construct the  $^3\text{He}$  circulation dilution cryocooler with new "still" concept.
7. Test the dilution/vortex cryocooler of task 6 to verify operation. This will use the same test facility that was used in task 5.
8. Submit a final report, including the test results developed in the above tasks.

This technical effort will extend over a 12 month period of performance.

## 6.2. <sup>4</sup>He Circulation, ACE, Inc., Dilution Cryocooler Cycle

The object of this effort is to determine the effect of "critical velocity" on the operation of the ACE, Inc., dilution cryocooler cycle. Zero-g operation can be simulated by arranging the cryocooler components in gravity, in order to eliminate gravity effects. The effort will consist of the following tasks:

1. Design a series of heat exchangers for the experimental facility developed under the technical effort covered by this report (NAS8-37260). These include:
  - a. 300 K - 4 K heat exchanger
  - b. 4 K - 1.3 K heat exchanger
  - c. 1.3 K - 0.5 K heat exchanger
  
2. Modify the existing test cell to minimize heat inputs to the dilution cryocooler. This includes:
  - a. Re-work <sup>3</sup>He flow circuit
  - b. New thermal anchors for superleaks.
  
3. Construct a new ACE, Inc., cryocooler. This will include:
  - a. New large area heat exchangers for the input and output segments.
  - b. Use demountable "drift" tubes so a variety of L/D ratios can be used.

4. Incorporate the improvements of the first three tasks into the test facility. The emphasis is on very low heat leak (< 1 micro watt) into the test cell.
  
5. Perform a series of tests to define the effect of critical velocity on the operation of the ACE, Inc., cycle. The variables to be considered are:
  - a. L, D, and the L/D ratio of a drift tube
  - b. Temperature
  - c. Flow velocity ( $^4\text{He}$ )
  - d.  $^3\text{He}$  concentration
  
6. Submit a final report, including the tests results developed in the above tasks.

The technical effort will extend over a 12 month period of performance.

## 7.0 REFERENCES AND BIBLIOGRAPHY

1. Atkins, K.R. and Narahara, Y. (1965), "Surface Tension of Liquid He-4", *Phys. Rev.*, 138, p. A437.
2. Bertran, B. and Kitchens, T.A., *Cryogenics* 8, 36 (1968).
3. Betts, D.S., Brewer, D.F., and Lucking, R. (19 ) "Effective Viscosity of Liquid Helium Isotope Mixtures, Low Temp. Physics - LT13, vol. 1, Plenum Press, New York, NY, p. 559.
4. Broulik, B. and Hess, G.B. (1978), "Characteristics of a Superfluid Fountain Pump," *Physica*, 94B, p. 169.
5. Brouwer, W. and Pathria, R.K. (1967), "On the Surface Tension of Liquid Helium II", *Phys. Rev.* 163, p. 200.
6. Castelijns, C.A.M., Kuerten, J.G.M., de Waele, A.T.A.M., and Gijnsman, H.M. (1985) "<sup>3</sup>He Flow in Dilute <sup>3</sup>He-<sup>4</sup>He Mixtures at Temperatures Between 10 and 150 mK," *Phys. Rev. B* 32, 2870.
7. Castles, S. (1980), Design of an Adiabatic Demagnetization Refrigerator for Studies in Astrophysics, NASA Pub. X-732-80-9.
8. Castles, S. (1983), Design of an Adiabatic Demagnetization Refrigerator for Studies in Astrophysics, NASA Conf. Pub. 2287, p. 389.
9. Condon, E.U. and Odishaw, H. (1958), Handbook of Physics, McGraw-Hill, New York.
10. Coops, G.M., A.T.A.M. de Waele, and H.M. Gijnsman (1982), "Experimental Evidence for Mutual Friction Between He-3 and Superfluid He-4," *Phys. Rev. B.*, 25, p. 4879.
11. Critchlow, P.R., Hemstreet, R.A. and Neppell, C.T. (1969), "A Single Charge He-3 - He-4 Dilution Refrigerator", *Rev. Sci. Inst.*, 40, p. 1381.
12. de Bruyn Ouboter, R., B. van den Brandt, and Tierolf, J.W. (1981), "Visual Observations of the Counterflow of the Two Liquid Phases in the 4He-Cycling 3He-4He Dilution Refrigerator" *Physica*, 107B, p. 557.
13. de Waele, A.T.A.M., Keltjens, J.C.M., Castelijns, C.A.M., and Gijnsman, H.M., (1983), "Flow Properties of He-3 Moving Through He-4 II at Temperatures Below 150 mK", *Phys. Rev. B*, 28, 5350.
14. Defay, R., Prigogine, I., Bellemans, A., and Everett, D.H. (1951), Surface Tension and Adsorption, John Wiley, New York.
15. Edwards, David O. ( ), "Helium-3 in Superfluid Helium-4," *Low Temp. Phys. - LT-13*, vol. 1, Plenum Press, New York, NY, p. 26.
16. Ellis, F.M. and Hallock, R.B. (1981), "Phase Separation in He-3/He-4 Films", *Physica* 107B, p. 35.

17. Esel'son, B.N., V.G. Ivantsov, and A.D. Shvets (1963), "Surface Tension of He-3/He-4 Solutions," *Sov. Phys. JETP*, 17, p. 330.
18. Franco, H. (1984), *Cryogenics*, Sept., p. 477.
19. Frossati, G., Hebral, B., Schumacker, G., and Thoulouze, D. (1978), *Cryogenics*, 18, p. 277.
20. Greywall, Dennis S., (1979), "Erratum: Specific Heat and Phonon Dispersion of Liquid  $^4\text{He}$ " [*Phys. Rev. B* 18 2127], *Phys. Rev. B* 21 No. 3, 1329.
21. Hendricks, J.B. and Dingus, M. (1987), "Long Lifetime, Spaceborne, Closed Cycle Cryocooler", Final Report, NASA Contract No. NAS8-35254.
22. Hendricks, J.B. and Karr, G.R. (1986), "Comparison of Flow States in the Porous Plug and the Active Phase Separator", *Proc. ICEC 11*, Butterworth, UK, p. 331.
23. Howell, J.R. and Siegel, R., Thermal Radiation Heat Transfer NASA SP-164, 114 vol. II (1969).
24. Huang, B.J. (1986) "Joule-Thomson Effect in Liquid He II," *Cryogenics* 26, p. 475.
25. Ilno, M., Suzuki, M., Ikushima, A. and Okuda, Y. (1984), "Surface Tension of He-3 Measured by Surface Wave Resonance" *Proc. LT-17*, Elsevier Science Pub., p. 1187.
26. Israelsson, U.E. (1988) Presented at International Cryocooler Conference, Monterey, California.
27. Jackson, J.D. (1962), Classical Electrodynamics, John Wiley and Sons, New York.
28. Jackson, H.W. (1982), "Can He-3/He-4 Dilution Refrigerators Operate Aboard Spacecraft?" *Cryogenics*, 22, p. 59.
29. Keller, W.E. (1969) Helium-3 and Helium-4, Plenum Press, New York.
30. Kittel, P. (1982), "Sub-Kelvin Temperatures in Space" Adv. in Cryo. Eng. Vol. 27, Plenum Press, p. 745.
31. Kuenhold, K.A., Crum, D.B., and Sarwinski, R.E., ( ) "The Viscosity of Dilute Solutions of  $^3\text{He}$  in  $^4\text{He}$  at Low Temperatures, *Low Temp. Phys.*-LT-13, Plenum Press, New York, NY, p. 563.
32. Landau, L.D. and Lifshitz, E.M. (1959) Fluid Mechanics, Pergamon, London.
33. Langer, S.A., DeConde, K., and Stein, D.C. (1984), "A Proposed Method for Polarizing Liquid He-3", *J. of Low Temp. Phys.*, 57, 249.

34. Li, Q., Watson, C.H., Goodrich, R.G., Haase, D.G. and Lukefahr, H., (1986) Cryogenics, 26, 467.
35. London, H., G.R. Clarke and E. Mendoza (1965), "Osmotic Pressure of He-3 in Liquid He-4, With Proposal for a Refrigerator to Work Below 1 K" Phys. Rev. 128, p. 1992.
36. London, H. (1968) "Refrigerators Operating at Very Low Temperatures" U.S. Pat. No. 3,376,712.
37. Lounasma, O.V. (1974) Experimental Principles and Methods Below 1 K, Academic Press, New York.
38. Mason, P., et.al. (1978), "The Behavior of Superfluid Helium in Zero Gravity" Proc. ICEC7, IPC Sci. & Tech. Press, p. 99.
39. McCarty, R.D. (1980) The Thermodynamic Properties of Helium II from 0 K to the Lambda Transition, NBS Tech. Note 1029.
40. Mikheev, V.A., Maidanov, V.A. and Mikhin, N.P. (1984) "Compact Dilution Refrigerator with a Cryogenic Circulation Cycle of He-3", Cryogenics, 24, p. 376.
41. Monchick, L., Mason, E.A., Munn, R.J. and Smith, F.J., (1965) "Transport Properties of Gaseous He<sup>3</sup> and He<sup>4</sup>," Phys. Rev. 139 No. 4A, A1076.
42. Neganov, B., Borisov, N. and Liburg, M. (1966), "A Method of Producing Very Low Temperatures by Dissolving He-3 in He-4" JETP, 23, p. 959.
43. Ostermeier, R.M., I.G. Nolt, and J.V. Radostitz (1978), "Capillary Confinement of Cryogenes for Refrigeration and Liquid Control in Space - 1 Theory" Cryogenics, 18, p. 83.
44. Pennings, N.H., de Bruyn Ouboter, R. and Taconis, K.W. (1976a), "The Leiden Dilution Refrigerator" Physica, 813, p. 101.
45. Pennings, N.H., Taconis, K.W. and de Bruyn Ouboter, R. (1976b), "The Leiden Dilution Refrigerator II" Physica, 84B, p. 102.
46. Pennings, N.H., de Bruyn Ouboter, R. and Taconis, K.W. (1976c), "On the Lowest Temperature Which can be Achieved in the Leiden Dilution Refrigerators", Physica, 84B, p. 249.
47. Polturak, E., R. Rosenbaum, and R.J. Soulen, Jr. (1979), "Anomalous Cooling Power of Dilution Refrigerators and Heat of Transport of He-3/He-4 Solutions" Cryogenics, 19, p. 715.
48. Radebaugh, R. (1967), Thermodynamic Properties of He-3/He-4 Solutions with Applications to the Dilution Refrigerator, NBS Tech. Note 362.
49. Radostitz, J.V., I.G. Nolt, P. Kittel, and R.J. Donnelly (1978), "Portable He-3 Detector Cryostat for the Far Infrared" Rev. Sci. Inst. 49 (1) p. 86.

50. Rice, O.K. (1977), "Interfacial Tension Near the Tricritical Point of He-3/He-4 Solutions", J. Low Temp. Phys., 29, p. 269.
51. Richardson, R.C. and Smith, E.N., ed. (1988) Experimental Techniques in Condensed Matter Physics at Low Temperatures, Frontiers in Physics Lecture Notes Series, Addison-Wesley Publ. Company.
52. Satoh, N., Satoh, T., Ohtsuka, T., Fukujawa, N. and Satoh, N. ( ) "<sup>4</sup>He-Circulating Dilution Refrigerator," Journal of Low Temp. Phys., vol. 67, p. 195.
53. Satoh, T. and Satoh, T ( ) "Studies of Cooling Effects in a Vortex Cooler," Proc. ICEC, p. 279.
54. Satoh, T., Shinada, H., and Satoh, T., (1982) "Turbulence and Cooling Effect in Adiabatic Flow of HeII," Physica 114B, North-Holland Publ. Co., p. 167-173.
55. Schuhl, A., Maegawa, S., Meisel, M.W., and Chapellier, M. (1985), "Production of Enhanced Liquid He-3 Magnetization by Dynamic Nuclear Polarization", Phys. Rev. Lett. 54, 1952.
56. Severijns, A.P. and H.E. Aarts (1977), "Helium-3/Helium-4 Dilution Refrigerating Machine" U.S. Patent No. 4,047,394.
57. Severijns, A.P., Staas, F.A. and Cense, W.A. (1978), "An Improved He-3/he-4 Mixing Chamber for Single - Cycle Experiments" Cryogenics, 18, p. 87.
58. Severijns, A.P. (1980), "A Novel He-3/He-4 Dilution Refrigerator with Superfluid He-4 Circulation," Cryogenics, 20, p. 115.
59. Shinada, H., Satoh, T., and Satoh, T., (1981) "Studies of Thermal Effect in Vortex Cooler," Physica 108B, North-Holland Publ. Co., p. 1109-1110.
60. Shu, Q.S., Fast, R.W., Hart, H.L. (1986), Cryogenics, 26.
61. Staas, F.A., and Severijns, (1969) "Vorticity in He II and Its Application in a Cooling Device," Cryogenics, 9, p. 422.
62. Staas, F.A. and A.P. Severijns, (1971) "Liquid Helium Refrigeration Apparatus and Method" U.S. Patent No. 3,581,512.
63. Staas, F.A. and A.P. Severijns (1974) "Device for Transporting Heat from a Lower to a Higher Temperature Level," U.S. Patent No. 3,835,662.
64. Staas, F.A. and A.P. Severijns (1975) "Helium-3/Helium-4 Dilution Refrigerator" U.S. Patent No. 3,922,881.
65. Sullivan, D.B., et.al. (1978), The Role of Superconductivity in the Space Program, NBS Pub. NBSIR 78-885.

66. Taconis, K.W., Pennings, N.H., Das, P., and de Bruyn Ouboter, R., (1971), "A He-3/He-4 Refrigerator Through Which He-4 is Circulated", *Physica*, 56, p. 168.
67. Taconis, K.W. (1978), "Dilution Refrigeration", *Cryogenics*, 18, p. 459.
68. Taconis, K.W. (1982), "Dilution Refrigeration" *Physica*, 109 and 110B, p. 1753.
69. van den Brandt, B., J.W. Tierolf and R. de Bruyn Ouboter (1981), "Visual Observations of the Counterflow of the Two Liquid Phases in the He-4 Cycling He-3/He-4 Dilution Refrigerator," *Physica*, 104B, p. 371.
70. van Haeringen, W. (1980), "On the Choice of Tube Lengths and Diameters in a He-3/He-4 Dilution Refrigeration System" *Cryogenics*, 20, p. 153.
71. Van Sciver, S.W., (1986) Helium Cryogenics, Plenum Press, New York, NY pp. 132-295.
72. Walker, G. (1983), Cryocoolers, Plenum Press, New York.
73. Wheatley, J.C., O.E. Vilches and W.R. Abel (1968), "Principles and Methods of Dilution Refrigeration" *Physics*, 4, p. 1.
74. White, G.K. (1979), Experimental Techniques in Low-Temperature Physics, Clarendon Press, Oxford.
75. Wilks, J. (1967), The Properties of Liquid and Solid Helium, Clarendon Press, Oxford.
76. Zemansky, M.W. (1957) Heat and Thermodynamics, McGraw-Hill, New York, NY, p. 211.
77. Zharkov, V.N., (1958) "The Influence of a He<sup>3</sup> Impurity on the Viscosity of Helium II," *Soviet Physics JetP*, vol 6 (33), p. 714.

## 8.0 APPENDICES

APPENDIX A

Fluid Flow Thermodynamics and  $^4\text{He}$  -  $^3\text{He}$  Refrigerators

by

Dr. Carl Brans  
Alabama Cryogenic Engineering, Inc.  
New Orleans, LA

FLUID FLOW THERMODYNAMICS  
AND  
 $^4\text{He}-^3\text{He}$  REFRIGERATORS

I. INTRODUCTION, SURVEY OF PROBLEM

Most discussions of He dilution refrigeration devices include at least informal reference to cooling associated with entropy production in mixing. For example, Radebaugh<sup>1</sup> prefaces his treatment of  $^4\text{He}-^3\text{He}$  dilution refrigeration by commenting that the mixing of  $^4\text{He}$  with the  $^4\text{He}-^3\text{He}$  mixture gives rise to entropy production and thus heat absorption by the system (cooling). The entropy production in mixing is of course a well known effect discussed in most thermodynamics texts. How well justified is the implication that this argument in fact leads to cooling? Consider the following situation in which all dissipative effects such as viscosity and component interactions are neglected:

ENTROPY OF MIXING  
IN FLOW THROUGH MEMBRANE

Side A	Side B
$N_{1A}, V_A$	$N_{1B}, V_B, T$
$P_{1A}, T$	$P_{1B}, N_{2B}, P_{2B}$

Equilibrium configuration, substances 1 and 2

In the diagram above, substance 1 is free to move thru the membrane, while substance 2 is trapped on the right side. Equilibrium implies that T is the same on both sides, as well as the chemical potential of substance 1. Thus,

$$\mu_{1A} = \mu_{1B} \tag{1}$$

Since  $\mu$  is intensive, it depends only on the ratios,  $N/V = n$ . Thus,

$$\mu_1(T, N_{1A}/V_A, 0) = \mu_1(T, N_{1B}/V_B, N_{2B}/V_B) \tag{2}$$

Further, assume that 1 and 2 do not interact strongly so that

$$\partial\mu_1/\partial n_2 \approx 0 \tag{3}$$

Thus, from (2) and (3) we get

$$N_{1A}/V_A = N_{1B}/V_B \tag{4}$$

The equation of state for substance 1 for pressure as a function of T and N/V will then result in  $P_{1A} = P_{1B}$ , giving rise to osmotic pressure,  $\pi = P_B - P_A = P_{1B} + P_{2B} - P_{1A} = P_{2B}$ .

Now, consider an infinitesimal part of the left-to-right flow as transferring a quantity  $\delta N_1$  across the membrane, resulting in a new equilibrium configuration. Assume that this transfer is accomplished by decreasing  $V_A$  by  $\delta V$ . *N.B. However, this assumption may not be valid for the continuous flow in a refrigerator. See more comments on this below.*

Obvious conservation laws then result in

$$\begin{aligned} N'_{1A} &= N_{1A} - \delta N_1 \\ N'_{1B} &= N_{1B} + \delta N_1 \\ N'_{2B} &= N_{2B} \\ V'_A &= V_A - \delta V \\ V'_B &= V_B + \delta B \end{aligned} \tag{5}$$

Also, assume that the process does not change T or  $P_{1A}$ , so

$$N'_{1A}/V'_A = N_{1A}/V_A \tag{6}$$

and thus

$$P'_{1A} = P_{1A} \tag{7}$$

$$\delta V = (V_A/N_{1A}) \cdot \delta N_1 \tag{8}$$

Equilibrium in the new configuration requires  $\mu'_{1A} = \mu'_{1B}$ , or

$$\begin{aligned} 0 &= (\partial\mu_1/\partial n_{1A})|_{T, n_2} \cdot (n'_{1A} - n_{1A} + n'_{1B} - n_{1B}) + \dots \\ &\quad + (\partial\mu_1/\partial n_2)|_{T, n_1} \cdot (n'_{2B} - n_{2B}) \end{aligned} \tag{9}$$

From (3) and (6), this then gives

$$N'_{1B}/V'_B = N_{1B}/V_B \tag{10}$$

From (4), (5) and (8) we then get

$$\delta_B = (V_B/N_{1B}) \cdot \delta N_1 = (V_A/N_{1A}) \cdot \delta N_1 = \delta V \tag{11}$$

Now consider the entropy of mixing in this process. Let  $S_1$  be the extensive entropy of substance 1 and again assume that on side B, the total entropy is the sum  $S_1 + S_2$ . The change in total entropy is then

$$\begin{aligned} \delta S &= (\partial S_1/\partial N_{1A})|_{T, V} \cdot (-\delta N_1) + (\partial S_1/\partial V_A)|_{T, N} \cdot (-\delta V) + \dots \\ &\quad + (\partial S_1/\partial N_{1B})|_{T, V} \cdot (\delta N_1) + (\partial S_1/\partial V_B)|_{T, N} \cdot \delta_B + (\partial S_2/\partial V_B)|_{T, N} \cdot \delta_B \end{aligned}$$

Now use the combined 1st and 2nd law and (8) and (11)

$$\begin{aligned}
 T \cdot \delta S / \delta V = & -(N_{1A} / V_A) \cdot \left[ (\partial U_{1A} / \partial N_{1A}) \Big|_{T,V} - \mu_{1A} \right] - \dots \\
 & - \left[ P_{1A} + (\partial U_{1A} / \partial V_A) \Big|_{T,N} \right] + (N_{1A} / V_A) \cdot \left[ (\partial U_{1B} / \partial N_{1B}) \Big|_{T,V} - \mu_{1B} \right] + \\
 & + \left[ P_{1B} + (\partial U_{1B} / \partial V_B) \Big|_{T,N} \right] + \left[ P_{2B} + (\partial U_{2B} / \partial V_B) \Big|_{T,N} \right] \quad (13)
 \end{aligned}$$

Equilibrium gives  $\mu_{1A} = \mu_{1B}$ . Further assume  $\partial U / \partial N \Big|_{T,V}$  depends only on T and that  $\partial U / \partial V \Big|_{T,N} \approx 0$ . The result is

$$T \cdot \delta S = \delta V \cdot (P_{1B} + P_{2B} - P_{1A}) \quad (14)$$

However, this is easily seen to be the net work done in the process. In other words, under the assumptions above, valid for ideal gases and presumably for dilute solutions, the heat associated with the entropy of mixing in a continuous, reversible flow across a membrane can be computed as the net work done by pistons driving this process in such a way as to maintain equilibrium.

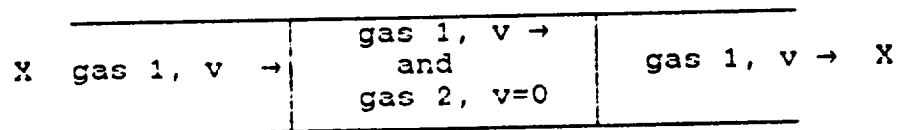
Now consider the situation for superfluid  $^4\text{He}$  (substance 1),  $^3\text{He}$  (substance 2) and a superleak as the "membrane". From standard analysis of superleaks, (1) is still valid and, to whatever extent the notion of partial pressure is applicable to  $^3\text{He}$ , so is the "osmotic" pressure argument. Of course, it may be argued that the quantity  $\partial S_1 / \partial N_1$  must be zero since SF does not carry entropy, but these terms do not contribute to the resulting (14) anyway. Thus, at first glance, it seems that the entropy of mixing argument does indeed predict  $^4\text{He}$ - $^3\text{He}$  dilution cooling. However, two points must be made: First, the above argument was for non-steady state changes across a single membrane, rather than for a continuous flow which is more appropriate to model a refrigerator, and second,  $T \cdot dS$  was directly equated to heat input. Both of these points must be looked at more carefully.

#### CONTINUOUS FLOW, MIXING AND COOLING

To illustrate the problems that might occur when the above "mixing implies cooling" argument is applied blindly to a continuous flow problem, replace the finite volumes on sides A and B by infinite volumes. Assume that the substances are ideal gas, with no

viscosity and no interaction between each other. Now assume that gas 1 is moving from left to right freely across the membrane, with constant  $P_{1A} = P_{1B}$ . Thus, the fluid dynamical equations for gas 1 are satisfied with constant velocity,  $v_1$ . Similarly, let gas 2 be at rest. The energy and entropy flow equations are consistent with constant  $T$  and specific quantities,  $s_{1A} = s_{1B}$ , and  $u_{1A} = u_{1B}$ . Another way to describe the situation is that it is a linear (i.e. completely non-interacting) superposition of a freely flowing gas 1 in an infinite volume with gas 2 at rest confined to the semi-infinite side B. Clearly, there is no absorption or generation of heat at any point in this process. Nevertheless, gas 1 is crossing a membrane from a region in which its concentration is 1 to one in which it is diluted by gas 2. The arguments leading to (14) above if taken naively, however, might lead us to suspect that cooling would occur at the membrane. This is certainly not intended to be a realistic model similar to the He flow across a superleak. Diffusive and dissipative effects must certainly be accounted for. Nevertheless, it does point out difficulty in taking the "cooling thru mixing" argument literally without further analysis.

Finally, it might be objected that the "infinite" extent of the two sides is unrealistic. This can be rectified by making a finite system:



Here identify points X, either topologically or by wrapping the system back on itself in a sufficiently big circle to make centrifugal effects negligible. This model then mimics the one in the diagram in section IV below.

In summary, we have a counter example to the idea that the mixing alone necessarily provides cooling in a continuous flow system.

## II. $^4\text{He}-^3\text{He}$ DILUTION REFRIGERATOR:REVIEW

An early discussion of this was provided by Wheatley<sup>2</sup>. More complete treatments on the Leiden dilution refrigerator are provided by papers published by the group at the Onnes Lab<sup>3</sup> and at

Eindhoven<sup>4</sup>. These works generally use thermodynamic equations for changes without explicit reference to flow. However, as point out above, the refrigerator is in fact a continuous operation, involving steady-state fluid flow. Thus, it is necessary to look at heating/cooling from mixing/demixing in terms of fluid thermodynamics. For superfluid He, the standard model was presented by Landau and Lifshitz, as summarized by Khalatnikov<sup>5</sup>. Other treatments were provided by London<sup>6</sup> and Prigogine and Mazur<sup>7</sup>, and Jackson<sup>8</sup>. All of these arrive at fluid flow equations involving specific, local thermodynamic quantities such as internal energy and entropy. Of course, in liquid Helium applications, the super and normal components are not in fact two separate substances, but the two-fluid idea is very successful in providing a successful mathematical model. However, the basic question for applications is to predict heat flow into or out of system at various points. A standard work looking at such questions is the book by deGroot and Mazur<sup>9</sup>.

### III. THERMODYNAMICAL FLOW AND IDENTIFICATION OF HEAT

The identification of particular energy flow as heat is a non-trivial problem. See e.g. deGroot and Mazur's<sup>9</sup> discussion in chapter III of various possible forms for  $J_q$ , heat flux. In the early part of this chapter they point out that  $T \cdot dS$  cannot in general be equated to quantity of heat flowing into system. For example from their (1) and (4), it follows that

$$T \cdot dS = dQ + d_i S$$

where  $d_i S$  is "internal entropy production", which includes, among others, terms involving  $\sum \mu_k dN_k$ , which are non-trivial when considering mixing, flow thru membranes or superleaks, etc. Thus, in reviewing the works mentioned in II above, care must be taken to insure the correct relationship between  $T \cdot dS$  and heat input to system.

Specifically consider the treatment by deGroot and Mazur, 413 ff, with the assumption of no external forces, all  $\psi$ 's = 0, and no chemical reactions,  $\nu_{kj} J_j^\alpha = 0$ .

Let  $\alpha = I, II, III$  index regions with I and II being left and right chambers and III a membrane. Assume that substance 1 is flowing from left to right in I thru III into II which contains both

substance 1 and substance 2, which cannot pass thru III. Further, assume steady state. In this approach, it is assumed that the flow is caused by a piston moving with constant velocity from left to right in I, which thus has a finite volume,  $V^I(t)$ . Similarly a piston in II maintains it at a volume  $V^{II}(t)$ . For simplicity, assume that  $V^\alpha$  are small, so that space variations can be neglected. In particular,  $V^{III}$  is infinitesimal, representing a thin membrane separating I and II. Thus the extensive quantities can be obtained merely by multiplying densities by the corresponding  $V^\alpha$ . dGM use symbols  $d_i/dt$  and  $d_e/dt$  to represent "internal" and "external" rates of changes of extensive quantities such as entropy,  $S^\alpha$  and internal energy,  $U^\alpha$ , as well as heat flux into the system. Thus,  $d_i Q^\alpha/dt$  is the rate of heat flow into side  $\alpha$  across the "internal" boundary, represented here by region III, while  $d_e Q^\alpha/dt$  is heat flow across external boundaries corresponding to system heating/cooling.

Now apply the assumptions above to expression for total entropy production,  $\sigma_{tot}$ , given in (55), using (42) and (16). Thus,

$$\sigma_{tot} = (d_i U^I/dt) \cdot (1/T^I - 1/T^{II}) - \sum_{\alpha=I}^{II} \left\{ \frac{\mu_1^\alpha}{T^\alpha} \frac{d_i M_1^\alpha}{dt} + \frac{\mu_2^\alpha}{T^\alpha} \frac{d_i M_2^\alpha}{dt} \right\}$$

Now, assuming III is a thin heat conductor,  $T^I = T^{II}$ , so the first term on the right side is zero. From (16),  $d_i M_1^I/dt + d_i M_1^{II}/dt = 0$ ,  $\mu_1^I = \mu_1^{II}$  if the flow of substance 1 across III is reversible. This implies that the first term inside the sum is zero. The second is also, since  $M_2^\alpha = \text{constant}$  for each  $\alpha$ . Thus,

$$\sigma_{tot} = 0.$$

Combining this with (46) and (47) leads to

$$\sum_{\alpha=I}^{II} \frac{dS^\alpha}{dt} = \sum_{\alpha=I}^{II} (1/T^\alpha) \cdot \frac{d_e Q^\alpha}{dt} = (1/T^I) \cdot \sum_{\alpha=I}^{II} \frac{d_e Q^\alpha}{dt} \quad (15)$$

In other words, the total rate of heat input to the system from external sources is just  $T^I$  times the time rate of change of the

total entropy in regions I and II,

$$\sum_{\alpha=I}^{II} \frac{d_e Q^\alpha}{dt} = T^I \cdot \left( \frac{ds^I}{dt} + \frac{ds^{II}}{dt} \right) \quad (16)$$

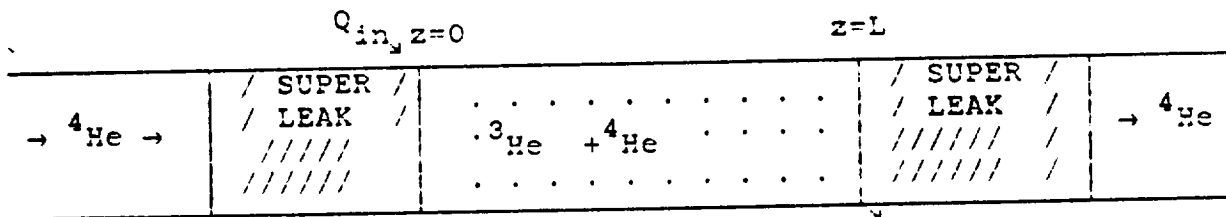
Assuming no change in density of substance 1 as it passes from I to II, the rates of changes of  $V^I$  and  $V^{II}$  are negatives of each other. Also, for small  $V^\alpha$ ,  $S^\alpha = V^\alpha \rho^\alpha s^\alpha$  where  $s^\alpha$  is the specific entropy. Thus,

$$\sum_{\alpha=I}^{II} \frac{d_e Q^\alpha}{dt} = T^I \cdot \frac{dV^I}{dt} \left( \rho_1 s_1^I - \left( \rho_1 s_1^{II} + \rho_2 s_2^{II} \right) \right) \quad (17)$$

This is just the entropy of mixing formula.

#### IV. STEADY FLOW ANALYSIS OF SOLUTION REFRIGERATOR

$^4\text{He}$  MOVING THRU TRAPPED  $^3\text{He}$



Let us now apply Landau-Lifshitz-Khalatnikov<sup>5</sup> equations to this diagram. Recall that, as mentioned in II above, although the fluid flow equations are effective models, normal and super components are not in fact two separate fluids. In this model,  $^4\text{He}$  is moving thru  $^3\text{He}$  trapped between two super leaks. All temperatures are assumed to be above phase separation. System is adiabatically insulated except at  $z=0$  and  $z=L$  where  $Q_{in}$  and  $Q_{out}$  can come in/out. Object of study is to build a mathematical model predicting  $T(z)$  and  $Q_{in}$  and  $Q_{out}$  in terms of known experimental parameters. SOURCE:Khalatnikov<sup>5</sup>, especially chapter 24.

- - UNKNOWNNS - -

- $P(z)$  Pressure  
 $T(z)$  Temperature  
 $v_n(z)$  Normal component velocity ( $^4\text{He}$ )  
 $v_s(z)$  Superfluid component velocity ( $^4\text{He}$ )  
 $\rho_s(z)$  Superfluid component density ( $^4\text{He}$ )  
 $v_3(z)$  Velocity of  $^3\text{He}$   
 $Q_{in}$  External heat in at  $z=0$   
 $Q_{out}$  External heat out at  $z=L$   
 $x(z)$   $\text{He}_3$  molar concentration  $= N_3/(N_3+N_4)$   
 related to Khalatnikov's  $c = \rho_3/(\rho_3+\rho_4)$  by  
 by  $c=x(m_3/m_4)/(1-x(1-m_3/m_4))$

- - ASSUMPTIONS AND KNOWNNS - -

Steady state  $\Rightarrow \partial (\text{All})/\partial t = 0$   
 Total mass of  $^3\text{He} = \text{constant} = \text{Area} \int_0^L \rho_3 dz$ ,

$\rho_n$  and  $\rho_s$  as functions of  $T$  and  $P$ .

$T(0)$

$v_s(0)$

$P(0)$

Expressions for chemical potential and dissipative parameters in terms of  $T, P$

Rewrite Khalatnikov's equations (24-36) and (24-37) as (18) thru (19)

$$\partial \vec{j} / \partial t + \nabla \cdot (\Pi + \tau) = 0 \quad (18)$$

$$\partial \vec{v}_s / \partial t + \nabla \cdot (\mu - Zc/\rho + v_s^2/2 + h) = 0 \quad (19)$$

$$\partial E / \partial t + \nabla \cdot \vec{Q} = Q_{in} \delta(z) - Q_{out} \delta(z-L) \quad (20)$$

and total matter conservation,

$$\partial \rho / \partial t + \nabla \cdot \vec{j} = 0 \quad (21)$$

$$\text{for } \vec{j} = \rho_n \vec{v}_n + \rho_s \vec{v}_s + \rho c \vec{v}_3$$

$$\text{and } \rho = \rho_n + \rho_s + \rho c$$

It is assumed that the  $^3\text{He}$  is diffusing thru the normal component of  $^4\text{He}$ . Thus, if Khalatnikov's  $\vec{j}$  is the  $^3\text{He}$  "dissipative diffusive current" then referring motion to normal  $^4\text{He}$  means that the c.o.m. velocity used in diffusion studies is  $\vec{v}_n$

thus  $\vec{v}_3 = (\rho c \vec{v}_n + \vec{g}) / (\rho c)$ . In this way, Khalatnikov's (24-38) is equivalent to conservation of  $^3\text{He}$  :

$$\partial(\rho c) / \partial t + \nabla \cdot (\rho c \vec{v}_3) = 0. \quad (22)$$

The superleaks can be thought of as membranes, concentrated at  $z=0$  and  $z=L$  respectively, having property that matter, temperature and chemical potential (of  $^4\text{He}$ ) are continuous across them, i.e., at  $z=0, z=L$

- - ANALYSIS - -

Since everything is along z-axis, vectors and tensors reduce to a single component. Apply  $\partial/\partial t = 0$  to (18), thru (22) to get

$$\Pi_{33} + \tau_{33} = \text{constant} \quad (23)$$

$$\mu - Zc/\rho + v_s^2/2 + h = \text{const} \quad (24)$$

N.B. (24) does not include a possible Gorter-Mellink term.

$$\rho c v_n + g = \text{const} \quad (25)$$

$$Q = \begin{cases} Q_L & \text{for } z < 0 \\ Q_0 & \text{for } 0 < z < L \\ Q_R & \text{for } L < z \end{cases} \quad (26)$$

where  $Q_L, Q_0,$  and  $Q_R$  are constants and

$$Q_0 - Q_L = Q_{in} \quad (27)$$

$$Q_R - Q_0 = -Q_{out} \quad (28)$$

$$\rho_n v_n + \rho_s v_s + \rho c v_3 = \text{const} \quad (29)$$

$$\text{Area} \int_0^L \rho c \, dz = \text{Total mass He}_3 \quad (30)$$

Khalatnikov and others provide an analysis of  $\Pi, \tau, Z, h, g, Q$  in terms of the variables listed above.

DETERMINATION OF FREE VARIABLES

Let the free variables be the functions  $T(z), P(z), v_n(z), v_s(z), x(z)$ , and the unknown constants  $Q_{in}$  and  $Q_{out}$ . First consider the five equations: (23), (24), (25), the middle of (26), (29), and (30). These five equations, with unknown constants on the right side of

the first four, would then determine uniquely the five functional unknowns in the absence of dissipation, for which derivatives do not occur, and assuming functional independence of the relevant expressions on the left side. Thus, in the absence of dissipation, and only then, each of the five functions,  $T$ ,  $P$ ,  $v_n$ ,  $v_s$ ,  $x$  would be constant in the steady state, and  $Q_{in} = Q_{out} = 0$ . This is consistent with the points raised in the discussion of dissipative-free ideal gas flow in section I above. This, of course, is not an adequate model for an actual  $^3\text{He}$ - $^4\text{He}$  refrigerator since dissipative terms and external work were neglected. The presence of dissipation, however, means that derivatives of these functions are present in the expressions on the right hand side, so that the determination involves solving first order differential equations yielding the functions uniquely in terms of an additional set of five constants. This form of the problem will require approximate computational work. Finally, this model neglects external driving forces. The discussion in I comparing driven versus free flow mixing apparently indicates that these must be considered.

#### V. SUGGESTED FUTURE WORK

There seem to be a good number of points in the theoretical analysis of heat production/flow in classical fluid thermodynamics that could well be studied more thoroughly, including especially the identification of heat. The same can of course be said more strongly for the superfluid case. Earth-bound experiments necessarily involve gravity whose magnitude easily overwhelms that of other effects. Thus, zero gravity fluid thermodynamics could be a very fruitful field for both theoretical and experimental work.

#### REFERENCES

1. Ray Radebaugh, chapter 12 in book *Cryogenics, Part 2: Applications*, Graham Walker Plenum Press, (N.Y. 1954).
2. John C. Wheatley, *Amer. J. Phys.* 36. 181(1968).
3. N. H. Pennings, R. de Bruyn Ouboter, K.W. Taconis, *Physica* 81B, 101, (1976), and *Physics* 84B, 249 (1976).
4. C. A. M. Castelijns, J. G. M. Kuerten, A. T. A. M. de Waele, H. M. Gijnsman, *Phys. Rev.* B32, 2870 (1985), and *Phys. Rev. Lett.* 56 2228 (1986).
5. I.M. Khalatnikov, *Introduction to the Theory of Superfluidity*, w. A. Benjamin (N.Y. 1965).
6. F. London, *Superfluids*, vol II, John Wiley (N.Y. 1954)
7. I. Prigogine and P. Mazur, *Physica*, XVII, 661 and 680 (1951).
8. H. W. Jackson, *Phys. Rev.* B19, 2556 (1979).
9. S. R. de Groot and P. Mazur, *Non-Equilibrium Thermodynamics*, North-Holland Publishing (Amsterdam, 1962).

## APPENDIX B

### Theory of Operation of the "Vortex Cryocooler"

The "vortex cryocooler" is based on the concept of a "superleak". The superleak can filter out the "normal" component of Helium II, leaving only the "superfluid" component. Since the superfluid component carries no entropy or heat, the "temperature" of the superfluid component should approach zero. This effect was demonstrated by Darent and Mendelssohn (1) and schematic of the apparatus is shown in Figure B-1. The superfluid component flows out of the container through the superleak P. Since no entropy is carried away, but the volume of Helium II in the vessel is reduced, the average entropy per unit volume is increased. If the process is adiabatic, the temperature in the vessel will rise. The heat that must be removed to keep the temperature constant is:

$$Q^* = T \rho S \quad (B-1)$$

This process results in heating. The opposite process, resulting from the injection of superfluid, can be used to provide cooling. This process is called the "mechano-caloric" effect.

Stass and Severijns (1963) have developed a device that uses the mechano-caloric effect to provide continuous cooling. They named the device the "vortex cryocooler". A simplified schematic of the device is shown in Figure B-2. Superfluid is injected into the cooling chamber (A) through a superleak (SL). The Helium II in the cooling chamber then flows out through a small capillary (C) and is returned to the Helium II bath. The cooling effect

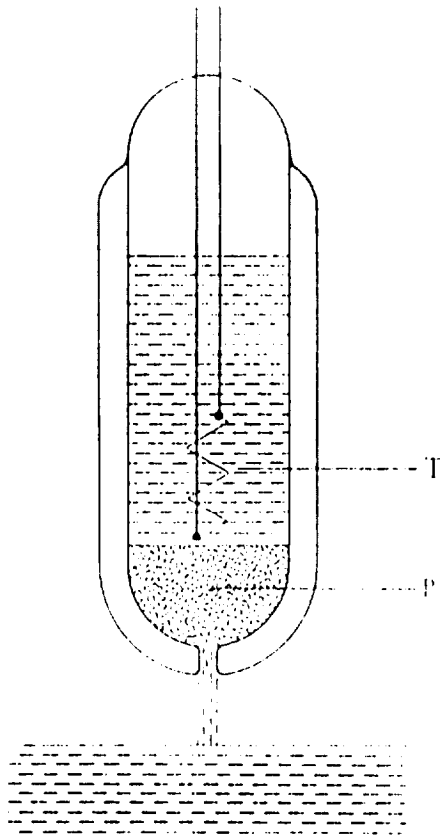


Figure B-1 Apparatus used to demonstrate the Mecano-Caloric effect.

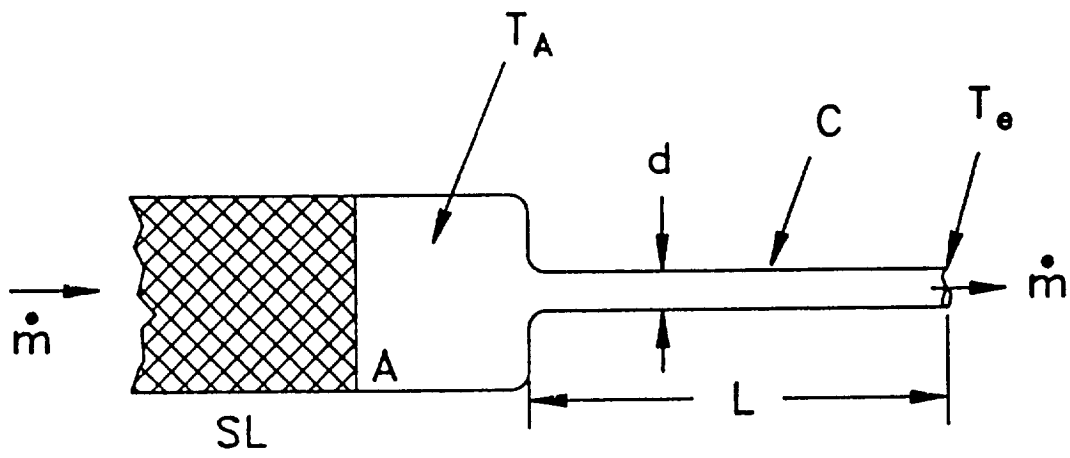


Figure B-2 Schematic of the vortex cryocooler.

is given by Eq. (B-1). This is balanced by the heat flow in the exit capillary. The device will cool if the heat flow is less than the cooling effect. The cooling effect for a typical device is illustrated in Figure B-3. At low flow rates (small velocities), the device does not cool, due to the large heat conduction in the capillary. Above the "critical velocity" of the capillary, the "heat resistance" of the capillary increases and the device begins to cool. As the velocity increases, the temperature continues to decrease until a "plateau" is reached. If the velocity is increased further, the chamber temperature begins to rise.

This plateau effect or minimum temperature has been one of the unsolved issues in the understanding of the vortex cryocooler. In a long series of papers, the Dutch have studied this effect, in order to resolve its source. They have been unable to develop a theory that explains the observed behavior. However, the extensive experiments have yielded an extensive "parametric" model of the vortex cryocooler, and this provides a good basis for users interested in applying the device.

In this Appendix we will present a theory of the vortex cryocooler that explains the observed behavior of the device. The theory forms the closing chapter in the development of the device, as the observed limits are shown to be intrinsic to its operation, and cannot be avoided. The theory is important, as it defines new limits on devices that utilize superfluid injection, such as the solution refrigerator and the dilution refrigerator.

The Appendix will begin with a review of heat conduction in capillaries. A section on the heat balance, and limiting behavior of the vortex cryocooler

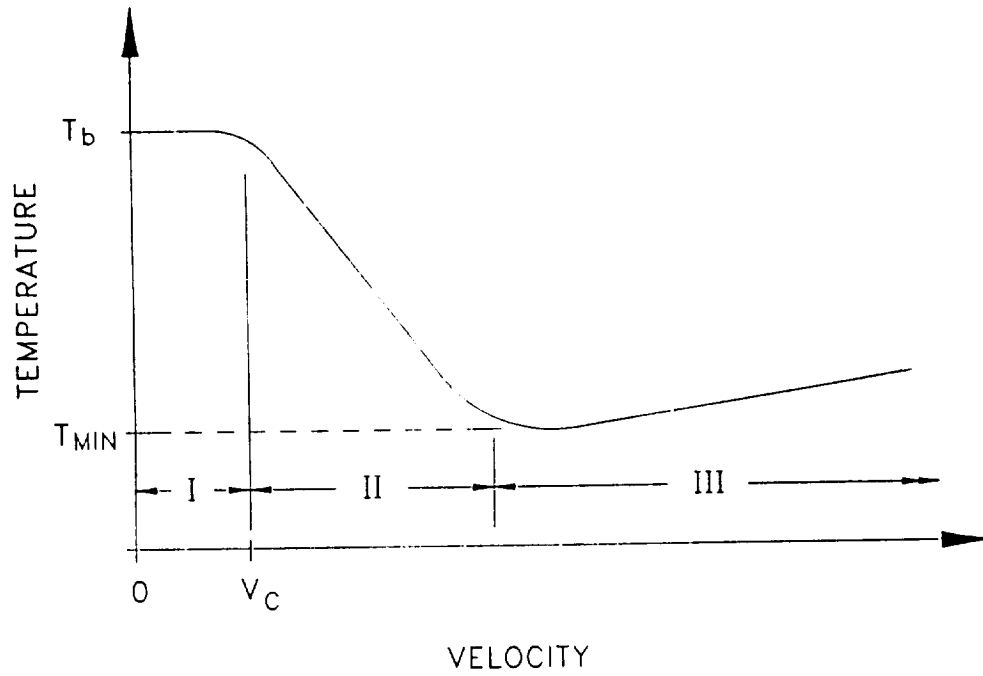


Figure B-3 Cooling effect of a vortex cryocooler (not to scale).

will follow. Finally, a section on the effect of hydrostatic pressure on the operation of the vortex cryocooler will be given. In a summary, the limits to operation will be given. This will be of use for considering the vortex cryocooler for a particular application.

### B.1 Review of Heat Transport in Capillaries

There is an extensive literature on the flow of heat in capillaries, particularly under zero net mass flow conditions. This can be reviewed in the work by Tough (1982). However, for the vortex cryocooler, we are interested in heat transport under "forced convection" conditions. This has received much less attention, but is an important issue for applications, such as cooling of superconducting magnets. Here we will review the results developed by Van Sciver (1986). A schematic of the experimental situation is shown in Figure B-4.

The first assumption in the analysis is that the heat conduction can be calculated as the sum of two mechanisms:

$$q = q_{fc} + q_{ic} \tag{B-2}$$

The forced convection term,  $q_{fc}$ , is assumed to be described by the flow of enthalpy:

$$Q_{fc} = \rho u \Delta h \tag{B-3}$$

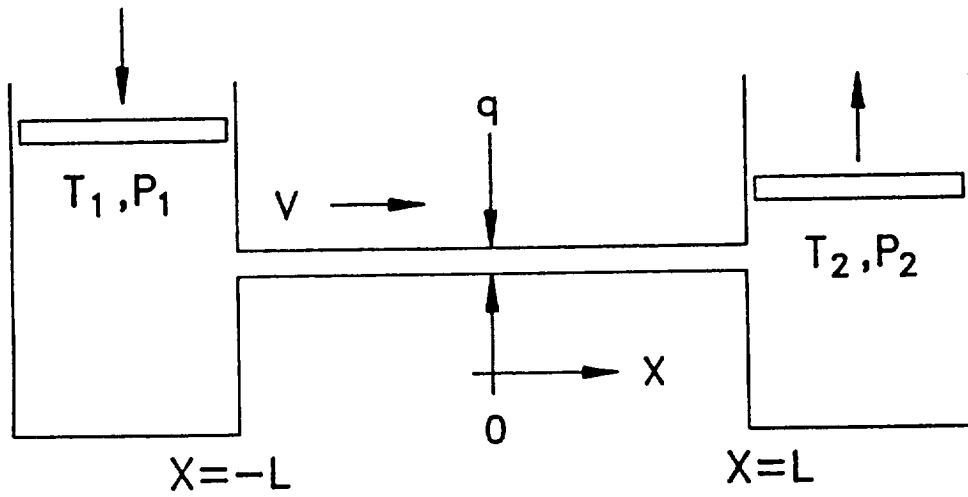


Figure B-4 Apparatus for measuring forced convection heat transfer in He-II.

where  $\Delta h = h_1 - h_2$  represents the specific enthalpy difference between two points in the system between temperatures  $T_1$  and  $T_2$ . That is:

$$\Delta h = \int_{T_1}^{T_2} c_p dT \quad (B-4)$$

Equation (B-3) assumes that the density,  $\rho$ , is a constant.

For internal convection,  $q_{ic}$ , we assume that the velocity is above the critical value, so that the heat transport is in the Gorter-Mellink regime. We will neglect the laminar flow regime, as this corresponds to low velocities, and high heat transport. The Gorter-Mellink heat transport can be described by:

$$q_{ic} = [(1/f(T)) (dT/dx)]^{1/3} \quad (B-5)$$

The form of  $f(T)$  as a function of temperature and pressure is shown in Figure B-5.

The heat balance equation can be written as:

$$d/dx [(1/f(T)) (dT/dx)]^{1/3} - \rho u (dh/dx) = \rho (dh/dt) \quad (B-6)$$

If we assume a steady state, then  $dh/dt = 0$ . If we make the assumption of constant properties, so  $\Delta h = c_p \Delta T$ , we can write:

$$- d/dx^* [(d\theta^*/dx^*)^{1/3}] + K' (d\theta^*/dx^*) = 0 \quad (B-7)$$

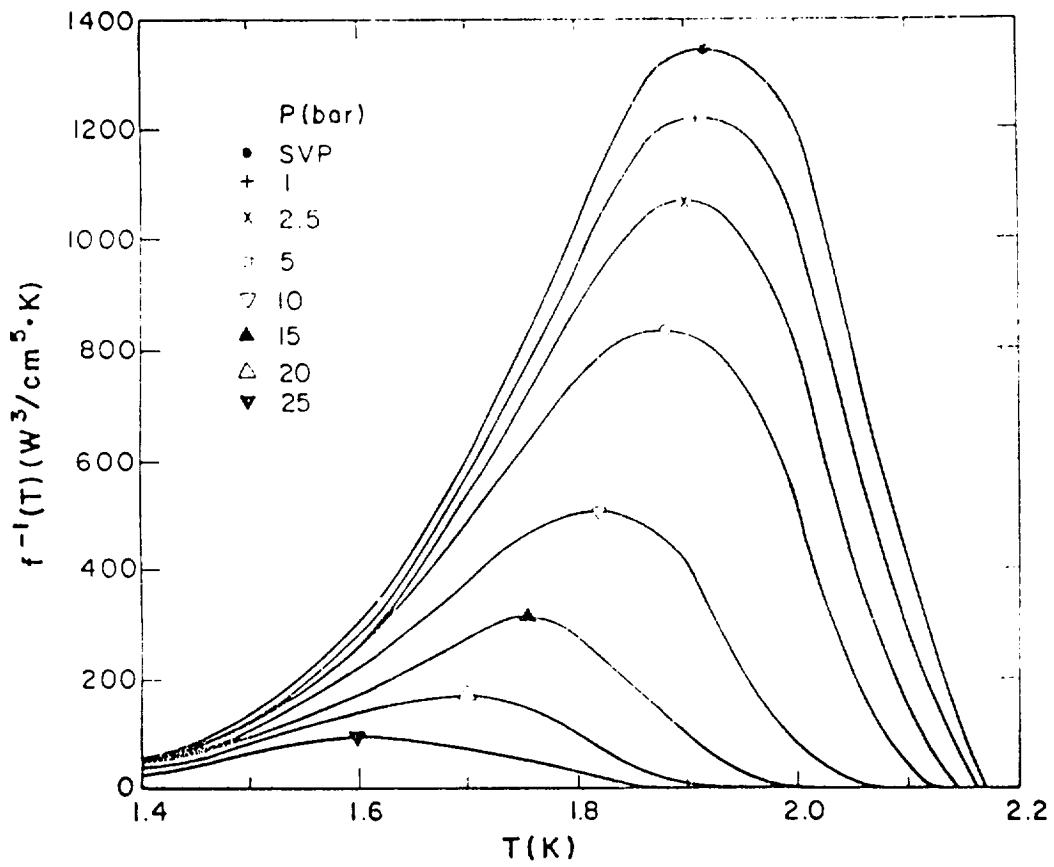


Figure B-5 The heat conductivity function  $f(T)$  for He-II as a function of temperature and pressure.

where

$$\begin{aligned}\theta^* &= (T-T_2)/(T_1-T_2) \\ x^* &= x/L \\ K' &= 2 \rho C_p u (fL)^{1/3} (T_1-T_2)^{2/3}\end{aligned}\tag{B-8}$$

A graph of the normalized temperature distribution along a capillary for various flow velocities, e.g. various values of  $K'$ , is shown in Figure B-6. We see that the temperature gradient is strongly affected by forced convection.

Given the solution to the temperature profile, the heat transport can be calculated. In normalized form the result is given by:

$$q/q_0 = -(d\theta^*/dx^*)^{1/3} + (K'/2) \theta^*\tag{B-9}$$

where

$$q_0 \equiv [(T_1-T_2)/fL]^{1/3}\tag{B-10}$$

Results are given in Figure B-7. Compared to experimental results, the theory seems to predict larger heat flows at relatively high velocities. The fit seems reasonable over a wide range, however.

In summary, the heat transport in a capillary is substantially changed when a transport current is present. In the case of interest, where the velocity is opposite to the heat flow, the apparent conductivity is substantially reduced. This reduction increases monotonically as the transport velocity is increased.

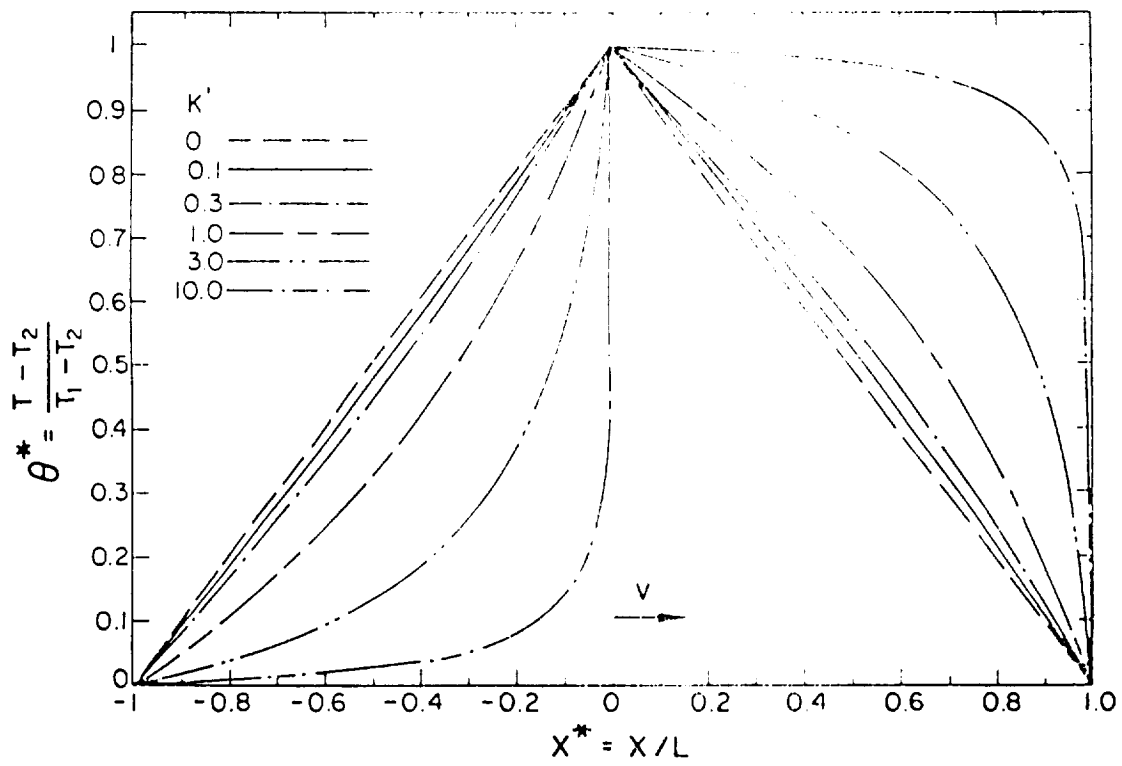


Figure B-6 Temperature distribution along a capillary for various flow velocities (quantities defined in text).

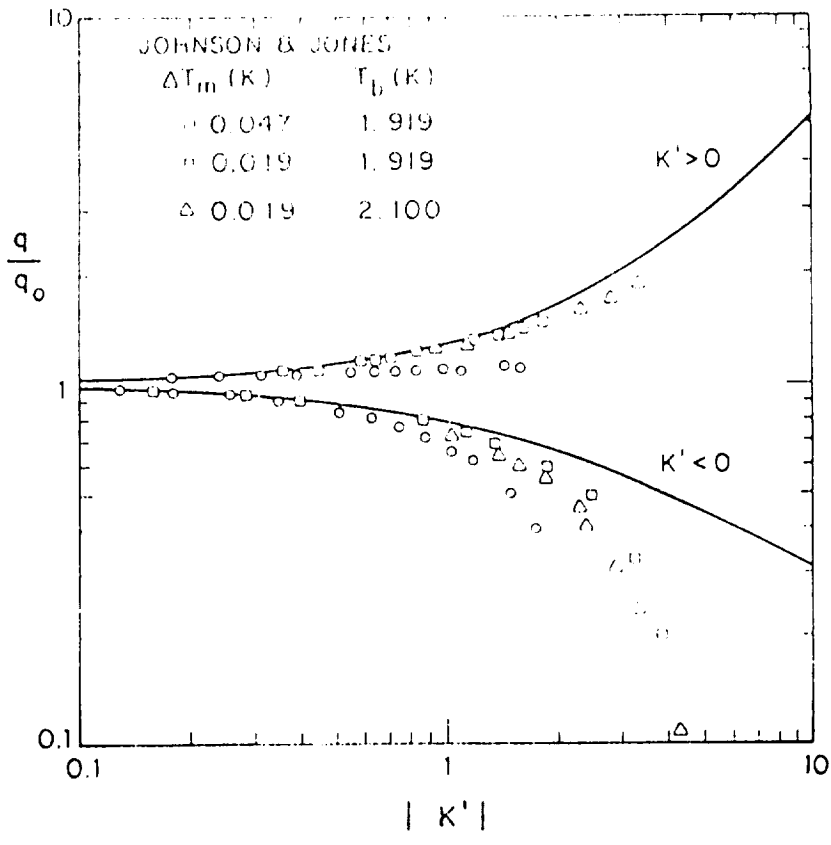


Figure B-7 Heat transport in a capillary as a function of flow velocity (quantities defined in text).

## B.2. Heat Balance in a Vortex Cryocooler

The heat balance for a vortex cryocooler can be written as a series of independent terms. There is one cooling term, due to the mecano-caloric effect. The heating terms include:

- i. heat conduction in the exit capillary, (internal and forced convection)
- ii. viscous heating in the exit capillary that is conducted back into the cooling chamber,
- iii. "Joule-Thomson" heating due to pressure gradients in the system, and
- iv. direct heat inputs to the cooling chamber.

This can be written as:

$$Q^* = q_{hc} + q_v + q_{jt} + q_i \quad (B-11)$$

These terms will be discussed in turn, and then the equations will be solved to give the minimum operating temperature.

### B.2.1. Heat conduction in the capillary.

The heat conduction process via the Gorter-Mellink conduction, was described in Section B-1. This process is usually the dominant one, however, at low temperatures and high velocities it can be negligible. At all temperatures, the direct "phonon" conduction process is available. In the phonon conduction mode the helium II can be treated as an "insulating"

crystal. In this regime the heat conduction is a function of temperature, pressure, and "size". The size effect is well known for crystals at low temperatures. Measurements of the thermal conduction of helium II in tubes is shown in Figure B-8. The low temperature results are for the "phonon" mechanism. At higher temperatures, other mechanisms are available, and the conduction rapidly increases.

For the purpose of this study, we will use the phonon heat conduction as the only heat conduction mechanism. This will underestimate the heat conduction, but it will allow a closed form solution to the problem. The experimental results can be approximately represented by ( $T \leq 0.6$  K):

$$k_{\text{HeII}} = 300 d T^3 \text{ kW/m}^2 \cdot \text{K}^4 \quad (\text{B-12})$$

This form is based on the assumption that the thermal conduction is limited by boundary scattering, and that the mean free path is equal to the tube diameter. In this analysis, the thermal conduction is directly proportional to the speed of sound in the material. Therefore, the pressure dependence of  $k$  is just the pressure dependence of the speed of sound. Therefore,

$$k(P) = k(0) \frac{c(P)}{c(0)} \quad (\text{B-13})$$

The speed of sound as a function of temperature and pressure can be obtained from the NBS Helium Properties Program.

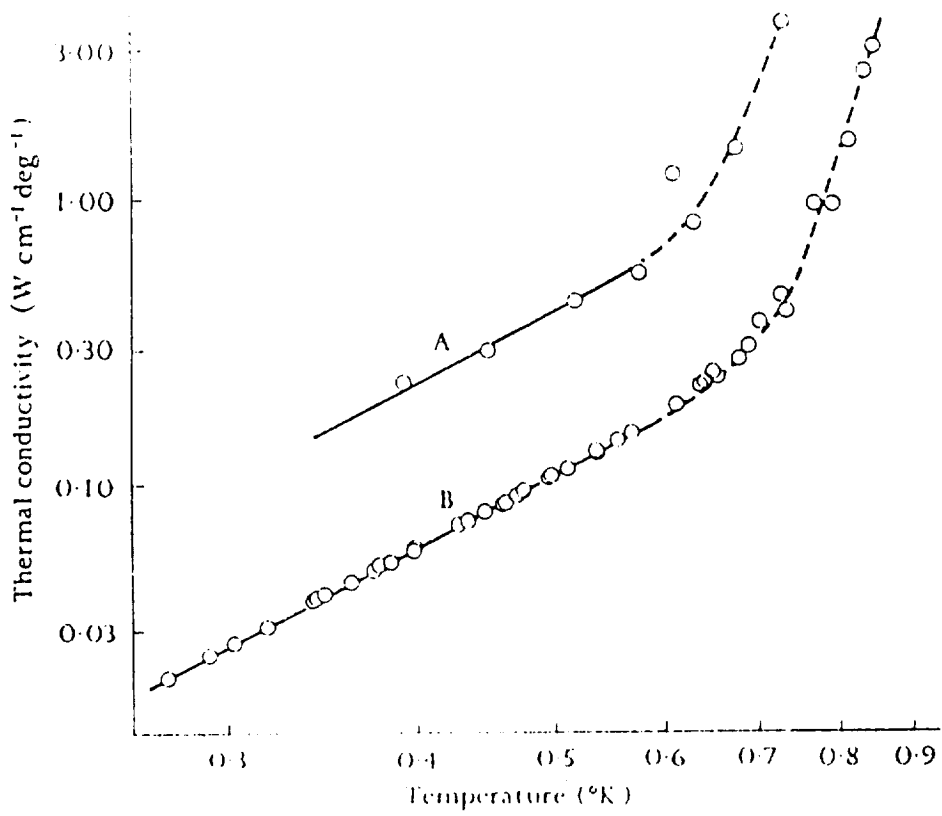


Figure B-8 Thermal conduction of helium II in tubes as a function of temperature and tube diameter, (A:0.8 mm dia., B:0.29 mm dia.).

### B.2.2. Viscous heating in capillary.

The friction loss of the helium flowing along the capillary will be converted to heat. The loss can be calculated from:

$$q_f = fLu^2/2d \quad (B-14)$$

The friction factor,  $f$ , will have the following forms

$$\begin{aligned} f &= 64/Re & Re < 2000 \\ f &= 0.316 Re^{-1/4} & 2000 < Re < 20,000 \\ f &= 0.184 Re^{-1/5} & Re > 20,000 \end{aligned}$$

$$Re = \rho u d / \eta \quad (B-15)$$

From the form of the equations we expect this effect to be important at high velocities. From the experimental work, we know that the flow velocity is in the range of  $25 \leq u \leq 100$  cm/sec.

The viscosity of helium II at temperatures below 0.9 K is rapidly increasing with temperature reduction. The form of the equation is complicated, but for temperatures below 0.65 K, it can be approximated as:

$$\eta = 16 \times 10^{-6} / T^2 \quad \text{MKS units (T < 0.65 K)} \quad (B-16)$$

Taking representative values ( $d = 0.2$  mm,  $Re = 20,000$ ,  $u = 1.0$  m/sec), we find that the heat generated in the capillary is:

$$Q_f = 5.8 \times 10^{-6} \text{ watt}$$

Clearly, this is not large enough to affect the vortex cryocooler, so we can assume that frictional heating in the capillary is negligible.

### B.2.3. Joule-Thomson Effect in Helium-II

The Joule-Thomson coefficient of a fluid is defined as:

$$j_m = (dT/dp)_h \quad (B-17)$$

It can be calculated from the thermodynamic identity:

$$j_m = (\alpha T - 1) / \rho C_p \quad (B-18)$$

where  $T, \alpha, \rho, C_p$  are the temperature, thermal expansion coefficient, bulk density, and specific heat at constant pressure respectively. The values of  $j_m$  for liquid He II have been calculated by Huang (1986). For temperatures below 1.3 Kelvin,  $\alpha T$  then becomes negligible, and the coefficient becomes:

$$j_m = - 1/\rho C_p \quad T < 1.3 \text{ K} \quad (B-19)$$

Since the density of He II is roughly constant in this temperature range, the JT coefficient is just proportional to the inverse of the specific heat at constant pressure. The specific heat values become very small at low temperatures, so this coefficient can become large. Also, it is always negative so the He II tends to heat in a flow process.

The specific heat values of He II have been measured by Greywall (1978). An expression that fits the data over the range  $0.2 \text{ K} < T < 1 \text{ K}$  and  $P_{\text{sat}} < P < 25 \text{ atm}$  is given. The equations have been incorporated into the National Institute of Standards and Technology data base program for helium properties. The subprogram is also available in a stand alone version called "Greywall".

#### B.2.4. Heat Balance Equation

The heat balance in the "mixing" chamber of the vortex cryocooler can be written as

$$TVS = q_{\text{cap}} + q_i \quad (\text{B-20})$$

That is, the cooling due to the mechano-caloric effect is balanced by the heat flow for the capillary and by direct applied heat inputs. We have shown that the heat input due to internal convection in the capillary is very small with high flow velocities. Also, viscous heating flow are also negligible. Therefore, the primary source of heat is due to the Joule-Thomson effect in the capillary. This heat flow is proportional to the temperature gradient.

$$Q/A = k \nabla T \quad (\text{B-21})$$

However, from the Joule-Thomson effect, we know that the temperature gradient is proportional to the pressure gradient. This can be written as:

$$Q/A = k (dT/dP)_h / (dP/dx)_h \quad (\text{B-22})$$

For the experimental situation, the flow in a capillary should be isenthalpic, as indicated.

The form of  $k$  was given in part B.2.1. of this section. The form of the Joule-Thomson coefficient was given in part B.2.3. The pressure drop can be calculated from:

$$dP/dx = (f\rho u^2/2d) \quad (B-23)$$

The friction factor,  $f$ , was given in part B.2.2. Experimentally, the friction factor has been found to be constant, rather than displaying the weak dependence of Reynold's number given in part B.2.2. Therefore, we will assume a constant value of  $f = 0.02$ . The terms can now be collected:

$$m T_a S_a = (3 \times 10^5) (dT^3 A_C) (1/\rho C_p) (0.02 \rho u^2/2d) + Q_i \quad (B-24)$$

The term on the left is simplified by the assumption that:

$$\nabla S = S_a - S_0 = S_a \quad (B-25)$$

$S_0$  is the entropy of the superfluid component entering from the superleak, and it is very small. Therefore, it is reasonable to neglect its contribution.

Using  $m = \rho u A_C$ , the equation can be rewritten as:

$$T_a S_a = [3 \times 10^3 (T_a^3 u) / (\rho c_p)] + Q_i/m$$

If we assume that  $Q_i$  is zero, then:

$$(S_a C_p / T_a^2) = 3 \times 10^3 (u/\rho) \quad (\text{B-26})$$

This places all the quantities that are functions of temperature on the left. Both S and C can be approximated by simple power law expressions.

$$\begin{aligned} S &= 1.78 T^{5.57} \text{ J/kg}\cdot\text{K} \\ C &= 1.01 \times 10^2 T^{6.56} \text{ J/kg}\cdot\text{K} \end{aligned} \quad (\text{B-27})$$

If we assume that  $u = 1.0$  m/sec, then:

$$T_a = 0.81 \text{ Kelvin}$$

The observed minimum temperature of the vortex cooler is roughly in the 0.7 Kelvin range. The very simple model developed above has been able to account for the experimental result, with no arbitrary assumptions. Note, also, that the temperature rises with higher velocities in keeping with the experimental results.

#### B.2.5. Pressure Effects in the Vortex Cryocooler

Sato et. al (1982) have found that the minimum temperature of the vortex cryocooler decreases with increasing background pressure, e.g., the pressure drops are not changed, just the background pressure. It would be a confirmation of the theory if we could predict the observed change. There are substantial problems that make this very difficult. The excitation spectrum of He II is a function of pressure, the "crossover" point where the behavior changes from "roton" domination to "phonon" domination changes, as does the

magnitude of the two mechanisms. This means that "kinks" develop in the temperature dependence and we are no longer able to get simple power law fits to the parameters.

To approach this problem, we have started from the specific heat fit equation given by Greywall (1979). The entropy values were obtained by integration of the specific heat equation

$$S = \int \frac{C}{T} dT \quad (B-28)$$

The Greywall fit equations already include a formula for the density as a function of pressure. The thermal conductivity is corrected for pressure according to eqn. (B-13). Rather than using a constant friction factor, we used eqn. (B-15), with viscosity values given by eqn. (B-16). The resulting equation was rearranged to put all functions of T and P on the left, and all constants and functions of velocity and channel diameter on the right. Thus the equation had the form

$$\Xi(T,P) = \Phi(u,d)$$

The two functions are solved numerically, using the programs developed above. The functions are plotted, and the actual solutions (Minimum Temperatures) are taken from the charts.

An example calculation is illustrated in Figure B-9. The line  $\Phi = 10980$  corresponds to a velocity of 1 m/sec and a capillary diameter of 0.1 mm. The  $\Phi = 8814$  line corresponds to a velocity of 1 m/sec and a capillary diameter of

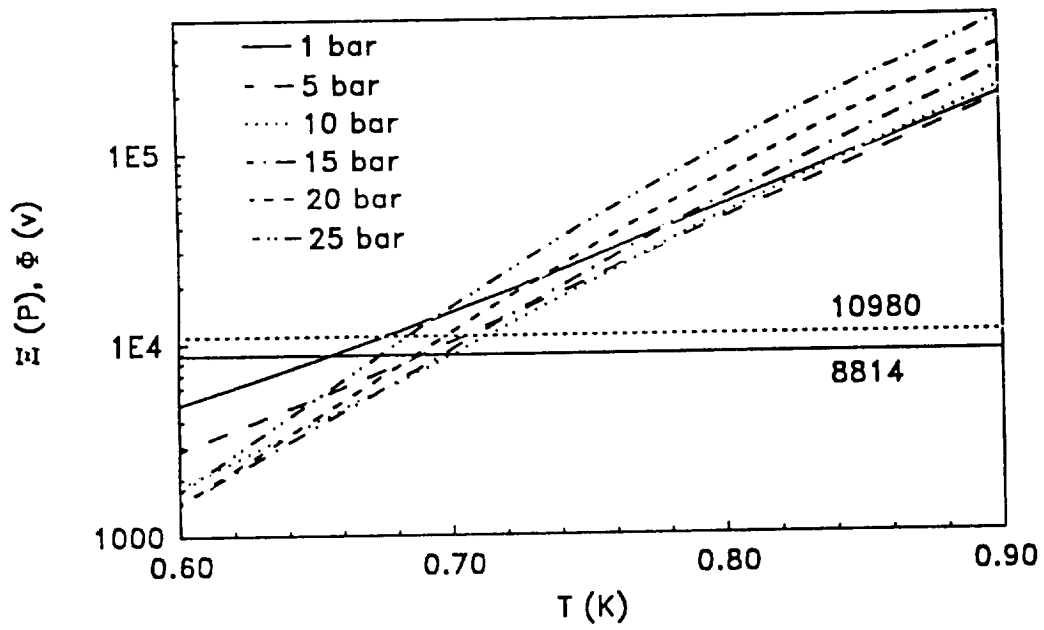


Figure B-9 The functions  $\Xi(T,P)$  and  $\Phi(u,d)$  as a function of temperature (quantities defined in text).

0.3 mm. An expanded scale version of the same situation is given in Figure B-10.

The two examples chosen above corresponds to the two capillaries used by Satoh, et al. (1986). A comparison of the predictions and the experimental results are shown in Figure B-11. The fit is reasonable, considering the number of approximations involved. However, we estimate that the primary source of error is in the form of the thermal conductivity equation. The experimental values given in Figure B-8 only fit the form used below 0.6 K. We note that the agreement is better at the lower temperatures. The higher temperature results are bound to have a different form and a different dependence of T and P than the low temperature results.

The diameter dependence in Figure B-11 is only due to the pressure drop equation. However, we know that the mean free path is temperature dependent, and that this dependence is not included in the thermal conductivity equation. This is another source of error.

The temperature as a function of position along the capillary has been measured by Satoh et al. (1986). The above analysis shows that the heating is greatest at the lowest temperatures. Thus, this effect will be most pronounced at the entry of the capillary. This is confirmed by experiment. The temperature gradient along the capillary is uniform for relatively low velocities. At high velocities, the entire temperature drop exists over a short region at the entrance of the capillary. A further confirmation comes from experiments with the bath cooled to 0.4 Kelvin. Even though the exit of

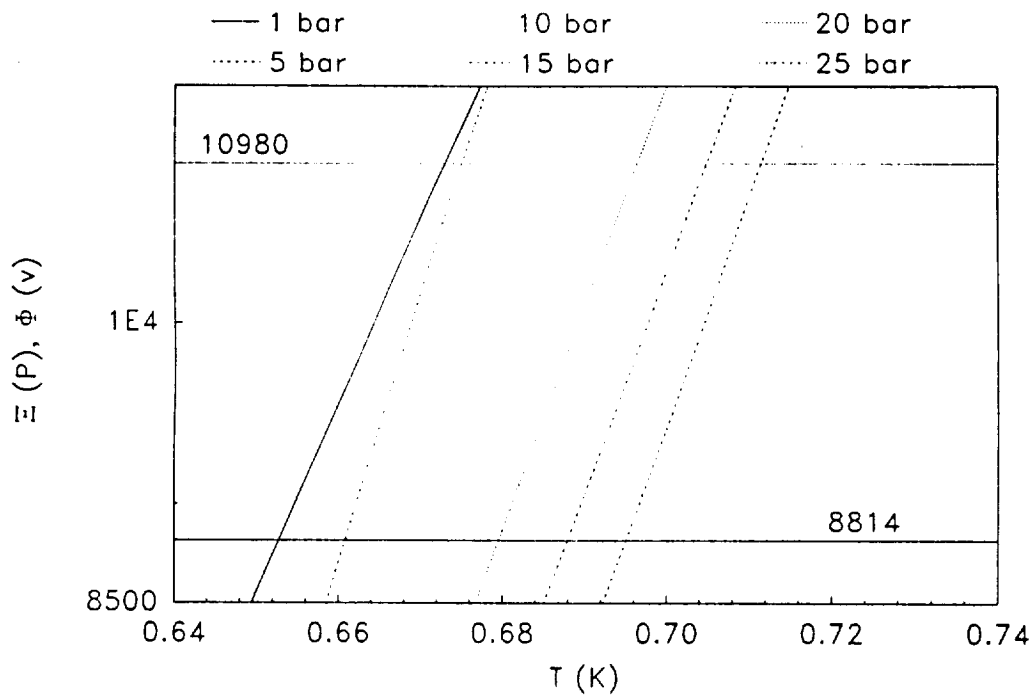


Figure B-10 An expansion of the graph given in Figure B-9 to show the intersection region.

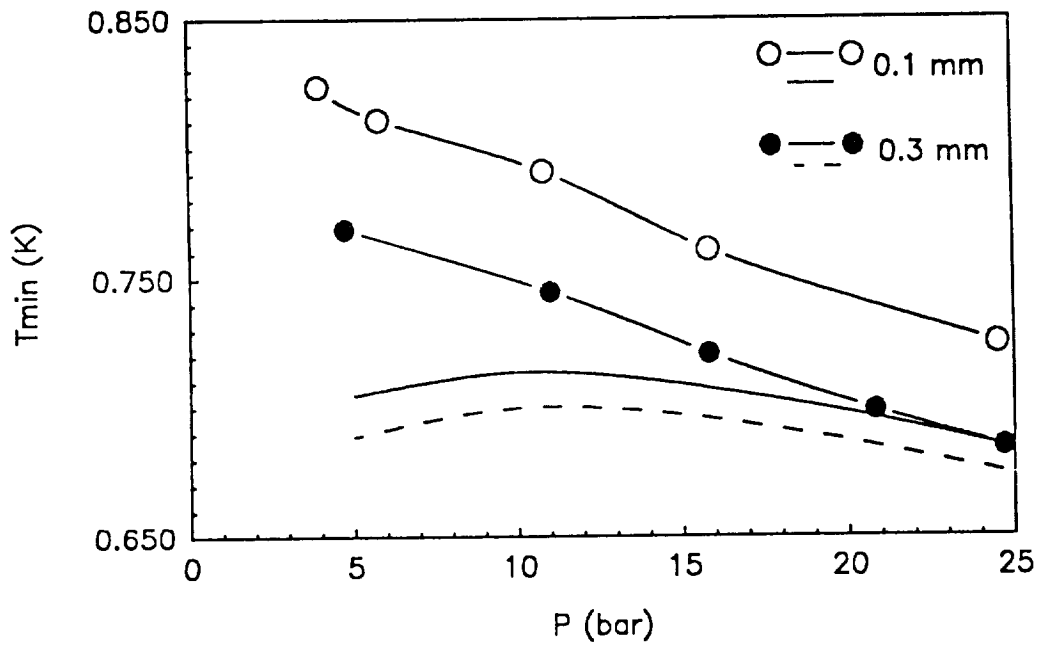


Figure B-11 A comparison of the experimental results of Satoh et al. (1986) and the theoretical predictions.

the capillary is at 0.4 Kelvin, the Joule-Thomson effect always brings the entrance to roughly 0.7 Kelvin.

### B.3 Summary of Theory and Comparison with Experiment

A typical  $T_A$  vs.  $u$  chart is shown in Figure B-3. The three principal operating regimes are identified. In regime I, the capillary flow is laminar, and the thermal resistance of the He II in the capillary is relatively small. Since the velocity is low, the mass flow is small, and the cooling effect is small. Thus, in regime I there is almost no cooling effect.

In regime II the flow in the capillary is in the "Gorter-Mellink" regime. The thermal resistance of the internal convection mode is rising with velocity. In addition, the forced convection due to the net mass flow also increases the thermal resistance. The increasing mass flow causes an increasing cooling effect, but the lower temperature means that the entropy change per unit mass flow is smaller. In this regime we expect the temperature to monotonically decrease with increasing velocity.

In region III, the increasing pressure gradient in the capillary generates increasing heating due to the Joule-Thomson effect. This effect will create increasing heating with increasing velocity.

The vortex cooler is a useful device, when operated in its effective range. At low pressures, a temperature of 0.8 Kelvin is easily reached, with a cooling load of a few hundred microwatts. By raising the pressure to 25

atm, the operating temperature can be pushed down to roughly 0.7 Kelvin with the same cooling load. Some other general observations include:

- i. Small capillaries (approx. 0.1 mm) have higher minimum temperatures, lower cooling loads, and slower time constants.
- ii. Large capillaries (approx. 0.5 mm) have lower minimum temperatures, higher cooling loads, and faster time constants. However, the larger units require more drive power to supply the superfluid flow.

## APPENDIX C

### Test Facility

The test facility is comprised of several components. These components include; gas handling system, cryostat and instrumentation. A description of each component is included in the following sections. Operating experience is also discussed.

#### C.1 DESIGN

A major concern in the overall design is to ensure long term leak-free operation. Welded stainless steel construction was used wherever feasible. If welding was impractical, components were brazed, as when joining Cu to stainless steel. The use of PbSn solder was limited mainly to electrical wiring, although it was used to plug a vacuum leak that developed in the  $^4\text{He}$  pot late in the contract period.

##### C.1.1 Gas Handling System

This system is used to contain a supply of  $^3\text{He}$  gas and to move it around where needed. As the cost of  $^3\text{He}$  is approximately \$150 per standard liter there is also a financial incentive for keeping the system leak tight. Figure C-1 contains a schematic of the system. There are two gas panels, each panel controls the flow from a separate reservoir of  $^3\text{He}$ . The two panels are connected together through a Metal Bellows Corporation model MBC-135 bellows pump, so that  $^3\text{He}$  can be moved between reservoirs.

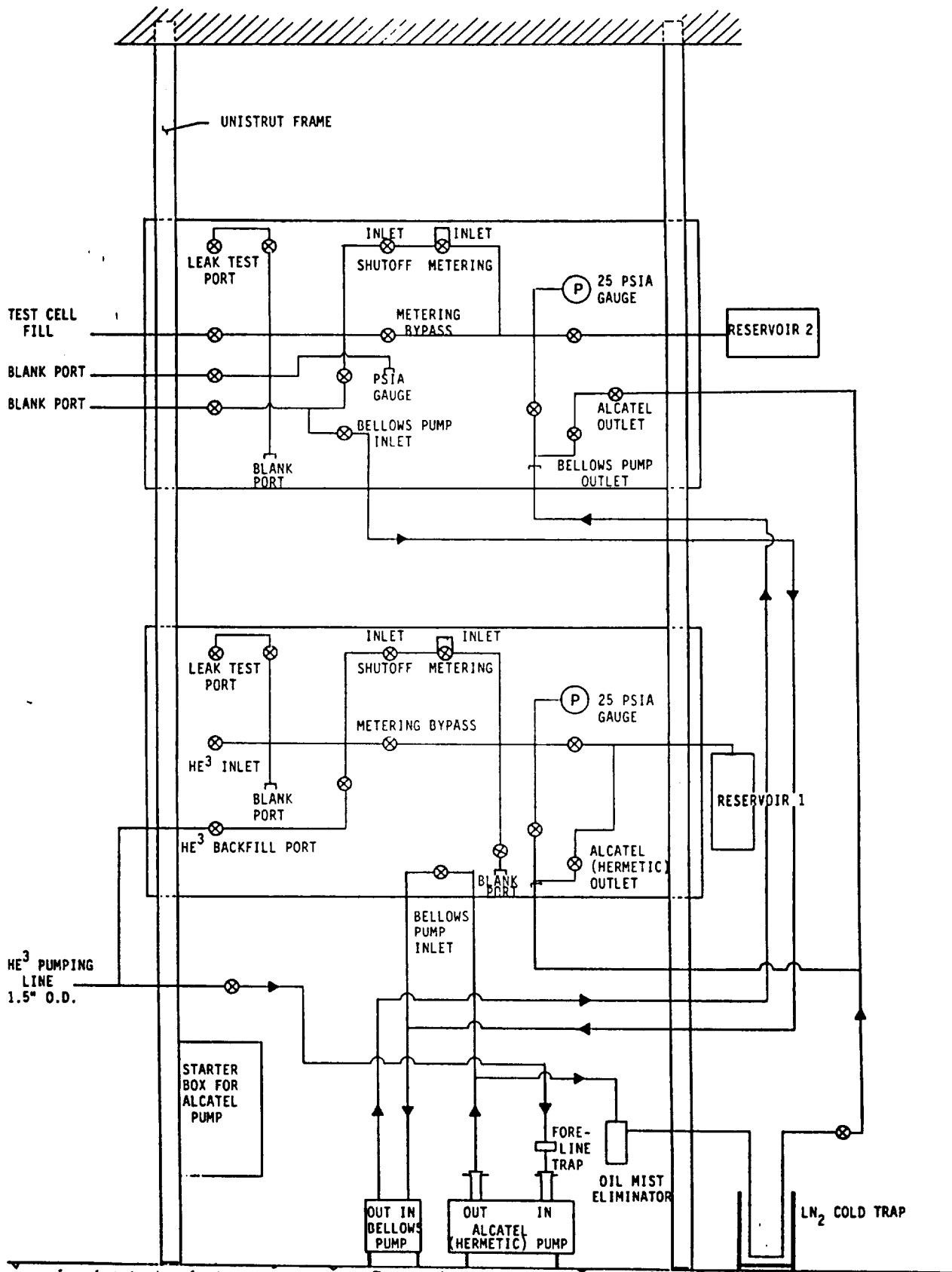


Figure C-1 Gas Handling System. Reservoir #1 feeds the  $^3\text{He}$  pot. Reservoir #2 contains  $^3\text{He}$  for loading into the test cell.

The valves on the gas panels are Nupro model SS-4D4L-V51 packless metal diaphragm valves with VCR fittings. When a valve fails, usually from an overtightened seat, it can be repaired and reinstalled without having to cut out any welded sections. We use Ag plated Ni gaskets and have had no trouble with the VCR fittings.

Gas panel No. 1 is used to control the  $^3\text{He}$  input to the  $^3\text{He}$  pot on the cryostat. An Alcatel model 2033H hermetically sealed two-stage rotary pump is used to pump on the  $^3\text{He}$  pot. This panel is operated at 5.9 psia for two reasons. If the Alcatel pump is operated above 7.3 psia, some leakage develops in the seals. Also, if a leak does develop, say for example in the reservoir, air leaks into the system and the  $^3\text{He}$  stays put. The resulting mixture can be purified by running it through a 4 K bath and freezing out all contaminants. Operating above atmospheric pressure would result in the  $^3\text{He}$  venting to the atmosphere.

The pumping line on the inlet of the Alcatel pump is a 1.5" O.D. stainless tube. There are 1.5" high vacuum valve is on the inlet and outlet of the pump, to isolate it when performing maintenance or repairs. The demountable connections use conflat, to prevent unintended removal possible when using quick flange type fittings. The pumping system is provided with a foreline trap on the inlet and an oil mist eliminator filter and  $\text{LN}_2$  trap on the outlet.

Gas panel No. 2 is used to meter quantities of  $^3\text{He}$  into the dilution test cell. Only small amounts of  $^3\text{He}$  are consumed per run. The resulting  $^3\text{He} - ^4\text{He}$  mixture is allowed to vent to the atmosphere as the dilution test cell

warms up. This reservoir was initially filled with  $^3\text{He}$  at a pressure of 21.5 psia.  $^3\text{He}$  is thus loaded into the test cell by the pressure differential between reservoir No. 2 and the test cell, which is loaded with  $^3\text{He}$  while at a temperature of 1.1 K.

Two types of pressure sensors were installed on the gas panels. Each panel has one absolute pressure sensor (0-25 psia, Setra model 204) and one differential pressure sensor (0-  $\pm$  30" W.C., Setra model 239). We experienced difficulty in making a leak free connection to the reference pressure port on the differential sensor. The fitting was an anodized aluminum female pipe thread connection. Teflon tape, epoxy and an aluminum solder were tried without success. We determined that the absolute pressure sensor had enough resolution so that we could operate without the differential pressure sensor. The gas panel port for this sensor was then plugged.

### C.1.2 Cryostat

The cryostat is designed to fit inside a 7.5" I.D. by 42" deep magnet dewar. A 3" thick Al hex flange mounts on top of the dewar, providing additional feedthroughs. A relief valve, cracking pressure set to 1 psig, is mounted on this flange along with a 3/4" ball valve. The cryostat mounts on top of the hex flange. An illustration of the cryostat is shown in Figure C-2.

There are three pumping lines, one each for the vacuum can,  $^4\text{He}$  pot and  $^3\text{He}$  pot, running through the top flange. Both lines for the helium pots are 1.5" O.D., the vacuum can pumping line is 2" OD. A hermetic 32 pin

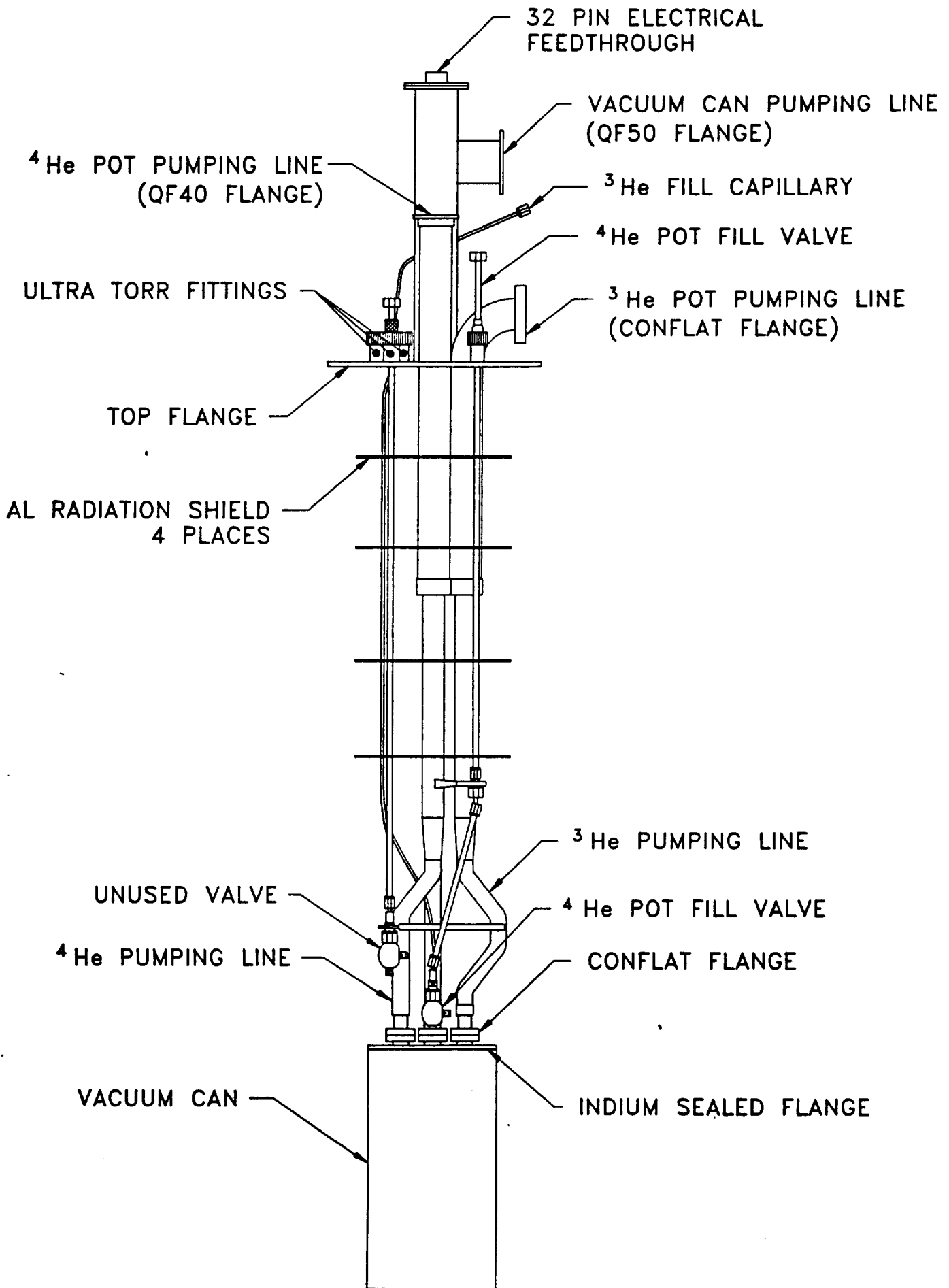


Figure C-2 Schematic Layout of the Cryostat.

feedthrough is mounted onto the tee of the vacuum can line. Instrumentation leads are run through this line, avoiding cold feedthroughs. The pumping lines are graded inside the dewar; starting at 1.5" O.D. at the top flange, they are reduced to .75" O.D. on top of the vacuum can lid. As shown in Figure C-2, the lines are offset through 45° ell fittings, forming a light trap to keep room temperature thermal radiation from impinging directly into the liquid pots and the vacuum can. Additional feedthroughs on the top flange are through Cajon Ultra-Torr fittings. The liquid helium level detector,  $^3\text{He}$  filling capillary and liquid helium transfer line run through these fittings. Unused ports are blanked off with brass plugs. Four Al radiation shields, anchored to the pumping lines keep thermal radiation from the top flange from impinging on the liquid helium in the dewar.

The liquid pots are insulated from the 4 K bath by a vacuum can. Its dimensions are 6" O.D. by 11.5" high. Figure C-3 shows the configuration inside the vacuum can. Copper cold fingers are welded into the vacuum can lid to provide 4 K heat sinks (not shown). The  $^3\text{He}$  and  $^4\text{He}$  pumping lines, 3/4" O.D. by .012" wall thickness, are welded to the top of the vacuum can lid and are brazed to the top of the  $^4\text{He}$  pot. The  $^3\text{He}$  pumping line runs through the  $^4\text{He}$  pot and out the bottom, where it is brazed in place. The  $^3\text{He}$  pot connects to the pumping line with an indium sealed flange. Conflats and VCR fittings are welded to the top and bottom of the  $^4\text{He}$  pot. Note that these are stainless steel to Cu welds. These welds have been very robust, no leaks have developed in the course of our work.

Both helium pots were fabricated out of 101 alloy Cu. The  $^4\text{He}$  pot was built in three pieces; the top, bottom and body are separate. After welding

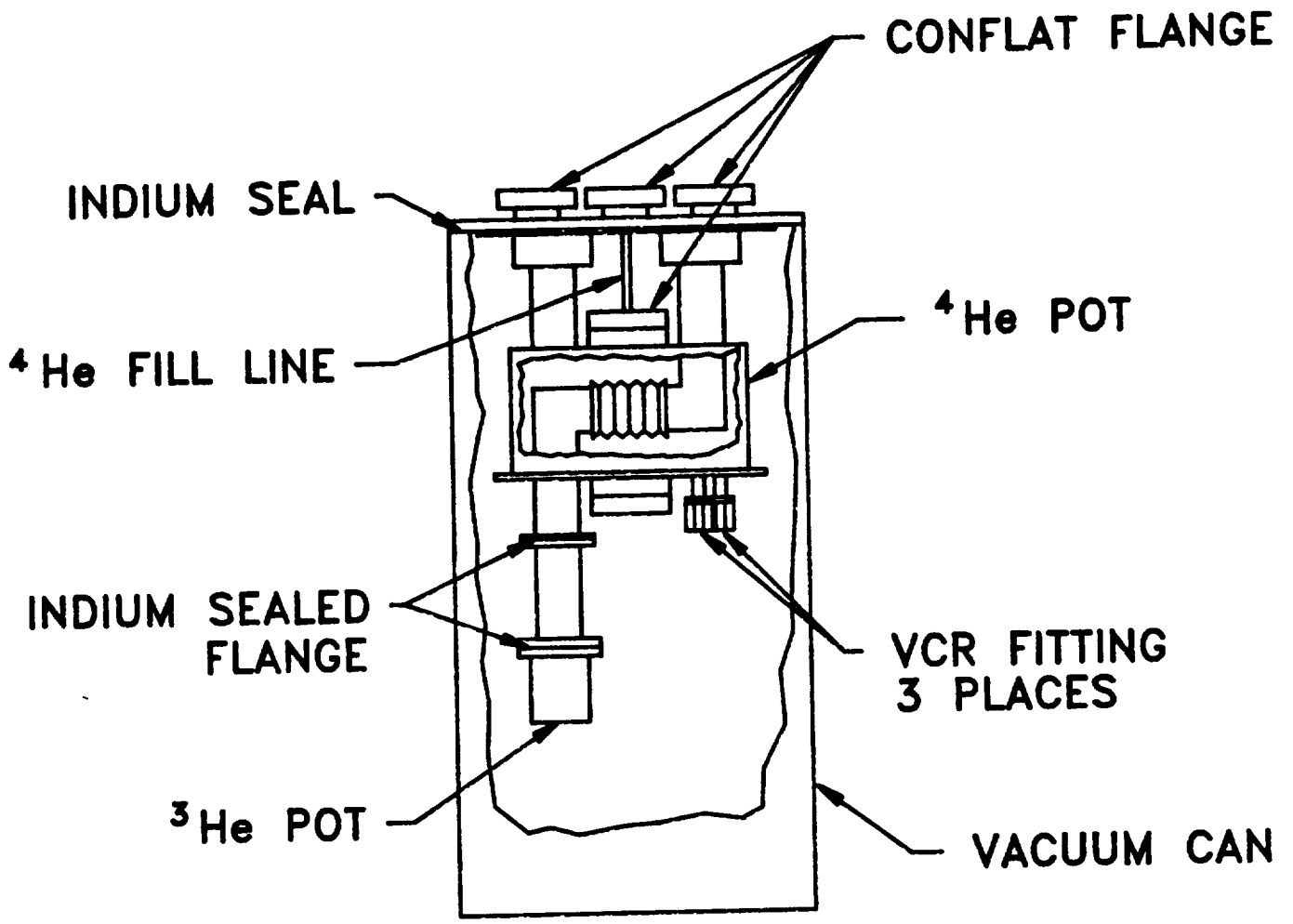


Figure C-3 Configuration of  $^4\text{He}$  pot and  $^3\text{He}$  pot and pumping lines.

the fittings in place in the top and bottom, the lids were brazed in place to the body. Initially, some leaks were present, but were sealed with PbSn solder. There were no further leak problems until late in the contract period when modifications to the  $^4\text{He}$  pot were deemed necessary. The  $^3\text{He}$  pot has a lid, into which was brazed a .75" O.D. pumping line, and a chamber. The lid and chamber are sealed with In. The bottom of the chamber has tapped mounting holes for attaching and thermally anchoring the test cell to the  $^3\text{He}$  pot. There have been no leaks associated with the  $^3\text{He}$  pot and pumping line.

### C.1.3 Instrumentation

Several types of thermometers are used when running the cryostat. The  $^4\text{He}$  pot temperature can be regulated with a Lake Shore Cryotronics model DRC-81C temperature controller. An uncalibrated Si diode is the sensor input to the controller. Although the sensitivity of Si diodes decreases for  $T < 1.8$  K, it is adequate to regulate the  $^4\text{He}$  pot.

Calibrated Ge sensors were used to calibrate some thick film chip resistors. The chip resistors are very small and have good sensitivity for  $T < 3$  K, Li et al. (1986). The film resistors are placed in several locations on the dilution test cell. Mounting Ge resistors is impractical due to their relatively large size. In Figure C-4, the calibration of film No. 1 is displayed. Two different types of fits are compared to the calibration data. For  $T \leq 0.9$  K, we calculate temperature from the equation

$$T = \left( \frac{B}{\ln R-A} \right)^4$$

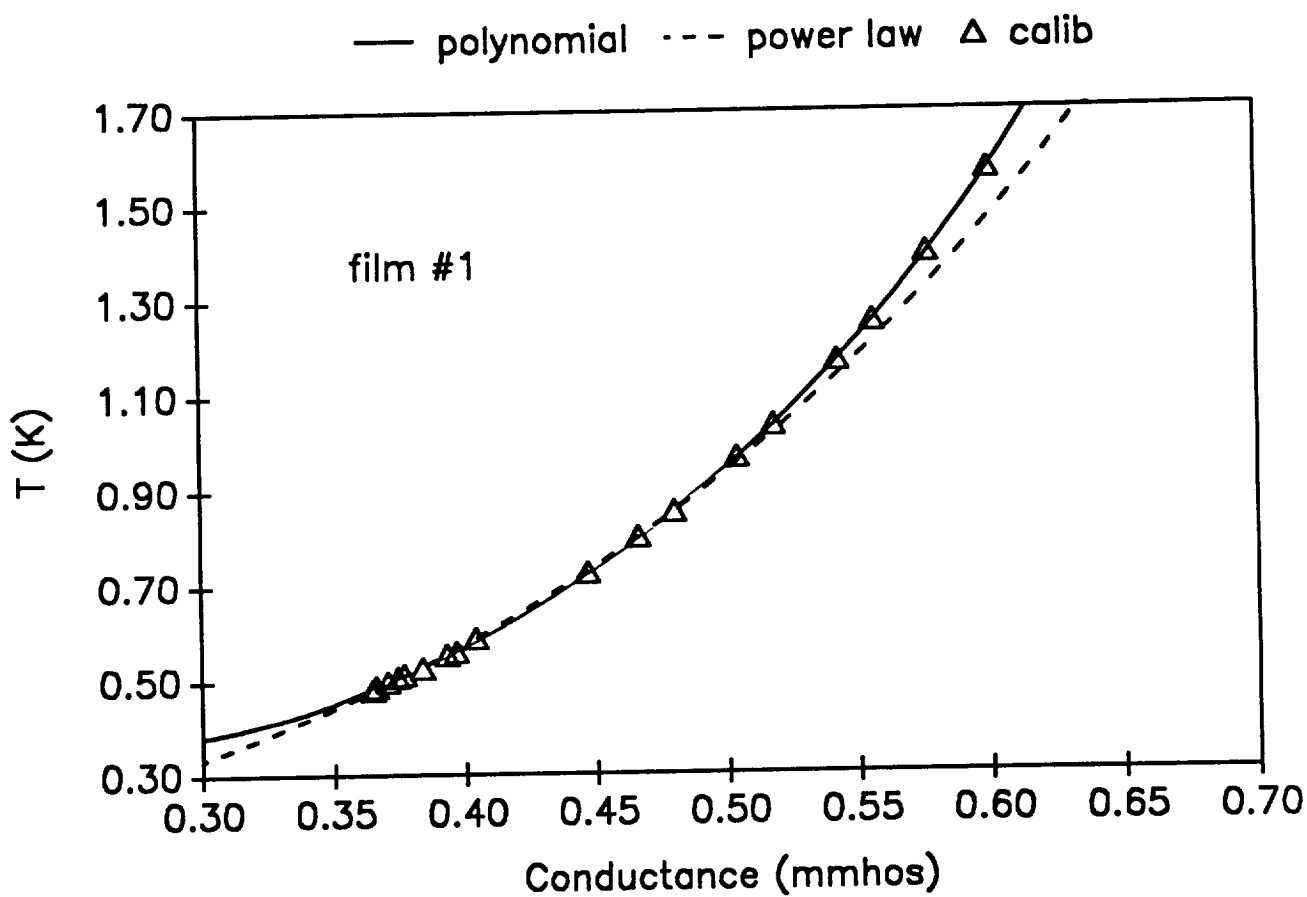


Figure C-4 Comparison of different fits to film resistor #1.  $\Delta$  calibration data — polynomial approx. ----  $T^{-\frac{1}{2}}$  power law.

where A and B are fit parameters and R is the film resistance. This equation is the form as reported in Li et al. (1986). Some experimental data were later taken below 0.47 K, which is the lowest temperature reached during the calibration run. This formula has some experimental justification for extrapolating the film resistor's behavior beyond the calibration range.

For  $T > 0.9$  K, a polynomial approximation is used

$$\ln T = \sum_{i=0}^4 a_i (\ln R - 7.55)^i$$

where the coefficients,  $a_i$ , are fit parameters.

Temperature sensors are read with a Biomagnetics Technology Inc. model 1000 conductance bridge. The excitation voltage is 100  $\mu$ V. At this excitation level, sensor self heating has not been observed. All conductance measurements are made using the 4-wire method. The AC excitation voltage of the bridge eliminates contributions from thermal emfs.

## C.2 OPERATION

The basic operation of the test facility is considered. Leak detection, cooldown procedure and baseline operating characteristics are described.

### C.2.1 Leak Detection

The most sensitive way to leak check the cryostat is with it mounted in the dewar. With the vacuum can in place (the indium seal having been

previously leak checked), the  $^3\text{He}$  pot,  $^4\text{He}$  pot and vacuum can are evacuated with the high vacuum system. The leak detector is hooked to the  $^4\text{He}$  pot and a small quantity of helium gas is admitted to the vacuum can. If the leak rate does not change over a period of 15 minutes, the  $^4\text{He}$  pot is leak free. The leak detector is connected to the  $^3\text{He}$  pot and helium is admitted to the  $^4\text{He}$  pot. The entire  $^3\text{He}$  pumping line is thus leak checked.

Having the vacuum can evacuated is essential for leak checking the dilution test cell. As the test cell uses a fountain pump to flow  $^4\text{He}$ , there are three superleaks in series, resulting in a very large flow impedance. During leak testing, the leak detector also pumps on the  $^3\text{He}$  fill capillary. By evacuating the vacuum can, much lower background signal is present in the leak detector when a leak is present. Adding helium gas to the vacuum would then produce a noticeable increase in the leak detector signal. Unfortunately, this method does not pinpoint the leak location so further work is required. However, it is the best way to determine if a leak is present.

### C.2.2 Cooldown

If the cryostat leak checks OK, the cryostat is pre-cooled with  $\text{LN}_2$ . The helium gas in the vacuum can from the leak test remains and acts as a heat exchange medium. One problem with using  $\text{LN}_2$  to pre-cool the cryostat is that  $\text{LN}_2$  collects in the packing of the  $^4\text{He}$  fill valve. Once the  $^4\text{He}$  pot temperature, as read from the temperature controller, is near 80 K, the remaining  $\text{LN}_2$  is blown out with helium gas. The  $^4\text{He}$  pot is pressurized with helium to about 4 psig and the fill valve is then opened. The helium flowing through the valve boils off any  $\text{LN}_2$  in the stem. We then proceed to transfer

LHe in the normal manner. When the  $^4\text{He}$  pot temperature reads  $< 5$  K, the exchange gas is pumped out. The vacuum can is pumped out overnight to ensure a good quality vacuum is attained.

### C.2.3 Baseline Operation

In order to be able to run for long period of time, the  $^4\text{He}$  pot was designed with a continuous fill line. A temperature of 1.4 K was reached with the fill capillary .020" I.D. by 10" long with a .018" diameter wire slid inside. The pot temperature increased slowly for about 90 minutes at which point the temperature rose rapidly to  $T_\lambda$  (2.17 K). We assume the  $^4\text{He}$  pot had emptied. The fill valve was then opened, refilling the pot and subsequently the  $^4\text{He}$  pot was pumped down to 1.4 K again. This  $^4\text{He}$  pot behavior was not ideal, but was sufficient for some data collection at 1.4 K.

We attempted to run the  $^3\text{He}$  pot to cool the test cell below 0.6 K. Initially the test cell cooled, however, there was a very long time constant associated with cooling down the test cell with the  $^3\text{He}$  pot. The major difficulty was with the temperature fluctuations in the  $^4\text{He}$  pot. Refilling the  $^4\text{He}$  pot caused the test cell to warm. The end result was that we could not cool the test cell below 0.88 K.

To remedy this situation, a shorter continuous fill capillary was installed. The drawback to this change was a higher  $^4\text{He}$  pot temperature. It ran at 1.7 K instead of 1.4 K. Very strong temperature oscillations also occurred. The  $^4\text{He}$  pot temperature increased to  $T_\lambda$  and then decreased to 1.7 K

in a period of about ten minutes. We attributed this effect to film flow up the pumping line.

To eliminate these thermal oscillations, an orifice was installed into the pumping line at the top of the  $^4\text{He}$  pot. This was a major modification to the cryostat and entailed cutting into the pumping line and brazing the orifice into place. Unfortunately, the brazing opened up several leaks on the lid of the  $^4\text{He}$  pot. As this occurred close to the end of the contract period, an intense period of leak chasing the  $^4\text{He}$  pot began. Eventually, the leaks were closed. In Figure C-5, the temperature vs. time behavior of the  $^4\text{He}$  pot is compared before and after the orifice was installed. The thermal behavior is substantially improved.

#### C.2.4 Thermal Analysis - $^4\text{He}$ Pot

Heat inputs to the cryostat come from a variety of sources. Conduction and radiation are the two principal heat transfer mechanisms. Convection is eliminated by the vacuum can. The estimated heat loads are compared to actual cryostat performance.

##### Electrical Leads

A total of 32 wires run from the room temperature feedthrough to solder tabs mounted on the side of the  $^4\text{He}$  pot. Where the leads enter the vacuum can, they are wrapped around a Cu cold finger for thermal anchoring at 4 K. The wires are;

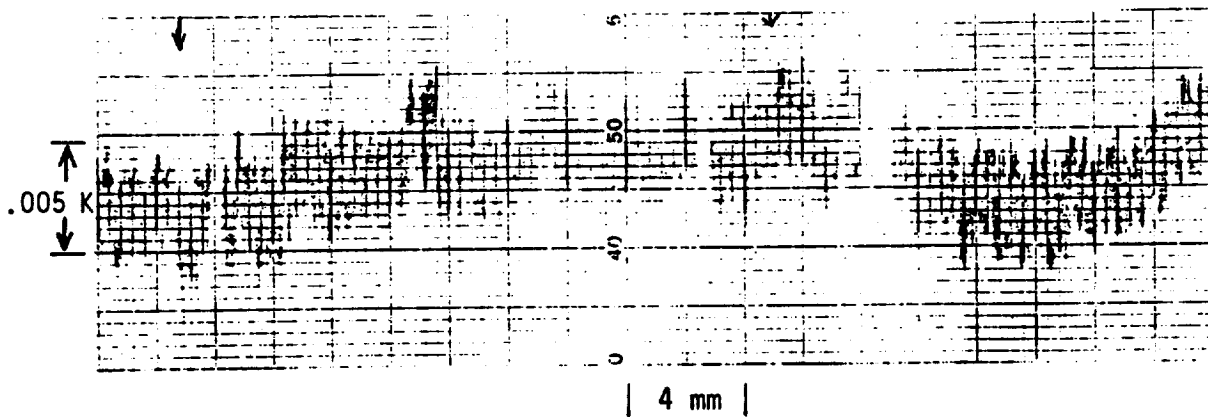
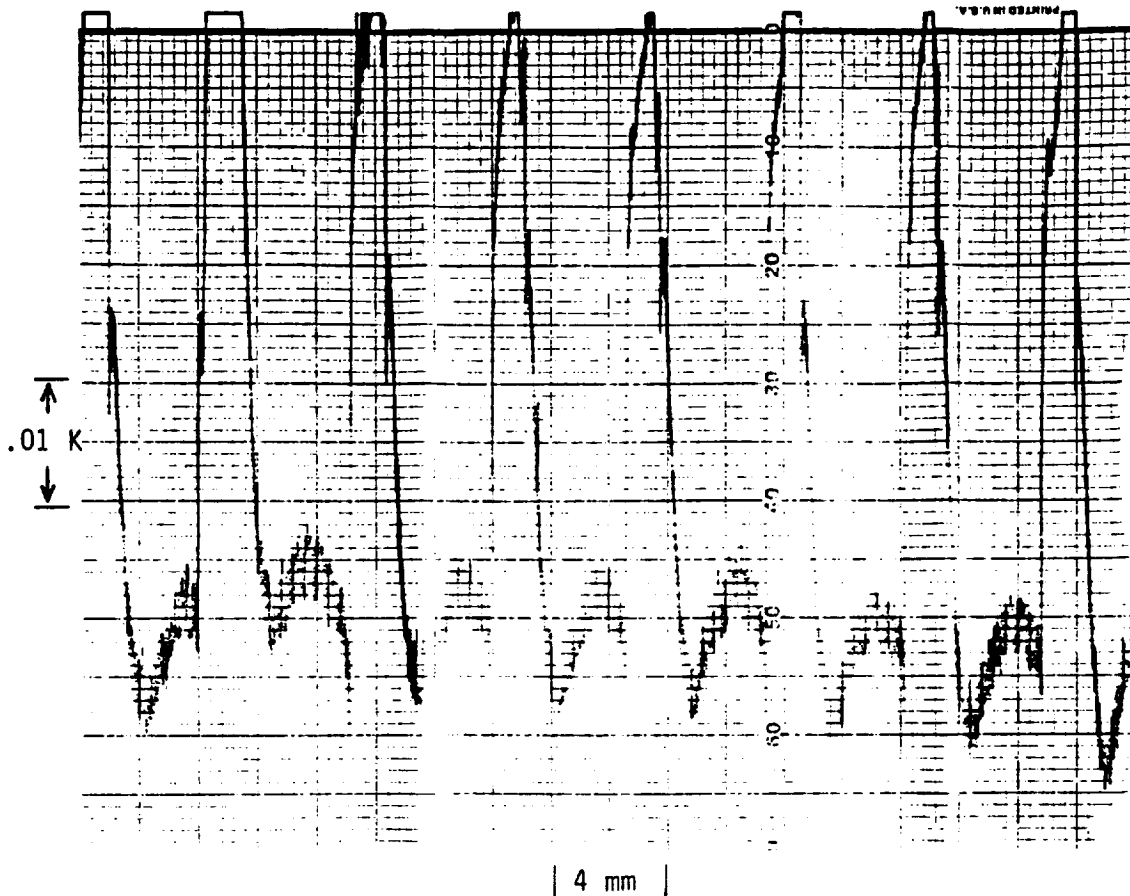


Figure C-5 The upper trace shows the steady state temperature behavior of the unmodified  $^4\text{He}$  pot. The lower trace shows the behavior after the orifice was installed in the pumping line.

<u>No. Wires</u>	<u>Composition</u>
28	No. 36 AWG Manganin
2	No. 36 AWG Cu
2	No. 32 AWG Cu

The overall length of the wires between the 4 K cold finger and the feedthrough is 153 cm. The conduction heat leak, as estimated from White (1979), for each group of wires is;

	<u>Q(mW)</u>
28 - No. 36 AWG Manganin	1.2
2 - No. 36 AWG Cu	7.1
2 - No. 32 AWG Cu	.49

- Structure

In addition, there are conduction loads from the <sup>4</sup>He and <sup>3</sup>He pumping lines and the <sup>4</sup>He fill capillary. These contributions are estimated to be

	<u>Q(mW)</u>
Pumping line	0.90
Fill capillary	.05

The estimated thermal radiation load on the 4 K pot is

$$Q_{\text{rad}}(4 \text{ K} - 1 \text{ K}) \approx 3 \times 10^{-8} \text{ W}$$

### C.2.5 Thermal Analysis - <sup>3</sup>He Pot

To keep the heat load on the <sup>3</sup>He pot as small as possible, the instrumentation leads running from the <sup>4</sup>He pot were 40 AWG manganin. The large gauge Cu wires were for the temperature controller heater on the <sup>4</sup>He pot. The other Cu leads ran to the fountain pump heater. A total of four thermometers are in place on the test cell. All thermometers are measured with a 4-wire technique. The heat load on the <sup>3</sup>He pot is

$$16 - \text{No. 40 AWG manganin wires} \quad Q = 0.8 \mu \text{ W}$$

The fluid lines from the <sup>4</sup>He pot all have 0.1 mm I.D. x 30 cm long capillaries leading from the pot to provide thermal isolation. The heat leak along these lines is estimated from Bertran and Kitchens (1968) to be around

$$\text{capillary heat leak} = 1.8 \mu \text{ W}$$

In addition, the inlet and exit flow passages have .083" I.D. x 10" long superleaks that provide additional isolation. A conservative estimate of the heat leak on the <sup>3</sup>He pot is

$$Q_{\text{heat leak}} (1 \text{ K} - 0.4 \text{ K}) = 2.6 \mu \text{ W}$$

This is well within the cooling capacity of a pumped <sup>3</sup>He bath.